The Role of Transforming Growth Factor β Signalling in Regulating the Sphingolipid Rheostat in Intrauterine Growth Restriction

by

Sarah Chauvin

A thesis submitted in conformity with the requirements
for the degree of Master of Science

Department of Physiology
University of Toronto

The Role of Transforming Growth Factor β Signalling in Regulating the Sphingolipid Rheostat in Intrauterine Growth Restriction

Sarah Chauvin

Master of Science

Department of Physiology
University of Toronto

2014

Abstract

Disruptions of sphingolipid metabolism contribute to the onset of several human pathologies. Herein, I examined sphingolipid metabolism in intrauterine growth restriction (IUGR), a pregnancy-related disorder that is commonly due to placental insufficiency. Lipid mass spectrometry revealed increased levels of pro-death sphingosine (SPH) in IUGR placentae relative to pre-term control placentae. This was accompanied by increased acid ceramidase (AC) expression and reduced sphingosine kinase 1 (SPHK1) expression and activity. Exposure of human choriocarinoma JEG3 cells to TGFβ1 and β3 recapitulated the sphingolipid regulatory enzyme expression profile observed in IUGR. Pharmacological inhibition of activin receptor-like kinase 5 (ALK5) in human villous explants and JEG3 cells reversed the TGFβ1 and β3 stimulatory effect on AC expression; whereas exposure of JEG3 cells to ALK1 inhibitor, Dorsomorphin, further suppressed SPHK1 expression. Of clinical significance, ALK5

expression and Smad2 activation is increased in IUGR placentae. Hence, altered TGFβ signalling may contribute to SPH accumulation in IUGR.

Acknowledgements

First and foremost I would like to acknowledge my supervisor Dr. Isabella Caniggia, who has been instrumental in my growth as a young professional and developing scientist. Throughout my master's degree, Dr. Caniggia has encouraged me to take ownership of my project, giving me the necessary tools to be successful while challenging me to think critically about my work. Dr. Caniggia has also afforded me many invaluable opportunities including attending and participating in the IFPA 2013 conference in Whistler, as well as supporting my desire to participate in an exchange course at the Karolinska Institute in Stockholm, Sweden. She will continue to be an inspirational role model to me in my future career.

I am also grateful for the guidance and support given to me by the members of my supervisory committee, Dr. Michelle Letarte and Dr. Theodore Brown. In addition to your advice and respective expertise, I deeply thank you for being as equally captivated by my project as I have been over the last two years. Your enthusiasm has truly made my master's program a rewarding experience.

I would further like to thank my colleagues, Andrea Tagliaferro, Sruthi Alahari, Megan Melland-Smith, Jayonta Bhattacharjee, and Julien Sallais, for orienting me in the lab, helping me troubleshoot my experiments, and providing me with an all-around culturally rich environment. I have learned many things both science-, and not science-related, which I will carry forward in my future endeavors.

Additionally, I would like to thank Canadian Institute of Health Research (CIHR) and my Ontario Graduate Scholarship award for funding this thesis project.

Last but not least, I would like to thank my parents for their ongoing support and encouragement. Specifically, my parents helped me to maintain perspective during the more challenging moments of my degree. I credit them both for taking the time to understand my work, and eternally thank them for supporting my living in the city of Toronto.

Contributors

The following people have contributed to the collection of materials and generation of the data:

Mount Sinai Hospital Biobank (Toronto, Canada) and Dr. Tullia Todors (University of Turin, Italy) for supplying normal and pathological human placental tissue and explants for immunoblot, immunohistochemistry, and immunofluorescence analysis.

Dr. Martin Post and Denis Reynaud from The Hospital for Sick Children at the Analytical Facility for Bioactive Molecules at Sickkids, Toronto, Ontario for analyzing the sphingolipid profiles in normal and pathological human placental tissue and explants.

Yoav Yinon, Jing Xu, Dr. Caniggia for their experimental data on activin receptor-like kinase 5 (ALK5) and phosphorylated Smad2 (pSmad) expression in normal and pathological human placental tissue.

Table of Contents

List of Tables

List of Figures

List of Abbreviations

AC	acid ceramidase
ACOG	American College of Obstetrics and Gynaecology
ALK	activin receptor-like kinase
alk-SM	alkaline sphingomyelinase
ANOVA	one-way analysis of variance
ASAH1	human acid ceramidase gene
ASM	acid sphingomyelinase
BafA1	bafilomycin A1
BMP	bone morphogenetic protein
CER	ceramides
CerS	dihydroceramide/ceramide synthases
DES1	dihydroceramide Δ4-desaturase 1
DMSO	dimethyl sulfoxide
EMEM	Eagle's minimal essential medium
ER	endoplasmic reticulum
ERK	extracellular signal-regulated kinase
EVT	extravillous trophoblast cells
FBS	fetal bovine serum
GA	gestational age
Grb2	growth factor receptor binding protein 2
HIF1	hypoxia-inducible factor 1
HPLC	high performance liquid chromatography
IF	immunofluorescence
IHC	immunohistochemistry
IUGR	intrauterine growth restriction
JNK	c-Jun amino-terminal kinases
KDHR	3-Ketodihydrosphingosine Reductase
LAP	latency associated peptide
LTBP	latent TGFβ binding proteins
LC3B	microtubule-associated protein 1 light chain 3
MAPK	mitogen-activated protein kinases
MRM	Multiple Reaction Monitoring
MS/MS	tandem mass spectrometry
NSM	neutral sphingomyelinase
Par6	partitioning defective 6
PBS	phosphate-buffered saline
Pen/strep	penicillin/streptomycin
PE	preeclampsia
PKC	protein kinase C
PTC	preterm control deliveries

RFU	relative fluorescence units
S1P	sphingosine-1-phosphate
S1PR	S1P receptor
SDK	sphingosine-dependent protein kinase
SPT	serine palmitoyltransferase
SBE	Smad binding element
siRNA	small-interfering ribonucleic acid
SAP	sphingolipid activator proteins
SK	syncytial knot
SM	sphingomyelin
SMS	sphingomyelin synthase
SPH	sphingosine
SPHK	S1P kinase
TβRI/II/III	Transforming growth factor beta type I/II/III receptor
TGFβ	Transforming growth factor beta

Chapter 1

1 Introduction

First described by the pathologist J.L.W. Thudichum in 1884 (1), sphingolipids have recently emerged at the forefront of cell biology owing in large part to their dynamic functions. Today this class of amino alcohols encompasses hundreds of structurally diverse molecules, which vary in chain length, number, position and stereochemistry in terms of double bonds, head-groups, and functionality (2). Sphingolipids were generally considered structural elements of the cell and sources of cellular energy. They are now emerging as bioactive signalling molecules in a variety of cellular processes including cell differentiation, proliferation, and apoptosis (3). Furthermore, dysregulated sphingolipid signalling plays a key role in the development of several human pathologies including lysosomal storage disorders, cancers, neurological disorders such as Alzheimer's disease, diabetes and heart disease, infection, and immune dysfunction (3-5). However, a role for sphingolipids in human pregnancy and pregnancy-related disorders has only recently been considered (6-8).

1.1 Sphingolipids

Sphingolipids represent a class of structurally diverse lipids that are ubiquitous components of all eukaryotic cell membranes (2). Unlike phospholipids, which are built on a glycerol backbone, sphingolipids are derived from long chain sphingoid bases, such as sphingosine (SPH) (2,4,9) **(Figure 1.1)**. Modifications to the C1-hydroxyl group or C2-amino group of a given sphingoid base contributes to the complexity and variety of sphingolipids, which play dynamic roles in membrane biology and signal transduction. For example,

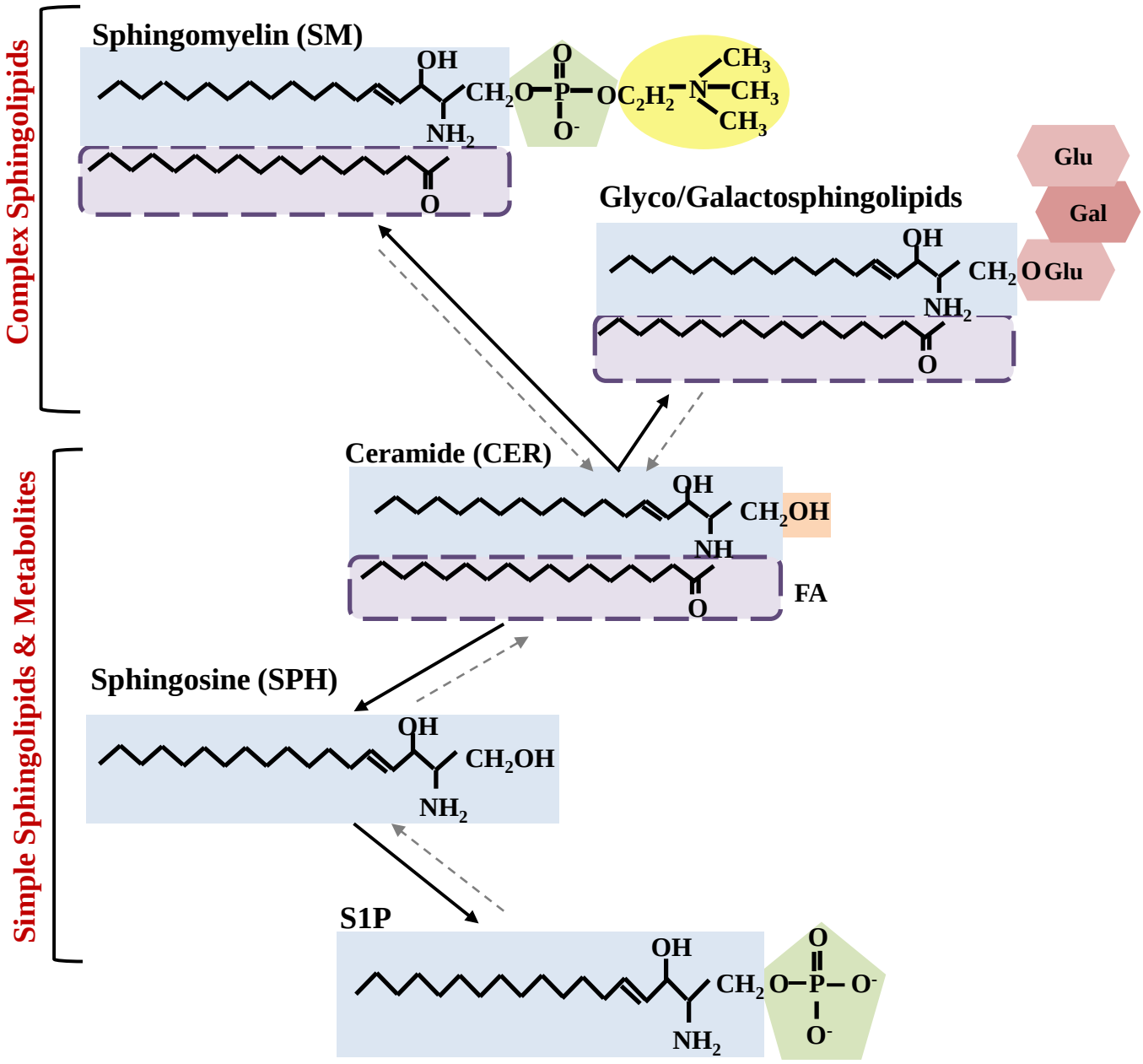

Figure 1.1 Basic sphingolipid structure

Sphingolipids represent a class of structurally diverse lipids. The simplest sphingolipid structure is ceramide, which is built on a sphingosine (blue) backbone and contains a fatty acid (FA) of variable chain length attached in amide linkage (purple). Ceramide is further distinguished by a hydroxyl headgroup (orange). The addition of a phosphocholine headgroup (green and yellow) to ceramide gives rise to sphingomyelin, whereas the addition of sugar moieties (red) gives rise to a broad class of glyco- and galactosphingolipids. Phosphorylation (green) of sphingosine generates the potent bioactive mediator sphingosine-1-phosphate (S1P).

phosphorylation at the C1-hydroxyl group of SPH produces important signalling molecule sphingosine-1-phopsphate (S1P). In contrast, the addition of a free fatty acid to the C2-amino group of SPH generates ceramides (CER), which are the simplest sphingolipid structures. Due to the possible number of acyl CoA molecules, CER truly represents a class of lipids, and can therefore have varying biological functions depending on the fatty acid chain content (4,9). Moreover, sphingolipids are further diversified through the addition of a complex head-group to the C1-hydroxyl group. Since CERs maintain a hydroxyl head-group they are considered as precursors to more complex sphingolipids such as sphingomyelins (SMs), which are distinguished by a phosphocholine head-group, and glycosphingolipids, which differ by the order and type of sugar residues attached to their head-groups **(Figure 1.1)**.

Sphingolipid structure dictates biophysical properties, which are critical in their compartmentalization, metabolism, and function. Similar to all membrane lipids, sphingolipids are amphipathic in nature meaning that they have both hydrophobic and hydrophilic properties to varying degrees depending on their composition (2,10). In general terms, the hydrophobic region consists of the sphingoid base and fatty acid attached in amide linkage, whereas the hydrophilic region consists of hydroxyl-containing or phosphate-containing head-groups. A sufficiently amphipathic lipid, such as SPH, is therefore capable of diffusing between membranes, and flipping between membrane leaflets, though it tends to accumulate in acidic organelles due to ionization of the free amino group (2). Likewise SPH metabolite S1P is relatively soluble/hydrophilic and is capable of exiting the cell via transporter proteins (11). In contrast, increasingly hydrophobic lipids such as CERs, SMs, and glycosphingolipids are much more spatially restricted to cellular membranes, and are thus likely modified by enzymes resident in the membrane of that cellular compartment (2). Hence, sphingolipid structure and subcellular distribution may contribute to distinct biological functions.

1.1.1 Sphingolipid Metabolism

At the core of sphingolipid metabolism are CERs, which are the only sphingolipids that can be synthesized *de novo* in the endoplasmic reticulum (ER) from non-sphingolipid precursors (13) **(Figure 1.2)**. The initial, rate-limiting step in CER synthesis is the condensation of serine and palmitoyl CoA into 3-ketodihydrosphingosine by serine palmitoyltransferase (SPT) enzyme. This is a critical step in sphingolipid synthesis as genetic deficiencies in SPT activity are linked with the onset of Hereditary Sensory and Autonomic Neuropathy Type I, a disease characterized by progressive motor neuron and dorsal ganglia degeneration (14). Furthermore, complete knockout of *Spt* in mice led to embryonic lethality suggesting a role for SPT in early developmental events (15).

Next, 3-Ketodihydrosphingosine Reductase (KDHR) rapidly reduces the ketone group of 3-ketodihydrosphingosine to a hydroxyl group in a NADPH-dependent manner (6). This forms the transitory sphingolipid backbone, dihydrosphingosine, which undergoes acylation at its C2-amino group to form dihydroceramide via the action of six distinct dihydroceramide/ceramide synthases (CerS) (16). In mammals, each CerS is thought to have a unique, yet overlapping preference for fatty acid chains thereby giving rise to the different species of dihydroceramide/ceramide. Once made, dihydroceramides are quickly converted into ceramide via dihydroceramide Δ4-desaturase 1 (DES1), which transforms the existing dihydrosphingosine backbone into sphingosine using molecular oxygen and NADPH (6). This represents an additional key step in sphingolipid metabolism as *Des1*$^{-/-}$ mice have highly elevated levels of dihydroceramide and significantly reduced ceramide, resulting in multi-organ dysfunction and failure to thrive (17).

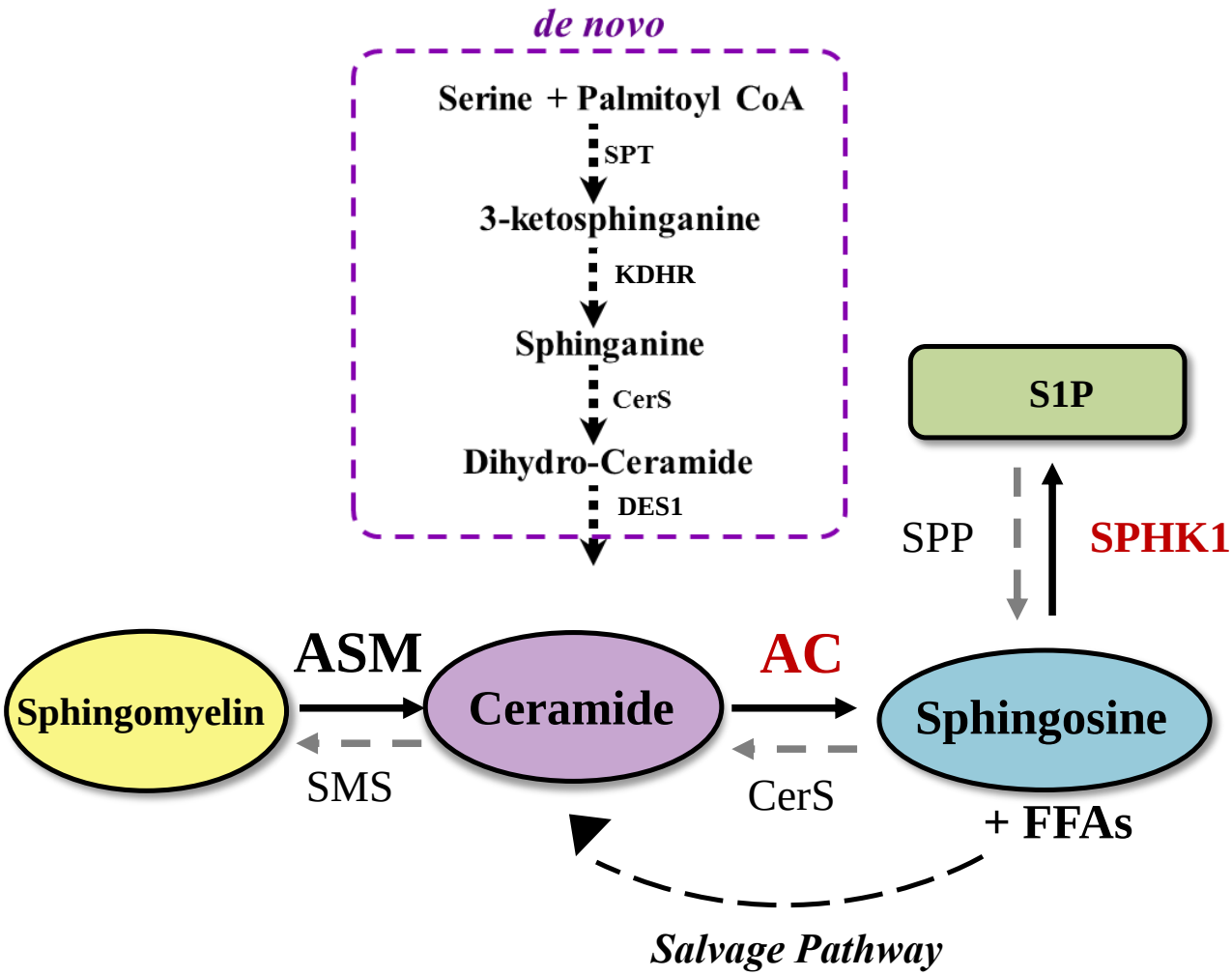

Figure 1.2 Sphingolipid metabolic pathway

At the core of sphingolipid metabolism is pro-death ceramide (CER), which is the only sphingolipid that can be synthesized *de novo* in the endoplasmic reticulum. CER *de novo* synthesis consists of 4 key reactions (purple box) initiated by the condensation of serine and palmitoyl CoA by serine palmitoyltransferase (SPT). CER levels are regulated by the balance between synthesis, modification, and breakdown. For instance, addition of a phosphocholine group to CER by sphingomyelin synthase (SMS) gives sphingomyelin (SM). Alternatively, SM can be reconverted into CER by acid sphingomyelinase (ASM). CER is further broken down by acid ceramidase (AC) into sphingosine (SPH). Phosphorylation of SPH by SPHK1 produces pro-survival molecule S1P. Dephosphoryaltion of S1P by S1P phosphatases (SPP) regenerates SPH, which can be reacylated by ceramide synthases (CerS) to produce CER. This is referred to as the salvage pathway of CER synthesis.

Newly synthesized CERs are next shuttled to the Golgi apparatus via vesicular transport and ceramide transfer protein, where membrane resident enzymes further modify them to produce complex sphingolipids (6). For example, CERs can be phosphorylated by kinases to produce the potent signalling molecules ceramide-1-phosphate. In addition, CERs can be modified through the addition of a sugar moiety to the C1-hydroxyl group by glycosylceramide synthase and galactosyltransferase **(Figure 1.1)**. This gives rise to a large class of molecules called the glycosphingolipids, which are particularly important for neuronal function and proper brain maturation (18). Lastly, CERs can be modified through the addition of a phosphocholine headgroup via the action of sphingomyelin synthases (SMS) to produce sphingomyelin (SM) **(Figure 1.2)**. Sphingomyelin is the most abundant complex sphingolipid, and it plays an important role in membrane structure and the myelination of neurons (6). Following processing, CERs, along with glycosphingolipids and SM, are transported from the Golgi to the plasma membrane or to the lysosomal compartment via vesicular trafficking (19).

In addition to *de novo* synthesis, CERs can be regenerated through the hydrolysis of SM by a family of sphingomyelinases (20). This family of enzymes is further classified according to their optimal working pH: 1) acid sphingomyelinase (ASM), 2) alkaline sphingomyelinase (alk-SM), and 3) neutral sphingomyelinase (NSM). The same classification system is used to define the family of ceramidase enzymes, which are responsible for the deacylation of CERs into SPH. Organelle-specific expression of sphingomyelinases and ceramidases is likely required to regulate CER levels in different subcellular compartments (6). Of particular interest are acid ceramidase (AC) and ASM, which are responsible for SM and CER breakdown in acidic environments, an event that occurs in the lysosomal compartment. Deficiencies in either AC or ASM result in human lipid storage disorders named Farber disease and Niemann-Pick disease,

respectively (21). Hence, the acidic forms of these enzymes have been attributed to degrading most cellular SM/CER content, and are thus the most commonly studied **(Figure 1.2).**

After SPH is produced, it can be phosphorylated by sphingosine kinase (SPHK1) to generate S1P, a pro-survival molecule that opposes CER/SPH pro-apoptotic functions (6). S1P is then further degraded by S1P lyase at the ER to produce hexadecenal and phosphoethanolamine. This marks the exit point of sphingolipid metabolism. Alternatively, S1P can be dephosphorylated by S1P phosphatase to restore SPH levels.

Due to their amphipathic nature, SPH and free fatty acids can be released into the cytosol by traversing the membrane compartment (22). Once released, they may act as substrates for ceramide synthases at the ER thereby resulting in the regeneration of CERs. This is defined as the sphingolipid salvage pathway, which is an alternative CER synthesis pathway originating from SPH and FFAs (6). Remarkably, the salvage pathway has been estimated to contribute from 50% to 90% of sphingolipid biosynthesis, highlighting the importance of the interplay of CERs with their metabolites (22).

1.1.2 Sphingolipids as Bioactive Mediators

Originally thought to be exclusively involved in energy metabolism and membrane structure, sphingolipids have recently been recognized as key signalling and regulatory molecules in select patho-physiological processes (2). Of notable interest are CERs, and their metabolites SPH and S1P, which mediate cell stress responses (23) **(Figure 1.3)**. In a variety of organ systems, CERs, SPH, and S1P production have been shown to be induced by stimuli such as UV radiation, chemotherapy, heat stress, growth factors, reactive oxygen species, and hypoxia (2,19) **(Figure 1.3)**. Once synthesized, bioactive sphingolipids are capable of acting in two ways, 1) through lipid-lipid interactions, whereby the bioactive lipid alters membrane structure

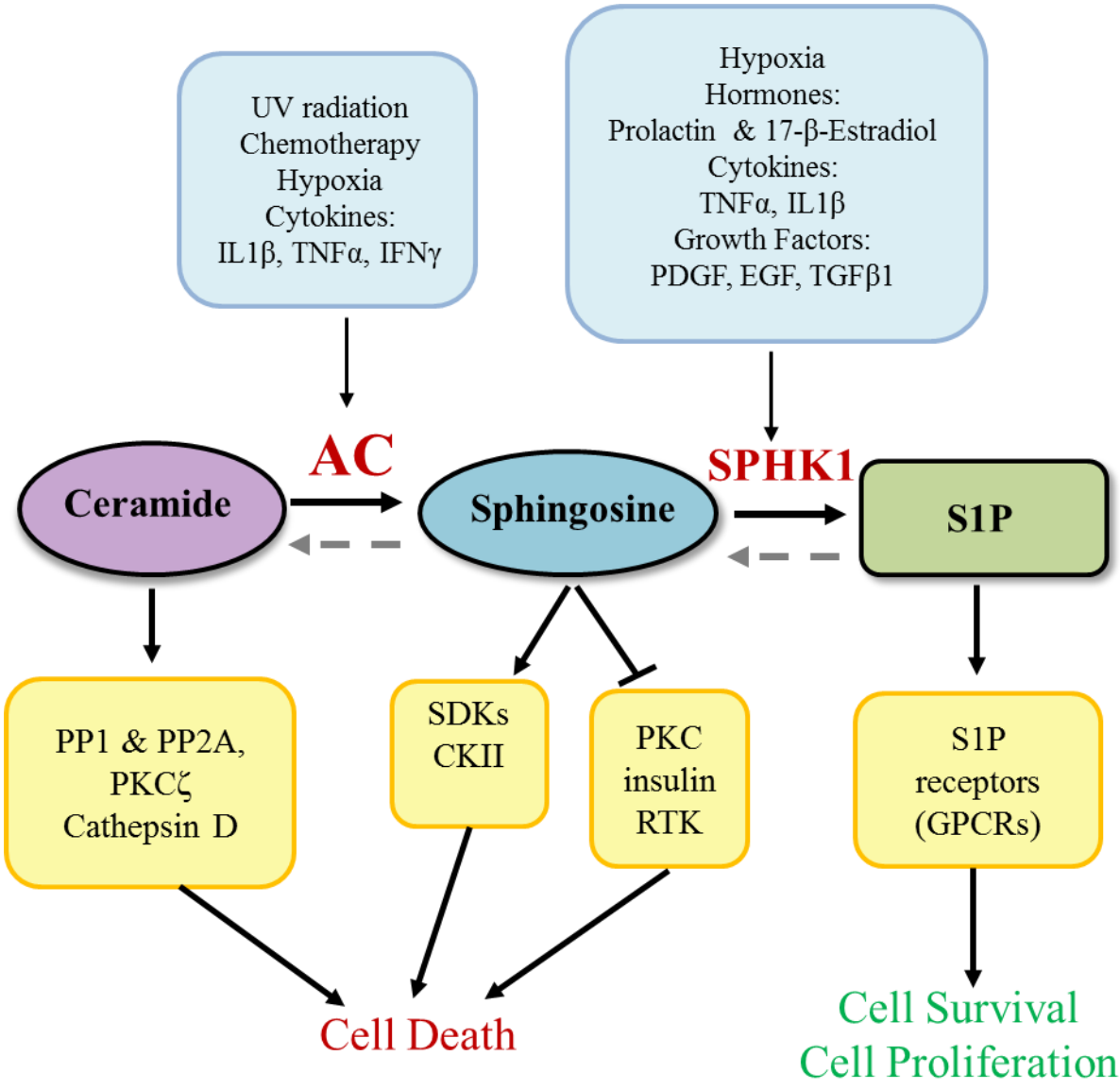

Figure 1.3 Sphingolipids as bioactive mediators

Sphingolipids function as bioactive mediators in a number of cellular processes including cell proliferation, differentiation, migration, and apoptosis. In particular, the balance between pro-death ceramide and sphingosine, and pro-survival sphingosine-1-phosphate (S1P) is critical to cell fate outcomes as they regulate a number of downstream targets (yellow). CER, SPH, and S1P levels are therefore tightly regulated by acid ceramidase (AC) and sphingosine kinase 1 (SPHK1). Alterations to AC/SPHK1 expression/activity due to external stimuli (blue) can disrupt the delicate sphingolipid rheostat thereby resulting in enhanced cell death or cell survival, which is common to a number of human pathologies.

or membrane protein interactions (10), or 2) through lipid-protein interactions, whereby lipids interact with specific downstream targets such as phosphatases, kinases, and G-coupled protein receptors, which in turn mediate their specific cellular effects (4).

Research studies have primarily focused on identifying direct protein targets through which bioactive lipids mediate their effects. Specifically, CER signalling has been implicated in inhibiting cell growth, differentiation, and proliferation, while promoting apoptosis and senescence (24). It is thought to function, in part, by activating protein phosphatases PP1A and PP2A, which have been shown to bind natural stereoisomers of ceramide *in vitro* (25). This results in the subsequent dephosphorylation of proteins such as retinoblastoma gene protein RB (26), protein kinase C (PKC) alpha (27), and protein kinase B (28), which are critical to cell cycle regulation and cell survival pathways. Similarly, CER has been demonstrated to activate PKCζ (29), serine/threonine-protein kinase raf-1, and kinase-suppressor of Ras, thereby affecting the phosphorylation status of downstream effector molecules of cell growth pathways (30). Lastly, lysosomal CER has been shown to bind and activate the cellular protease cathepsin D, a lysosomal enzyme that has been implicated in the initiation of the mitochondrial cell death pathway (31).

Similar to CER signalling pathways, sphingosine has been associated with inducing cell cycle arrest and promoting apoptosis by regulating protein kinases. For example, SPH has been shown to inhibit PKC, which has implications on cell growth by preventing gene transcription (32). Moreover, studies have found that SPH inhibits calmodulin-dependent kinases and insulin receptor tyrosine kinase, but enhances casein kinase II (33). A unique feature of SPH signalling is the downstream activation of proteins designated as sphingosine-dependent protein kinases (SDKs), which were first identified in the human T-lymphocyte-derived Jurkat cells (34) and in

the mouse embryonic fibroblast derived Balb/3T3 cells (35). Notably, the latter and subsequent studies found that SDK activation by sphingosine resulted in the phosphorylation of 14-3-3 proteins (35,36). The 14-3-3-proteins are a conserved family of dimeric phosphoserine binding proteins that function as adaptor proteins in a number of signalling pathways (37). Specifically, dimeric 14-3-3 has been shown to prevent apoptosis by associating with pro-death molecule Bad; thereby preventing its interaction with the membrane bound death agonist BCL-XL (38). Following sphingosine-mediated activation of SDKs, 14-3-3 proteins get phosphorylated at the dimeric interface thereby preventing their association with target proteins and disrupting their anti-apoptotic function (33). Hence, SPH is also capable of promoting cell death and inhibiting cell survival by directly interacting with downstream effector molecules.

In stark contrast to CER and SPH, S1P signalling has been implicated in promoting cell proliferation, cell survival, cell migration, inflammatory processes, angiogenesis, and resistance to cell death (2). As mentioned, S1P is much more soluble than SPH/CER, and is therefore capable of being exported from the cell by protein transporters. Once released to the extracellular space, S1P interacts with one of five S1P receptors (S1PRs), which are differentially expressed on different cells and tissues giving rise to unique cellular responses (39). S1PRs are in fact a subset of high affinity G-protein coupled receptors that use a number of well-known G-protein-responsive pathways to activate Rac, Ras-extracellular signal-regulated kinase (ERK), phosphoinositide 3-kinase-AKT-Rac, phospholipiase C (PLC) and Rho (40). Intracellular S1P is also capable of acting in an S1PR-independent mechanism to stimulate calcium release (41); however, intracellular targets of S1P have not yet been identified and thus its intracellular role is not well understood.

It is important to stress that the physiological levels of bioactive lipids differ in order of magnitude and this dictates their mode of action (2). For example, there is a greater abundance of CERs than there is of SPH, and there is even less S1P in cells under homeostatic conditions. Hence, CERs act with intermediate affinity for their targets, whereas less abundant SPH and trace levels of S1P interact with high affinity targets that are capable of sensing their low concentrations. Hence, small fluctuations in CERs may have relatively minute biological outcomes, while the same changes in SPH and S1P can have greater biological impact.

Collectively these studies illustrate a role for CERs, SPH, and S1P as secondary messenger molecules in signal transduction pathways. Remarkably, where CER/SPH accumulation has been shown to promote cell death, cell cycle arrest, and senescence, S1P accumulation promotes cell proliferation, differentiation, and survival (2,23,42). The opposing functions of these lipids therefore highlight the delicate balance of the cellular sphingolipid rheostat, and the dynamic role of sphingolipids in regulating cell fate.

1.1.3 Sphingolipid Regulatory Enzymes: AC and SPHK1

Acid ceramidase is a lysosomal enzyme that catalyzes the deacylation of cellular CER into SPH. It is therefore considered the rate-limiting enzyme in both SPH and S1P production. Complete absence of AC expression causes embryonic lethality in mice at the two-cell stage, suggesting its importance during early development (43). In humans, AC is encoded by the *ASAH1* gene located on chromosome 8 (44). It is synthesized in the ER as a 55 kDa monomeric precursor protein, and then undergoes glycosylation in the Golgi apparatus to ensure proper trafficking to the lysosome (44) **(Figure 1.4a)**. Specifically, *in vitro* studies have revealed that AC contains 6 N-linked oligosaccharides and that disruption of these glycosylation sites prevents AC maturation and activity (44). Upon reaching the lysosomal compartment (pH~4.5), AC

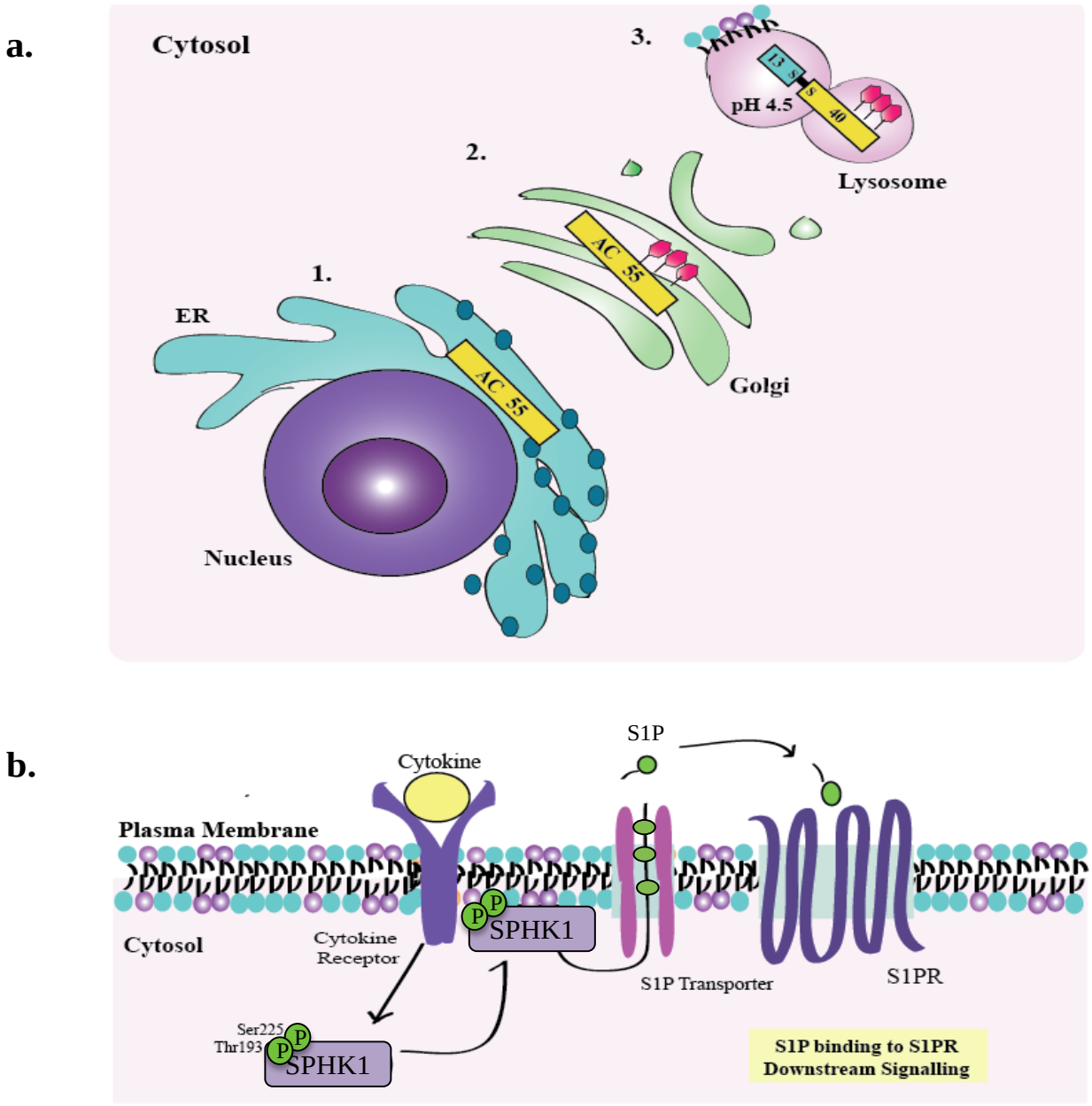

Figure 1.4 AC and SPHK1 regulatory enzymes

(a) AC is synthesized in the endoplasmic reticulum (ER) as a 55kDa propeptide (1). It is then shuttled to the Golgi Apparatus where it is glycosylated at its C-terminus (2). Upon reaching the lysosome, AC undergoes autoproteolytic cleavage forming a 53 kDa protein consisting of 2 subunits (*i.e.*, 13 kDa α-subunit/40 kDa β-subunit) attached by a disulfide bridge (3). It is in the lysosome that AC carries out its function. **(b)** SPHK1 is recruited from the cytosol to the inner leaflet of the plasma membrane following cytokine-mediated phosphorylation at Serine 225 and Threonine 193. SPHK1 phosphorylates sphingosine to generate S1P, which can exit the cell via transporter proteins and interact with S1P receptors (S1PR) to initiate downstream signalling.

undergoes autoproteolytic cleavage to produce a 53 kDa dimeric active form of the enzyme (45). This maturation process is pH dependent and relies on cysteine dependent proteolysis similar to the mechanism used by the N-terminal nucleophile hydrolase superfamily (45). Active AC consists of two covalently bonded subunits: 1) the 13 kDa α-subunit, containing the enzymatic active site, and 2) the 40 kDa β-subunit, containing six N-linked oligosaccharides (44). Total AC processing, from synthesis to activation, is estimated to take approximately twelve hours and the half-life of mature AC is estimated at twenty hours (44).

To sufficiently carry out its function, AC requires the expression of sphingolipid activator proteins (SAPs), which are enzymatically inactive proteins that enhance AC binding affinity for its substrate ceramide (46). In particular, SAP-D has been shown to be a necessary cofactor for AC activity *in vivo* (47). This was later confirmed by *in vitro* studies showing that SAP-D expression enhanced AC activity by roughly 5-fold (48). Recently, tyrosine phosphorylation has been considered as an important regulator of AC activity; however, it remains unclear as to whether AC is directly phosphorylated (49). Currently, a putative phosphorylation site at tyrosine residue 305 has been identified but site-directed mutagenesis studies are needed to confirm its role in regulating AC activity (49).

Sphingosine kinases are cytosolic enzymes that utilize ATP to phosphorylate the C1-hydroxyl group of sphingosine. They represent additional rate-limiting enzymes in S1P production and the absence of their expression results in d7 embryonic lethality in mice (50). Despite catalyzing the same reaction, SPHK1 and SPHK2 have differences in their substrate specificity, and somewhat distinct subcellular localizations, which determine their effects (2). SPHK1 has been extensively studied as it displays enhanced substrate specificity for SPH and acts at the plasma membrane; whereas the function of SPHK2 is poorly understood. However, it

has been established that SPHK2 has broader substrate specificity and acts within the nucleus (50). Herein, the regulation and activity of SPHK1 will be discussed.

SPHK1 belongs to the diacylglycerol kinase family and is encoded by the *SPHK1* gene, which maps to human chromosome 17 (6). It is synthesized as a 49kDa protein, and has intrinsic kinase activity that is primarily regulated by its ability to gain access to its substrate SPH **(Figure 1.4b)**. Stimulants such as phorbol ester have been shown to cause the translocation of SPHK1 from the cytosol to the plasma membrane (50), an event that depends on phosphorylation at Threonine 193 and Serine 225, likely mediated via ERK proteins (6). Furthermore, phosphorylated SPHK1 had an enhanced affinity for anionic phospholipids, which are highly abundant in the membrane thereby facilitating translocation. Activation by phosphorylation also coincided with increased S1P production and extracellular release (2).

Although sphingolipid metabolism is mediated by a vast number of regulatory enzymes, the AC-SPHK1 axis of regulation is a particular research focus given that it is responsible for maintaining intracellular levels of bioactive CERs, SPH, and S1P **(Figure 1.3)**.

1.1.4 Mechanisms of AC and SPHK1 Regulation

Dysregulated AC expression can lead to the accumulation of pro-death or pro-survival lipids thereby tilting tissue homeostasis. For example, heritable deficiencies in AC activity caused by a defective AC gene product results in Farber disease, a lysosomal storage disorder characterized by the accumulation of CERs in acidic compartments (51). This disease is clinically characterized by symptoms including swollen joints, subcutaneous nodules, hoarseness, and mental disabilities (52). In contrast, enhanced AC activity in cancer has been shown to increase S1P levels thereby stimulating tumour progression and cancer resistance to chemotherapy (51,52). Additionally, Alzheimer's disease is characterized by AC overexpression

resulting in an accumulation of pro-death SPH, which contributes to increased neuronal cell death typical of this pathology (53). Hence, AC expression must be tightly regulated as disruption in its expression/activity may result in human pathologies.

In vitro studies have identified several external stimuli capable of altering AC expression **(Figure 1.3)**. For instance, cancer treatments such as irradiation (54) and chemotherapeutic Daunorubicin (49) have been shown to upregulate AC activity in prostate cancer cells and hepatoma cells, respectively (49,54). This conferred increased radioresistance and proliferation to cancer cells, presumably by increasing S1P production. As a result, scientists are currently exploring the benefits of administering AC inhibitors in conjunction with cancer therapies (49). In addition, hypoxia, which is characteristic of the tumour environment, was demonstrated to increase AC expression in cancer cell lines derived from the Ewing's family of tumours (55). Emerging evidence also points to a role for cytokines in regulating AC expression. Specifically, TNF-α, IL-1β, and IFN-γ have been shown to stimulate AC in pancreatic β-cells, possibly contributing to the altered sphingolipid profile detected in diabetes (28). Lastly, Sato *et al.* reported decreased CER levels following TGFβ1 treatment of serum-starved human fibroblasts, suggesting a role for TGFβ in regulating AC (56). However, no reports have directly addressed this hypothesis.

Deficient SPHK1 activity has also been associated with Alzheimer's disease (57), and has been found to promote vascular defects (8,58) and pregnancy loss (58). In contrast, enhanced SPHK1 expression has been associated with the induction of tumorigenesis (59). Consequently, the proper regulation of SPHK1 is also critical to maintenance of the cellular sphingolipid rheostat.

SPHK1 is also regulated by a number of external stimuli **(Figure 1.3)**. In line with AC, hypoxia was shown to stimulate *SPHK1* mRNA, protein expression, and activity in endothelial cells and glioma-derived cells (60,61). In depth analysis of this finding revealed two hypoxia-responsive elements in the SPHK1 promoter suggesting a role for hypoxia-inducible factor 1 (HIF1) in SPHK1 regulation. Interestingly, where HIF1α was shown to be an inhibitor of SPHK1, HIF2α was reported to enhance SPHK1 expression. Hence, competitive binding of HIF1α/HIF2α to the *SPHK1* promoter may impinge on the expression of this enzyme (60,61). In addition, hormones such as prolactin and 17 beta-estradiol were demonstrated to have a biphasic effect on SPHK1 activity in the breast adenocarcinoma cell-line MCF7 (62). Doll *et al.* further established that SPHK1 activation by hormones likely involved STAT5 activation as well as PKC (62). Given the role of S1P in inflammation and cell growth, most research studies have focused on the role of cytokines and growth factors in regulating SPHK1 expression. To date, TNF-α, IL-1, epidermal growth factor, and platelet-derived growth factor have been shown to activate SPHK1 resulting in transient increases in S1P (~2-3 fold) (2). Investigators concluded that SPHK1 stimulation by cytokines/growth factors involved PKC, phospholipase D, and/or ERK mitogen-activated protein kinases (MAPKs), which aided in SPHK1 translocation. Lastly, studies have also supported a role for TGFβ1 in upregulating SPHK1 activity and expression in human and mouse fibroblasts thereby preventing apoptosis (63). Scientists are currently exploring the possibility of a cross-talk between TGFβ and S1P signalling axes due to the role of ERK proteins, which are downstream signalling targets of TGFβ, in SPHK1 activation (64).

1.2 Transforming growth factor betas

The transforming growth factor beta superfamily is comprised of over thirty structurally related proteins including activins, inhibins, anti-müllerian hormone, bone morphogenetic

proteins (BMPs), myostatin, and others (12). Members of the TGFβ superfamily regulate a variety of cellular processes including cell differentiation, migration, recognition, proliferation, and apoptosis (13-15). In general, these responses are initiated by ligand binding to transmembrane receptor kinases that transduce their signal to downstream effector molecules thereby regulating cellular events. As a result TGFβs play key roles in physiological processes such as embryonic patterning, immunity, and tissue remodelling (16). Inappropriate TGFβ signalling has also been implicated in several human pathologies such as arthritis, fibrosis, preeclampsia (PE), and cancers (16,17).

In humans, TGFβ exists in 3 isoforms (β1, β2, β3) that share high structural homology and some functional overlap (18). Since a unique gene on a distinct chromosome encodes each isoform, TGFβs are secreted in a temporal and tissue specific manner. TGFβ isoforms are all synthesized as large precursor proteins, where TGFβ1 contains 390 amino acids and TGFβ2 and 3 have 412 amino acids (15). In addition, they each contain an N-terminal signal peptide that is needed for their secretion; a pro-region called the latency-associated peptide (LAP) that controls their bioactivity, and a C-terminal region that becomes mature TGFβ following proteolytic cleavage. With respect to the C-terminus, mature TGFβ2 was found to share 71% structural identity with TGFβ1 (19), whereas mature TGFβ3 was 72% identical to TGFβ1 and 76% identical to TGFβ2 (20). These structural differences may explain why the isoforms display differential binding affinities for TGFβ receptors *in vitro*. Specifically, TGFβ1 and TGFβ3 preferentially bind to TGFβ Type II receptors (TβRII) and TGFβ Type I receptors (also termed activin receptor-like kinase (ALK) 1 & 5), which are both serine/threonine kinases (21). Additionally, TGFβs can interact with so-called TGFβ type III (TβRIII) receptors, endoglin and betaglycan. TGFβ1 and β3 can dimerize through their association with TβRII (22). In contrast,

TGFβ2 does not interact with endoglin, and has a higher affinity for betaglycan than for TβRII alone (23).

Typically, TGFβ isoforms share three major functions: 1) regulating cell proliferation/apoptosis, 2) modulating immune responses, and 3) stimulating extracellular matrix deposition (15). However, TGFβs also possess unique biological functions as demonstrated by studies using *Tgfβ* knockout mice that displayed isoform-specific phenotypes. For instance, *Tgfβ*-null mice die *in utero* as the result of defective vasculogenesis and hematopoiesis, implying a role for TGFβ1 in blood cell lineage and cardiac development (24). Those mice that survived TGFβ1 deficiency die shortly after birth due to excessive inflammation and immune cell recruitment to several organs (25). This suggests a role for TGFβ1 in suppressing immune responses. In contrast, *Tgfβ2*-null mice display several tissue and organ malformations leading to perinatal death, implying a key role for this isoform in several developmental processes (26). Moreover, as TGFβ2 is highly expressed by neurons and astroglial cells in the embryonic nervous system, its absence was associated with neural crest deficiencies (26). Lastly, *Tgfβ3* knockouts displayed impaired lung development and defective palate development, suggesting TGFβ3 importance in development of these tissues (27). Intriguingly, during early human pregnancy, the placenta expresses high levels of TGFβ3 (28), which has been shown to be an important regulator of trophoblast differentiation (17,29,30).

Similar to bioactive sphingolipids, TGFβ signalling must be tightly regulated. Consequently, TGFβs are synthesized as precursor proteins that require processing before becoming active (15). After folding, TGFβs are proteolytically cleaved by furin-type enzymes giving rise to mature TGFβ and a latency associated peptide (LAP). LAP remains noncovalently bound to TGFβ, thereby preventing association with its receptors. This complex is termed the

small latent TGFβ complex, which is capable of interacting with latent TGFβ binding proteins (LTBPs) in the extracellular matrix to form large latent complexes (31). LTBPs are instrumental in enhancing the secretion and stability of the TGFβ latent complex as they ensure proper TGFβ folding, and assist in its trafficking to the extracellular matrix. In order to become active, LAP is removed from the complex by proteases like plasmin, matrix metalloproteases, or cathepsin. Other mechanisms of activation involve exposure to reactive oxygen species (32) or to an acidic environment (33). Following activation, mature TGFβ homo- or heterodimers bind to receptor complexes that initiate downstream signalling pathways.

1.2.1 Transforming growth factor beta signalling

Most cells express three surface proteins that recognize TGFβs including the Type I (TβRI), Type II (TβRII), and Type III (TβRIII) receptors. The Type I and Type II receptors are transmembrane serine/threonine kinases, which form heterodimeric complexes that are essential for signal transduction (21). These receptors differ in that TβRII is constitutively active whereas TβRI contains a conserved glycine/serine rich cytoplasmic domain that needs to be phosphorylated by TβRII in order to be active (14). In humans and mice, seven type I receptors (*i.e.*, ALK1 to ALK7) have been identified; however, TGFβs signal through ALK5, which is ubiquitously expressed, and through ALK1, which is predominately expressed on the surface of endothelial cells (15).

In contrast, Type III receptors are transmembrane glycoproteins that are not directly involved in intracellular signalling as they lack a kinase domain (22). However, they control the access of TGFβ to its receptors thereby modulating signal transduction. Betaglycan is an abundant protein expressed on most cell types in foetal and adult tissues (23). In its transmembrane form, betaglycan has been shown to bind to, and enhance TGFβ2-mediated

responses. However, soluble betaglycan potently inhibits TGFβ2 signalling by preventing its association with the receptor complex. In contrast, endoglin, also known as CD105, is expressed on a limited number of cell types, primarily vascular endothelial cells, some hematopoietic cells, stromal cells, chondrocytes, and trophoblast cells (22). Moreover, endoglin shows a binding preference towards TGFβ1 and β3 rather than TGFβ2. Hence, Type III receptors modulate ligand binding thereby functioning as accessory receptors.

Canonical TGFβ signalling is initiated when mature TGFβ binds to TβRII receptors thereby recruiting dimeric TβRI receptors to form a heterotetrameric complex (14) **(Figure 1.5).** Ligand binding also induces a conformational change in the kinase domain of TβRII, which allows it to transphosphorylate the glycine/serine regulatory region in ALK5. This in turn activates ALK5 kinase activity, resulting in the phosphorylation of receptor-regulated (R-) Smad2 and Smad3 at their C-terminal serine residues. Phosphorylated Smad2 or Smad3 form heterotrimeric complexes with the common-partner Smad4, which translocates to the nucleus where it interacts with transcription factors to modulate the expression of target genes.

While in most cell types TGFβs signal via ALK5, recent studies have discovered a role for ALK1-mediated TGFβ signalling in endothelial cells (34) **(Figure 1.5)**. Specifically, ALK1 expressed at sites of epithelial-mesenchymal interactions was found to stimulate Smad1 and Smad5 phosphorylation, which is typical of BMP-mediated signalling (35). Notably, the TGFβ/ALK5 and TGFβ/ALK1 pathways have opposing effects on endothelial cell behaviour; whereby ALK5 inhibits migration and proliferation, whereas ALK1 promotes these processes (36). Furthermore, ALK5 and ALK1 were demonstrated to have unique downstream targets. Recent studies have shown that ALK5 is required for TGFβ/ALK1 signalling, and that ALK1 directly antagonizes ALK5/Smad signalling (37). Thus, the balance between ALK1 and

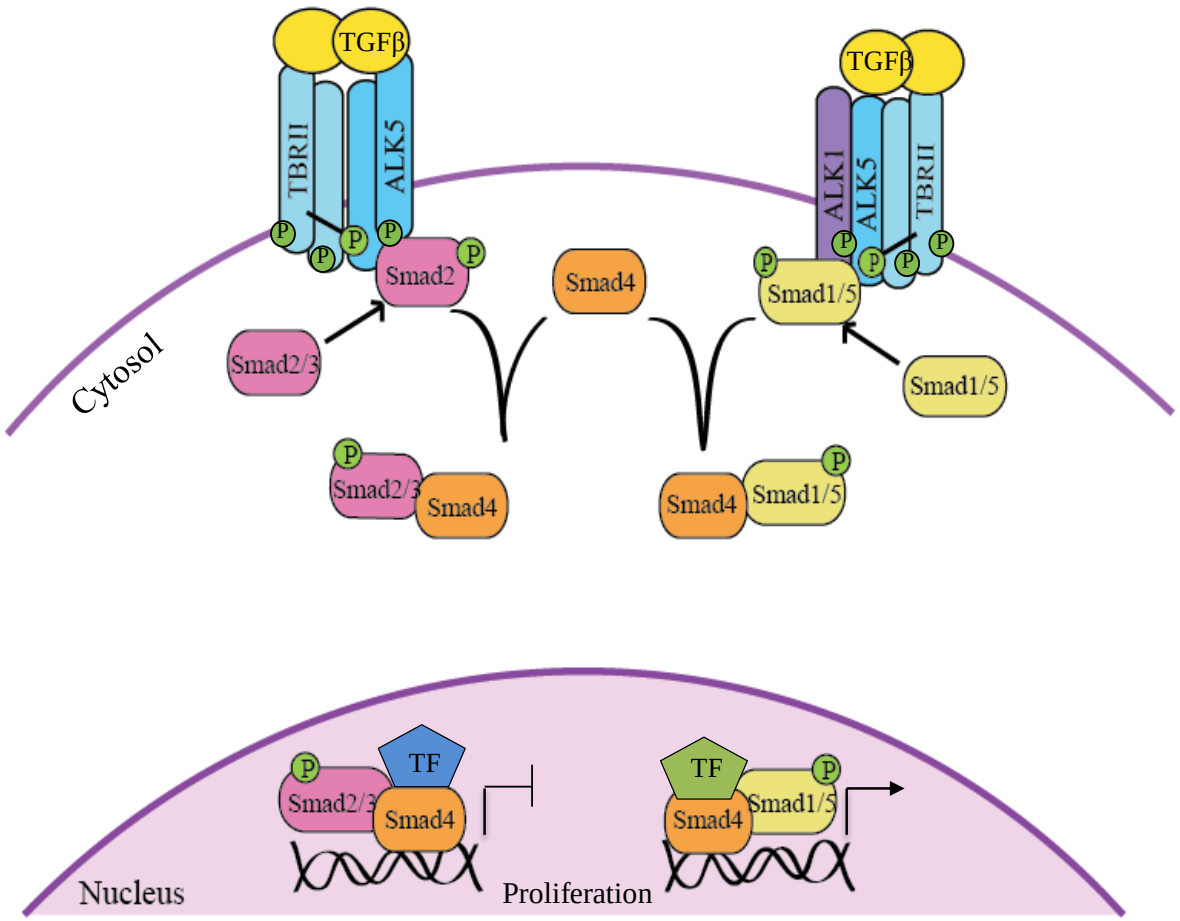

Figure 1.5 TGFβ mediated Smad signalling pathways

Canonical TGFβ signalling is initiated by TGFβ binding to a constitutively active serine threonine kinase receptor called the TGFβ type two receptor (TβRII). This results in the subsequent phosphorylation of the TGFβ type one receptor (TβRI) otherwise known as activin receptor-like kinase 5 (ALK5). Activated ALK5 in turn phosphorylates Smad2/3, which is capable of forming a complex with co-Smad4 and translocating to the nucleus to modulate the expression of target genes through its association with transcription factors (TF). Recent studies conducted in endothelial cells have identified ALK1 as an additional TβRI. In contrast, TGFβ can activate ALK1, in complex with ALK5, leading to phosphorylation of Smad1/5. Moreover, ALK5-signalling and ALK1/ALK5-signalling have opposing functions whereby ALK5 inhibits proliferation and ALK1/ALK5 activates proliferation in endothelial cells. The decision for TGFβ to activate the ALK5- or ALK1/ALK5-mediated pathway is thought to depend on the expression levels, ratio, and functionality of these receptors on a given cell type.

ALK5 signalling in endothelial cells represents a unique mechanism for regulating TGFβ-mediated cellular responses.

Alternatively, TGFβ can signal through Smad-independent mechanisms, collectively termed the "non-Smad pathways" (38). One such pathway is involved in regulating epithelial-to-mesenchymal transition in polarized epithelial cells (39). Studies have shown that the TGFβ receptor complex at the tight junctions is associated with the polarity regulator, partitioning defective 6 (Par6) (40). Upon TGFβ binding, TβRII phosphorylates Par6, which in turn activates the E3 ubiquitin ligase Smurf1 thereby promoting the ubquitination and subsequent degradation of the GTPase, RhoA. Degradation of RhoA promotes the disassembly of the actin cytoskeleton leading to the dissolution of tight junctions, which is one of the hallmarks of epithelial-to-mesenchymal transition (40). Interestingly, CERs have recently been demonstrated to induce the formation of an apicolateral polarity complex consisting of PKCζ, Par6, and the small GTPase Cdc42 (41). This ceramide-induced complex was thought to mediate morphogenesis in primitive ectoderm cells. Yet, the cooperation between TGFβs and CERs in regulating cell polarity remains to be explored.

Additionally, TGFβ has been shown to activate mitogen-activated protein kinases (MAPKs) including the ERKs, the p38 MAPKs, and the c-Jun amino-terminal kinases (JNKs) (38). Typically, the ERK pathway is activated through growth factor binding to receptor-tyrosine kinases. Despite TRβI and II being serine/threonine kinases, TβRII has been shown to undergo autophosphorylation of three specific tyrosine residues namely, Y259, Y336, and Y424, albeit at a much lower level than on serine and threonine residue (42). These phosphorylated tyrosine residues serve as docking sites for the adaptor proteins growth factor receptor binding protein 2 (Grb2) and Src homology domain 2 containing protein, which are involved in ERK activation

(38). As mentioned, activated ERK1/2 has been shown to phosphorylate SPHK1 thereby inducing its translocation to the cell membrane (2). This represents an additional link between TGFβ and sphingolipid signalling. Lastly, ALK5 has been shown to interact with the E3 ubiquitin ligase TRAF6, which upon ligand binding induces its polyubquitination (38). Polyubiquitinated TRAF6 then serves as a scaffold protein for TGFβ activated kinase 1, which subsequently activates JNK/p38. Following activation, JNK and p38 work in conjunction with Smad proteins to regulate apoptosis and epithelial to mesenchymal transition (39).

Evidently, TGFβs and bioactive sphingolipids mediate a variety of similar cell fate events thereby sharing an overlap in biological function. This overlap in function may relate to both the ability of TGFβs to regulate sphingolipid signalling as well as the ability of lipids to transactivate TGFβ signalling cascades. The tight regulation of cell fate events may play a critical role in early placental development. In the present study, I aim to investigate the relationship between TGFβs and sphingolipids in the human placenta.

1.3 Human Placental Development

The human placenta is a specialized organ of pregnancy that supports the growth and development of the fetus (43). During pregnancy its primary function is to create a fetal-maternal interface that is capable of performing nutrient and gas exchange via the maternal blood supply to the developing fetus. Specifically, the placenta provides oxygen, water, sugars, amino acids, lipids, vitamins, minerals and other nutrients to the fetus while removing waste products. It also creates a selective physical barrier that protects the fetus against xenobiotic molecules, infections, and maternal diseases, while supplying the fetus with maternal immunoglobulin G antibodies as a form of passive immunity. Lastly, it functions as an endocrine organ that secretes

hormones into the maternal and fetal circulations to maintain pregnancy, promote fetal growth, and aid in parturition.

The mature placenta is composed of fetal tissue derived from the chorionic sac, and maternal uterine tissue that comes from the gravid endometrium (44). The fetal side of the placenta, termed the chorionic plate, contains fetal chorionic blood vessels that branch off from the umbilical vessels of the placenta. The maternal interface, termed the basal plate, is the site of contact of the placenta with the uterine arteries and veins. The space between the chorionic and basal plates is called the intervillous space, which is densely packed with villous structures containing fetal blood vessels to permit sufficient gas and nutrient exchange. Chorionic villi are lined with a specialized, multinucleated layer of epithelial cells called the syncytium, which is the external facing layer of the fetal membrane. However, the fetal membrane is composed of three additional cell layers, including a layer of mitotically active cytotrophoblast cells, placental mesenchyme, and lastly the endothelial lining fetal capillaries **(Figure 1.6a)** (43). When maternal blood enters the intervillous space via the maternal spiral arteries, oxygen, nutrients, and waste are exchanged at the syncytium of chorionic villi. Then, maternal blood carrying fetal waste products is carried away via the endometrial veins. Meanwhile, fetal blood enriched with oxygen and nutrients return to the fetus via the chorionic veins and umbilical vein. Around 20 weeks of gestation, the cytotrophoblast cell layer of placental villi becomes discontinuous (43). This causes the membrane to become thinner, allowing the maternal and fetal blood to come into close proximity.

During early placentation, cytotrophoblast cells function as mitotically active progenitor cells, which either fuse to form and replenish the overlaying syncytiotrophoblast, or acquire an invasive/migratory phenotype to anchor the villus to the maternal decidua (45). Specifically,

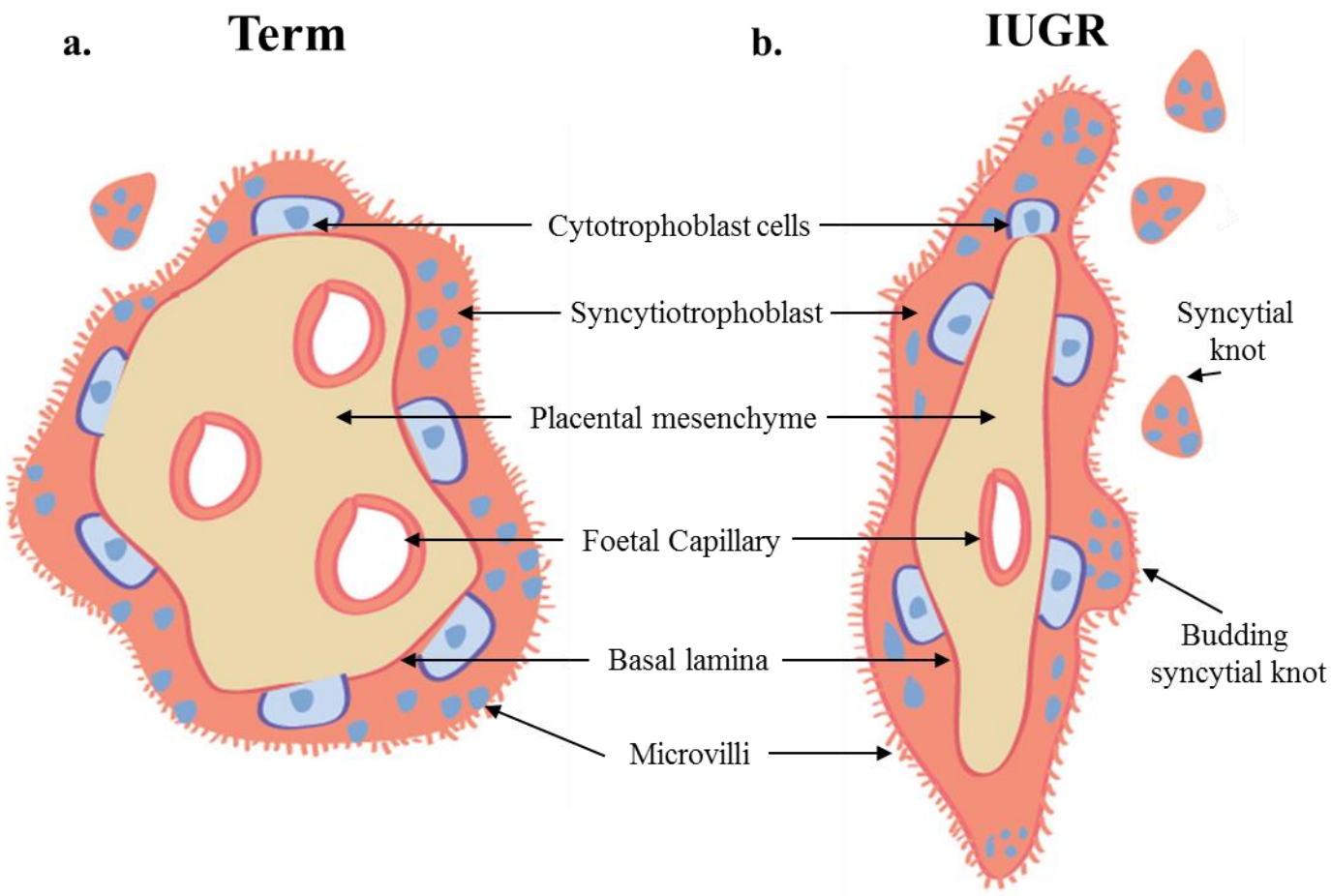

Figure 1.6 Diagram of the cross-section of a human floating chorionic villus from normal term and IUGR placentae

(a) The chorionic villi are the functional units of the placenta. They are predominately composed of proliferative cytotrophoblast cells (blue) and a terminally differentiated syncytiotrophoblast (pink). Within the villus is the placental mesenchyme, consisting of fibroblasts (yellow), and the foetal capillaries lined by endothelial cells. The syncytiotrophoblast is a multi-nucleated layer that performs critical placental functions such as nutrient and gas exchange as well as hormone production. It is continuously shed throughout pregnancy and replenished by the fusion and differentiation of the underlying cytotrophoblast cells. **(b)** Placental villi from women with intrauterine growth restriction (IUGR) are typically thinner, elongated, and hypovascularized. They are also characterized by accelerated rates of trophoblast cell turnover resulting in the increased formation and extrusion of syncytial knots into maternal circulation.

cytotrophoblast cells at the tips of anchoring villi acquire this invasive phenotype allowing them to penetrate into the syncytiotrophoblast thereby forming columns of extravillous trophoblast cells (EVTs) (43). EVTs continue to invade the decidua and remodel the maternal spiral arteries by replacing maternal endothelial cells resident in maternal spiral arteries and by becoming endovascular trophoblasts that repress maternal vasomotor responses and dilate uterine arterioles. EVTs can also penetrate the interstitial space to recruit arterioles and promote the expansion of the placental site. The phenotypic switch from epithelial-like cells to mesenchymal like-cells is dependent on the dissolution of tight junctions and the secretion of factors that degrade the decidual extracellular matrix, including type IV collagenase, matrix metalloproteinases, cathepsins B, and urokinase-type plasminogen activator (45). These events are under the control of autocrine and paracrine factors expressed at the fetal-maternal interface such as growth factors, and particularly TGFβs, which play a pivotal role in inhibiting invasion (46).

As alluded to earlier non-invasive cytotrophoblast cells are highly proliferative and serve to replenish the syncytium, which is responsible for performing nutrient and gas exchange, and secreting placental hormones (44). This requires the fusion of cytotrophoblast cells, an additional differentiation event needed for proper placentation. Since the syncytium is composed of terminally differentiated cells, aging content and condensed nuclei are continuously shed throughout pregnancy as membrane-enclosed vesicles called syncytial knots (SKs) (47). Excessive shedding of SK into the maternal circulation is a hallmark of placental pathologies such as preeclampsia (PE) and intrauterine growth restriction (IUGR) (48). Hence, the regulation of trophoblast cell proliferation, fusion, and death is critical to the maintenance of the syncytium.

1.3.1 TGFβs and placentation

TGFβ superfamily members are abundantly and dynamically expressed in the human placenta, where they play key roles in mediating trophoblast cell proliferation, differentiation, fusion, and apoptosis (46). Specifically, TGFβ2 is produced at the feto-maternal interface and regulates trophoblast cell invasion into the uterus (49). In contrast, TGFβ1 and β3 are predominately expressed by placental villi and may play a role in sustaining the syncytium in a non-proliferative state while inhibiting trophoblast cell differentiation (29,45,50).

Although TGFβ1 and β2 remain constant throughout gestation, TGFβ3 displays a unique temporal pattern of expression. Prior to 10 weeks of gestation, placental development occurs in a relatively hypoxic environment (~2%-3% O_2) likely due to an upregulation of transcriptional regulator HIF1, which turns on a variety of oxygen responsive genes (51). Interestingly, HIF1 expression is associated with increased TGFβ3 expression in villous explants, which is consistent with promoter analysis showing that HIF1A transactivates TGFβ3 (17,51,52). Under these conditions, TGFβ3 has been shown to play a key role in inhibiting extravillous trophoblast cell differentiation towards an invasive phenotype (17). Around 10-12 weeks of gestation the oxygen tension rises to 8-10% thereby reducing HIF stability and decreasing TGFβ3 expression (51,52). As a result, EVTs are able to invade the uterine wall (90/104). Hence, TGFβ3 specifically plays a determining role in regulating trophoblast cell differentiation during early placental development (52).

1.3.2 Sphingolipids and placentation

Recently, sphingolipid biosynthesis and metabolism have been implicated in altering the biochemical and morphological aspects of trophoblast differentiation and syncytialization (6,53). Using *In vitro* studies, Singh *et al.* showed that endogenous levels of CER increased in primary

isolated term cytotrophoblast cells at the onset of trophoblast differentiation, and decreased upon spontaneous syncytialization in culture (6). This decline was accompanied by a concomitant increase in the expression of CER metabolizing enzyme, AC (6). The same group later reported decreased intracellular sphingosine and S1P during trophoblast syncytialization (53). Notably, treatment of primary isolated cytotrophoblast cells with exogenous sphingosine or an inhibitor of SPHK1 also inhibited trophoblast differentiation as measured by decreased levels of human chorionic gonadotropin (hCG) secretion (53). Together these findings suggest that sphingolipids may also play a key role during early placental development.

Additionally, SPHK1-mediated production of S1P has been implicated in the growth and differentiation of uterine tissues during pregnancy (8). Jeng *et al.* demonstrated a 30-fold increase in SPHK1 expression in the glandular epithelium, vasculature, and myometrium of pregnant rats in response to rising progesterone levels (54). They also showed that overexpressing human SPHK1 in the rat myometrial/leiomyoma cell line, ELT3, induced cell cycle regulator cyclin D1 expression, thereby increasing rates of proliferation. In contrast deficiencies in SPHK1 expression has been shown to cause defective decidualization and poor blood vessel formation, culminating in pregnancy loss (7). *Sphk1* knockouts were further characterized by SPH accumulation accompanied by increased decidual cell death, reduced proliferation of stromal cells, and leaky decidual blood vessels (7). Similar to rats, pregnant sheep express high levels of SPHK1 in the uterine vasculature, and in trophectoderm cells and epithelial syncytium (55). These findings stress the importance of SPHK1 and S1P signalling in uterine/placental angiogenesis and development.

Altered sphingolipid metabolism has also been detected in preeclampsia (PE), a pregnancy-related disorder that is clinically diagnosed by the sudden onset of maternal

hypertension (systolic: ≥140mmHg diastolic: ≥90mmHg) (56). For instance, increased levels of pro-death CERs and SPH have been detected in the Wharton's jelly of preeclamptic newborns, and may contribute to altered umbilical cord composition typical of PE (57). Additionally, recent observations by lipidomics analysis of human placental syncytiotrophoblast microvesicles (STMs) revealed a 3-fold increase in the sphingomyelin (SM) content of STMs from the preeclamptic patient group relative to the healthy age-matched control patient group (58). Lastly, our lab has detected impaired AC and ASM expression leading to an accumulation of CERs and SM in preeclamptic placentae (Melland-Smith, M., manuscript under consideration). Collectively, these findings support a role for bioactive sphingolipids in the development of placental pathologies such as PE.

1.3.3 Intrauterine Growth Restriction (IUGR)

Intrauterine growth restriction (IUGR) is defined as a foetus that fails to achieve its inherent growth potential and exhibits a birth weight below the 10th percentile for gestational age (GA) **(Figure 1.7)** (59). IUGR affects approximately 4 to 7% of births, and is associated with an estimated 6- to 10-fold increased risk of perinatal mortality (60-62). IUGR is clinically diagnosed by determining the GA of the foetus by crown-rump length, then tracking fetal size and growth by serial ultrasonic biometry (59). Doppler ultrasound of the umbilical artery is also used to identify a compromised foetus by assessing fetal-placental circulation (63).

During pregnancy IUGR can develop as the result of maternal insults, such as smoking, substance abuse, poor nutrition, and high altitude, and as the result of fetal origins, which include chromosomal abnormalities and infection **(Figure 1.7)** (64). However, a higher percentage of severe IUGR cases (birth weight below the 5th percentile for GA) are linked to placental

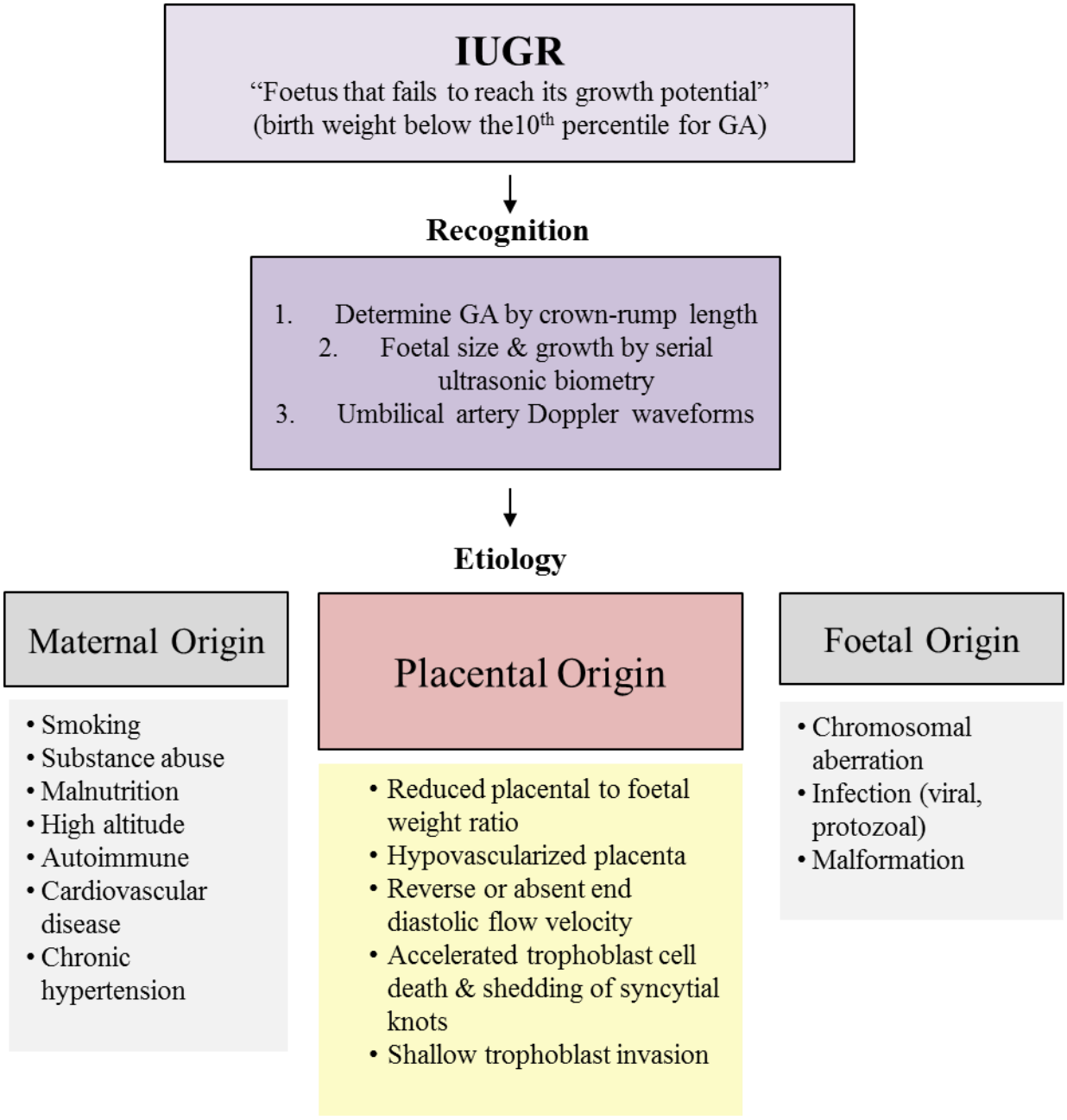

Figure 1.7 Schematic outlining the diagnosis and causes of IUGR

IUGR is defined by the American College of Obstetrics and Gynaecology (ACOG) as a foetus that fails to achieve its growth potential. Typically, an infant with a birth weight that is less than the 10th percentile for gestational age (GA) is considered to be IUGR. There are three main etiologies of IUGR including maternal conditions, foetal conditions, and placental conditions; however, the majority of cases are due to placental insufficiency.

insufficiency caused by disruptions in the balance between trophoblast cell survival and death **(Figure 1.6b)** (61,65). Specifically, IUGR is associated with accelerated rates of trophoblast cell differentiation and turnover, impaired trophoblast invasion, and inadequate vascular remodelling, leading to poor uteroplacental perfusion that impinges on proper foetal development (51,65) **(Figure 1.7)**. Altered trophoblast cell fate events typical of IUGR are, in part, caused by sustained placental hypoxia and high TGFβ3 expression levels, which inhibit trophoblast cell differentiation along the invasive pathway (17,51,60); however, the contribution of bioactive sphingolipid mediators to the pathogenesis of this disorder remains elusive.

1.4 Rationale, Hypothesis, and Objective

Disruption of sphingolipid metabolism contributes to the onset of a variety of human pathologies (3). This is primarily due to the fact that sphingolipids function as key bioactive mediators in several cell-signalling events. Importantly the balance between pro-death ceramide (CER) and sphingosine (SPH), and pro-survival sphingosine 1 phosphate (S1P) is tightly controlled by sphingolipid metabolizing enzymes such as acid ceramidase (AC) and sphingosine kinase 1 (SPHK1).

Early placental development requires the tight coordination of trophoblast cell proliferation, differentiation, and apoptosis, which is largely controlled by oxygen and growth factors, namely TGFβs. Recent evidence highlights a role for TGFβ1 in the regulation of CER and sphingolipid regulatory enzyme expression in human dermal and cardiac fibroblasts (15) (13). We have previously established the importance of altered TGFβ signalling in preeclampsia and intrauterine growth restriction (IUGR); and have recently found altered sphingolipid profiles in preeclamptic placentae. I now ***hypothesize*** that TGFβ1 and β3 play a role in regulating sphingolipid metabolism in the human placenta under physiological and pathological conditions. However no information is currently available on the role of TGFβs, specifically TGFβ3, in regulating the sphingolipid rheostat in the human placenta or its possible role in placental pathology. Hence, the ***objectives*** of my project were to 1) characterize the sphingolipid prolife and sphingolipid regulatory enzyme expression in IUGR, and 2) systematically decipher a role for TGFβ1 and β3 signalling in regulating sphingolipid regulatory enzyme expression in the human placenta and in IUGR.

Chapter 2

2 Materials and Methods

2.1 Placental tissue collection

Informed consent was obtained from all participants prior to tissue collection, which was performed by the Biobank of Mount Sinai Hosptial and by the Ospedale Infantile Regina Margherita (O.I.R.M) Sant'Anna Hospital, University of Turin, Italy, in accordance with the Institutions ethics' guidelines (Ethics guidelines of the University Of Toronto Faculty Of Medicine and the University Of Turin Faculty Of Medicine). Early gestation human placental tissues (5-8 weeks of gestation, n=12) were obtained from the elective termination of pregnancies by suction evacuation, or dilation and curettage. The gestational age was determined using the date of the last menstrual period and the first trimester ultrasound measurement of crown-rump length. Placental tissue obtained from intrauterine growth restricted (IUGR) pregnancies (n=33) were selected based on the American College of Obstetricians and Gynaecologists (ACOG) clinical and pathological criteria (59). All women were healthy non-smokers, having no signs of preeclampsia (PE), infection, or known causes of IUGR. The IUGR patient group was characterized by an average gestational age of 32 weeks, absent or reverse-end diastolic flow velocity of the umbilical artery, and a birth weight below the 5th percentile for gestational age. This group also exhibited normal maternal blood pressure of 128/85 (systolic/diastolic) and showed no signs of proteinuria suggesting that these IUGR cases were not superimposed with preeclampsia. Placental tissues collected from healthy, age-matched preterm deliveries (PTC) were included as controls. The PTC patient group delivered at an average gestational age of 33 weeks, exhibited normal Doppler and blood pressures (124/76),

and delivered with a fetal weight considered appropriate for gestational age (AGA). These women endured healthy pregnancies and showed no signs of placental dysfunction, abnormal fetal growth, or PE (PTC, n=27). Mean gestational age at delivery, fetal sex and weight, and other clinical parameters relevant to the health of the mother are summarized in Table 3.1. Tissue showing signs of damage (*i.e.*, calcification, necrosis, or ischemia) were excluded from sampling. Following delivery, samples were collected randomly from central and peripheral placental areas and immediately snap-frozen in liquid nitrogen for lipidomics, protein, and RNA analysis, or fixed in paraformaldehyde to be processed for immunohistochemical (IHC) or immunofluorescence (IF) analysis.

2.2 First trimester villous explant culture

First trimester human placental tissue (5-8 weeks gestation) obtained from the elective termination of pregnancies was stored in sterile, ice-cold phosphate-buffered saline (PBS) upon receipt and processed within 2 hours of collection. Tissue was washed in PBS and aseptically dissected under a microscope to remove decidual tissue and fetal membranes. Small sections of placental villi (~15-25 mg wet weight) were excised and cultured in 500μL of serum-free DMEM/F12 (GIBCO-BRL, Grand Island, New York, USA), supplemented with 10,000 units/ml of penicillin/streptomycin (pen/strep) in 24 well plates. Since early placental development (<10 weeks of gestation) occurs in a relatively hypoxic environment (~2-3% O_2), villous explants were maintained at 37°C in an atmosphere of 3% O_2/92% N_2/5% CO_2, which is considered normoxic for villous placentae of this gestational age. To establish the effect of TGFβ1 and β3 on the sphingolipid and regulatory enzyme profile, explants were treated overnight with 10 μM of SB431542 (Sigma-Aldrich Corp., St. Louis, MO, USA), a pharmacological inhibitor of activin receptor-like kinase 5 (ALK5) activity. In parallel, culture explants treated with vehicle,

dimethyl sulfoxide (DMSO) (Sigma-Aldrich Corp., St. Louis, MO. USA), were included as controls. Following overnight incubation, explants were collected in eppendorf tubes and snap frozen on dry ice. Samples designated for lipid extraction were sent directly to the Analytical Facility for Bioactive Molecules at the Hospital for Sick Children (Sickkids), Toronto, Ontario to be analyzed by high performance liquid chromatography (HPLC) linked to tandem mass spectrometry (MS/MS). Samples designated for protein extraction were snap-frozen in liquid nitrogen and stored at -80°C.

2.3 Choriocarcinoma cell culture

Human choriocarcinoma JEG3 cells (ATCC, Manassas, VA, USA) were cultured in 75 cm^2-flasks in complete Eagle's minimal essential medium (EMEM) (ATCC, Manassas, VA, USA) supplemented with 10% heat-inactivated fetal bovine serum (FBS) and 1% (10,000 units/ml) of pen/strep at 37°C in standard culture conditions (5% CO_2 in 95% air). Upon reaching confluency, cells were washed twice in PBS, trypsinized with 0.25% Trypsin-EDTA (Life technologies, Carlsbad, CA, USA), and passaged at a dilution of 1:5 into a new 75 cm^2-flask. For *in vitro* experiments, cells were stained with trypan blue and counted using a hematocytometer; on average, cell culture viability was ~95%. Cells were seeded at a density of 1.5 x 10^5 cells/well into 35 mm x 6-well plates (Life technologies, Carlsbad, CA, USA).

2.3.1 TGFβ1 and β3 treatments

TGFβ1 and β3 (R&D Systems, Minneapolis, MN, USA) were reconstituted in 4 mM HCl (aqueous) and 1mg/mL BSA solution to create a 10 μg/mL stock solution. JEG3 cells were seeded at a density of 1.5 x 10^5 cells/well into 6-well plates and maintained at 37°C under standard oxygen conditions. Upon reaching approximately 70% confluency, JEG3 cells were treated with TGFβ1 or TGFβ3 (1, 5, or 10 ng/ml in warm complete media) for 3, 8, and 24 hours.

Control wells were treated with the TGFβ vehicle (4 mM HCL/1mg/mL BSA solution) diluted similarly for the same time points. Following incubation, cells were collected on ice in either TRIzol (Life technologies, Carlsbad, CA, USA) for RNA extraction, RIPA buffer (150 mM NaCl, 50 mM Tris at pH 7.5, 1% NP-40) with a protease inhibitor cocktail (Roche, Indianapolis, IN, USA) for Western Blotting, or fixed in 3.7% paraformaldehyde for 15 minutes at room temperature to perform immunofluorescence staining.

2.3.2 Serum starvation assay

The effect of growth factors present in the cell culture media on sphingolipid regulatory enzyme expression was established by culturing JEG3 cells in low-serum EMEM supplemented with 1% FBS, 24 hours prior to TGFβ1 and β3 treatment. In parallel cultures, JEG3 cells were treated with TGFβ1 and β3 under standard culture conditions (10% FBS). Cells were collected on ice in RIPA buffer solution with protease inhibitor cocktail for Western blot analysis.

2.3.3 Pharmacological inhibitor studies

All pharmacological inhibitors were diluted in DMSO to generate a 10 mM stock concentration. JEG3 cells were then seeded at a density of 1.5×10^5 cells/well into 6-well plates and treated the next day with either 5 μM of SB431542 (ALK5 inhibitor), 10 μM of Dorsomorphin (Compound C) (ALK1 inhibitor) (Abcam, Cambridge, England, United Kingdom), 10 μM of U0126 (ERK inhibitor) (Sigma-Aldrich Corp., St. Louis, MO, USA), 10 μM of SB23906 (p38 inhibitor) (Sigma-Aldrich Corp., St. Louis, MO, USA) or 10 μM of SP600125 (JNK inhibitor) (Sigma-Aldrich Corp., St. Louis, MO, USA). Following a 1 hour incubation with individual inhibitors, JEG3 cells were treated with TGFβ1 or TGFβ3 (5 ng/ml) for 24 hours. Each experiment included two control wells treated with control vehicle, DMSO (Sigma-Aldrich Corp., St. Louis, MO, USA). Twenty-four hours later, cells were collected on ice

in RIPA buffer solution with protease inhibitor cocktail for Western blotting.

2.3.4 Transient transfection studies

Smad2 expression was knocked down in JEG3 cells using a Smad2 siRNA-containing plasmid kindly provided by Dr. Chun Peng (York University, Toronto). In short this construct was generated by cloning the published Smad2 siRNA sequence (UCUUUGUGCAGAGCCCCAAtt (66)) into the pSuper vector (Oligoengine, Seattle, WA, USA). To begin, JEG3 cells were plated at a density of 1.5 x 10^5 cells/well in 6-well plates and cultured for 24 hours in EMEM media supplemented with 10% FBS and 1% pen/strep at 37°C under standard culture conditions. At approximately 80% confluency cell culture media was replaced with pen/strep-free EMEM and cells were transfected with 1.0 μg of either control pSuper vector or the Smad2 siRNA-containing vector. Transfections were performed using Lipofectamine™ 2000 transfection reagent (Life Technologies, Carlsbad, CA, USA) according to the manufacturer's protocol. In detail, Lipofectamine™ 2000 (6 ml/well) was diluted in the appropriate amount of Opti-MEM® I Reduced Serum Medium (Life Technologies, Carlsbad, CA, USA) (250 μl/well) and incubated at room temperature for 5 minutes. Meanwhile, constructs were diluted in the appropriate volume of Opti-MEM® I Reduced Serum Medium (250 μl/well) to ensure 1.0 μg of plasmid DNA per well. After a 5 minute incubation period, the diluted constructs were combined with the diluted Lipofectamine™ 2000 and mixed by gentle inversion. To allow for complex formation, mixtures were left to incubate at room temperature for 20 minutes. During this time, culture medium was replaced with serum- and antibiotic-free medium. Once the incubation was complete, 500 μl of either pSuper-containing solution or siSmad2-continating solution were added to the designated wells. Following 6 hours of incubation with the transfection complex, the media was replaced with complete EMEM containing 10% FBS and 1% pen/strep. The next day, cells were treated with TGFβ1 (5 ng/ml),

TGFβ3 (5 ng/ml), or control vehicle for an additional 24 hours. Cells were then collected on ice in either TRIzol for RNA extraction or RIPA buffer solution with protease inhibitors for Western blotting.

2.4 Sphingolipid profiles by mass spectral analysis

Placental tissue from IUGR pregnancies and healthy age-matched controls were collected as previously described, and processed for lipid extraction and sphingolipidomics analysis at the Analytical Facility for Bioactive Molecules at Sickkids, Toronto, Ontario. The extraction procedure was performed on human villous explants treated with SB431542, or control vehicle DMSO, and JEG3 cells treated with TGFβ1 and β3 or control vehicle. Both tissue and cells were subjected to the Bligh and Dyer method of lipid extraction (67), described below in detail.

Extraction procedure- Twenty five mg of frozen tissue or 5 mg of cell lysate was lyophilized and then homogenized in 2 mL of (1:1) methanol/water. Next, samples were spiked with 10 ng of internal standards (C17 (d18:1/17:0) ceramide, (d17:1) sphingosine, (d17:1) sphingosine-1-phosphate (S1P), and 17:0 (d18:1/17:0) Sphingomyelin. Following addition of 2 mL of chloroform, samples were vortexed for 1 minute, kept on ice for a 10 minutes, then centrifuged at 1000xg for 5 minutes. Lipids were extracted by removing the chloroform layer and drying under a stream of nitrogen. To perform mass spectrometry (MS) analysis, samples were reconstituted in 100 µl of ethanol acidified with 0.2 µl of formic acid, and transferred to siliconized minivials.

HPLC and mass spectrometry- Reverse phase HPLC linked to tandem MS was done using an Agilent 1200 Series binary pump (Agilent Technologies Inc., Santa Clara, CA, USA) coupled to an API4000 triple-quadruple mass spectrometer (SCIEX, Concord, ON., Canada). Multiple Reaction Monitoring (MRM) mass transition parameters were first optimized by infusion of pure

standards (5 µl/min of 1 µg/ml). Reverse phase HPLC was done using a kinetex C18 Column (Phenomenex, Torrance, CA, USA), which had a mobile phase consisting of water/acetonitrile/methanol (2/1/1, v/v/v) and tetrahydrofuran/acetonitrole/methanol (2/1/1, v/v/v), both containing 0.05% formic acid. The HPLC gradient was injected with a flow of 400 µl/min as follows: initial conditions of 60:40 (A:B) were held for 4.5 minutes prior to injection, then an additional 2 minutes post injection, and ramped to 15:85 (A:B) over a period of 13 minutes. These conditions were held for 15 minutes, at which point the gradient returned to the initial conditions for 17 minutes. Sample injection volume ranged from 1 to 5 µl. The MS analysis was performed using positive electrospray ionization. The source temperature was 400°C with an ion spray voltage of 5000 V. Nitrogen was used as the Collision Induced Dissociation gas. MRM Mass Transitions and Chromatographic Retention Times were in accordance with previously published conditions (68). For quantitative analysis a separate standard curve was made for each analyte measured using MRM area ratios (analyte peak area/IS peak area). The results were calculated by plotting the sample area ratios against their respective analyte-specific standard curve (69).

2.5 RNA isolation and analysis

Total RNA was extracted from frozen placental tissue and choriocarinoma JEG3 cells using the TRIzol® (Life Technologies, Carlsbad, CA, USA) extraction method. Consistent with this method, cells were collected in 1 mL of TRIzol® reagent and stored overnight at -80°C. Tissue samples (50-100 mg) were thawed on ice and homogenized in 1 mL of TRIzol® reagent using a power homogenizer (Ultra-Turrax T25 basic, IKA, Wilmington, NC, USA). For every 1 mL of TRIzol® reagent, 200 µl of chloroform (Sigma-Aldrich Corp. St. Louis, MO, USA) were added to each sample. Samples were subsequently mixed for 15 seconds by inversion and

incubated on ice for an additional 30 minutes. Following this period, samples were centrifuged (4°C) at >12,000 x g for 15 minutes, and the supernatant was transferred to new eppendorf tubes. Next, 250 µl of isopropanol (Fisher Scientific, Fair Lawn, NJ, USA) were added to each sample and samples left to incubate on ice for 30 minutes. Again, samples were centrifuged (4°C) at 12,000 x g for 10 minutes and their supernatant discarded. The resulting pellet was then washed with 500 µl of 75% ethanol (diluted in DEPC water) and centrifuged (4°C) at >7500 x g for 5 minutes. The supernatant was aspirated and the pellet was left to dry at room temperature prior to suspension in 20 µl of DEPC water. Following isolation, RNA concentration was determined using a NanoDrop 1000 Spectrophotometer (Thermo Scientific, Wilmington, DE, USA). RNA quality and integrity were qualitatively evaluated by running samples on a 1% denaturing agarose gel. All samples were treated with RNase-free DNase I (Fermentas Inc, Burlington, ON) for 30 minutes at 37°C to eliminate genomic DNA contamination, and then heated at 65°C for 10 minutes in the presence of EDTA. Next, 1 µg of RNA from each sample was subjected to reverse transcription using random hexamers (Applied Biosystems, Foster City, CA, USA) in the PTC-100™ Thermal Cycler (MJ Research, Inc., Waltham, MA, USA). Upon completion, template-specific cDNA was amplified by 40 cycles of semi-quantitative Real-time PCR (5 min at 95°C, cycle: 30s at 95°C, 30s at 55°C and 1.5 min at 72°C) using the DNA Engine Opticon 2 System (MJ Research, Waltham, MA, USA) as previously described (70). Taqman primers and probe for AC (encoded by *ASAH1*), SPHK1 (encoded by *SPHK1*), ASM (encoded by *SMPD1*), Smad2 (encoded by *SMAD2*) and 18S (Assay-on-Demand™, Applied Biosystems, Foster City, CA, USA) were used in the presence of Taqman® Universal PCR Master Mix (Applied Biosystems, Foster City, CA, USA). Data were normalized against 18S ribosomal RNA using the $2^{-\Delta\Delta Ct}$ formula as previously described (70).

2.6 Antibodies and HRP substrates

Antibodies against AC (T-20, goat [IHC: 1:200, IF 1:250, WB 1:350]), ASM (H-181 rabbit l [IF 1:200, WB 1:350]), TGFβ RI/ALK5 (goat [IF: 1:350, WB: 1:500]), pSmad1 (Ser 463/465) (goat [WB: 1:500]), ZO1 (goat [IF: 1:100 WB: 1:350]) and β-actin (I-19, goat [WB 1:1000]) were purchased from Santa Cruz Biotechnology, Santa Cruz, CA. Rabbit anti-pSmad2 (S465/467) [WB 1:1000, IF:1:250], total Smad2 (86F7 rabbit monoclonal [WB 1:1000]), and total Smad1 ((D5907) XPR rabbit monoclonal [WB 1:1000]) antibodies were obtained from Cell Signalling Technology, Inc. Beverly, MA. SPHK1 (rabbit [IF: 1:500, WB 1:1000]) antibody and competing peptide were purchased from Abcam (Cambridge, England, UK). The secondary antibodies were used at a dilution of 1:2000 and include: horseradish peroxidase (HRP)-conjugated donkey anti-goat, goat anti-rabbit, and biotinylated donkey anti-goat from Santa Cruz Biotechnology, Santa Cruz, CA, USA; and Alexa Fluor® 594: donkey anti-goat/-rabbit, and Alexa Fluor® 488: donkey anti-goat/-rabbit [IF 1:200] from Life technologies, Carlsbad, CA, USA.

2.7 Western blot analysis

Western blotting was performed using placental tissue lysates from IUGR and PTC placentae, first trimester villous explants or JEG3 cell lysates following the various experimental hindrances. For whole placental tissue, protein extraction was carried out by crushing frozen chunks of tissue in liquid nitrogen using a mortar and pestle, and then homogenizing with a homogenizer (Ultra-Turrax T25 basic, IKA, Wilmington, NC, USA) in 1ml of RIPA with a protease and phosphatase inhibitor cocktail. For villous explants, tissue was thawed and digested in 50-100 µl of RIPA buffer with a protease inhibitor cocktail, followed by homogenization on ice with a glass pestle (Wilmad, Vineland, NJ). Samples were then vortexed three times for 5

seconds each, and left to incubate in RIPA for 1 hour on ice. In contrast, JEG3 cell lysates were obtained by collection in RIPA buffer containing a protease inhibitor cocktail, then centrifuging (4°C) at max speed (16,300 x g) for 10 minutes. Protein concentrations for tissue and cell lysates were determined using a Bradford assay (Bio-Rad Laboratories, Hercules, CA., USA).

Either 50 μg of total protein from placental tissue or 30 μg of total protein from JEG3 cell lysates were run on a 10-15% SDS-PAGE acrylamide gel in running buffer solution consisting of 25 mM Tris base, 192 mM glycine, and 0.1% sodium dodecylsulfate (SDS) at 120 volts. Once sufficiently separated, proteins were transferred from the gel to a methanol-hydrated polyvinylidene fluoride (PVDF) membrane for 1 hour and 30 minutes in ice-cold transfer buffer (25 mM Tris base, 192 mM glycine and 20% methanol). Following transfer, PVDF membranes were incubated in 5% nonfat dry milk in tris-buffered saline solution (20 mM Tris-Cl and 136 mM of sodium chloride) containing 0.1% Tween-20 (TBST) for 1 hour at room temperature to block non-specific binding. After blocking, membranes were probed at 4°C overnight with primary antibody against the protein of interest. All primary antibodies were diluted in the appropriate volume of 5% nonfat milk in TBST to achieve the aforementioned dilutions. The next day, membranes were washed in TBST for three, 10-minute washes, and then incubated with secondary HRP-conjugated polyclonal antibody against the primary antibody for 1 hour at room temperature. All secondary antibodies were diluted in the appropriate volume of 5% non-fat milk in TBST to achieve a dilution of 1:2000. After incubation, membranes were washed for 3, 10-minute washes in TBST. To develop blots, membranes were incubated in 1 mL of chemiluminescence ECL-plus reagent (PerkinElmer Inc., Waltham, MA, USA) at room temperature and then exposed to film (GE Healthcare Limited, Pollards Wood, Buckinghamshire, UK). To confirm equal protein loading, gels were re-probed for β-actin by first washing blots for 1 hour with stripping buffer (0.2 M glycine, ddH2O, pH=2.2), followed by

blocking the membrane in 5% nonfat dry milk in TBST for 1 hour, and then incubating blots in a 1:1000 dilution of the primary antibody β-actin to 5% nonfat dry milk in TBST 4°C overnight. To validate the AC and SPHK1 antibodies, samples were run in duplicate under the same conditions and the membrane was then cut in half. After blocking, one half of the membrane was incubated with primary antibody and the other half was incubated with primary and competing peptide in a one-to-five ratio. All blots were processed for developing as previously described. For protein quantification purposes, bands of interest were analyzed by scanning developed blots using a CanoScanLiDE20 image scanner (Canon Canada Inc. Mississauga, ON). To quantify proteins of interest, densitometry was performed on Western blots using Image Quant 5.0 software (Molecular Dynamics, Piscataway, NJ, USA). Protein expression was normalized to the housekeeping gene, β-actin.

2.8 Immunofluorescence staining

Immunofluorescence staining was performed on placental tissue and JEG3 cells according to a protocol previously described (71). Placental tissues from IUGR, age-matched PTC, and TC were fixed in 3.7% paraformaldehyde and then embedded in paraffin. Paraffin-embedded issue was then cut into 5μm thick sections and mounted on glass microscope slides. Before immunofluorescence staining, every 20^{th} section of tissue was stained with haematoxylin and eosin in order to assess the quality of the tissue and to select the most representative sections. Intact sections were next deparaffinized in xylene followed by rehydration using a descending ethanol series diluted in ddH_2O (100%, 95%, 90%, 85%, 70%, and 50%). Antigen retrieval was carried out in 10mM sodium citrate (pH 6.0) by placing slides in the microwave for 5 minutes, then removing and keeping slides at 95-99°C for 15 minutes. Next, slides were placed back in the microwave for 3 minutes followed by a 30 minute cool down. To quench the autofluoresence

of red blood cells, slides were treated with Sudan Black (0.3% sudan black in 70% ethanol) for 30 minutes, then rinsed with PBS for three 5-minute washes.

JEG3 cells were seeded onto glass cover slips previously sterilized by UV light, and were fixed in 3.7% paraformaldehyde diluted in media for 15 minutes at room temperature. Following fixation, cells were washed in PBS for three 5-minute washes. Cells were then permeabilized with 0.2% Triton X-100 (Bishop Canada Inc., Burlington, ON) in PBS on a gentle rotator and washed 3 times again in PBS.

To prevent nonspecific binding, cells/tissue sections were incubated for 1 hour at room temperature with 5% normal horse serum diluted in PBS. Cells/sections were then probed for the enzymes of interest by incubating in primary antibody diluted in 5% blocking serum and antibody diluent (0.4% sodium azide, 0.625% gelatin in PBS filtered with 0.22mm syringe-driven filter) in a 1:1 ratio, at 4°C overnight. The following primary antibody dilutions were used: Goat polyclonal anti-human AC at 1:200; rabbit polyclonal anti-human ZO1 at 1:100; rabbit polyclonal anti-human SPHK1 at 1:100; goat polyclonal anti-human ALK5 at 1:300; and rabbit polyclonal anti-human pSmad2 at 1:100. Instead of primary antibody, negative control slides were incubated with equal concentrations of rabbit or goat IgG diluted in a 1:1 ratio of 5% blocking serum and antibody diluent. The next day, slides were washed 3 times for 8 minutes in PBS and incubated with an Alexa fluorochrome-conjugated secondary antibody against the IgG of the primary antibody at a 200-fold dilution (Alexa Fluor® 594: donkey anti- goat/-rabbit and Alexa Fluor® 488: donkey anti- goat/-rabbit, Life Technologies, Carlsbad, CA, USA) for 1 hour at room temperature. From this point onwards, slides were covered in aluminum foil to prevent light from affecting the fluorophore. After incubation with the secondary antibody, slides were washed 3 times for 8 minutes in PBS. For chromatin visualization, sections/cells were treated

with DAPI (4',6-diamino-2-phenylindole) for 7 minutes at room temperature. To mount, a 20µL drop of mounting solution (50% glycerol diluted in PBS) was placed at the center of each section followed by a cover slip, which was then sealed with nail polish. For cells, tweezers were used to lift the cover slips and place them onto glass microscope slides followed by sealing with nail polish. Fluorescence images were viewed and captured using the DeltaVision Deconvolution microscopy with z-stacking (Applied Precision, LLC, Issaquah, WA, USA).

2.9 Immunohistochemical analysis

Three samples of IUGR and preterm control placentae respectively were selected for immunohistochemical (IHC) analysis by visualizing H&E stained sections under a microscope, verifying the quality and morphological features of the tissue. The protocol that was followed for IHC was previously described (17). Briefly, placental tissues embedded in paraffin were sectioned and mounted on glass slides, dewaxed in xylene, and rehydrated in descending ethanol gradient as described above. Antigen retrieval was done by heating in 10 mM sodium citrate solution (pH 6.0), similar to the protocol described above. Endogenous peroxidase was quenched with 3% (v/v) hydrogen peroxide in PBS for 30 minutes at room temperature. Slides were next washed in PBS for three 10-minute washes. To block nonspecific binding, slides were placed in a moist chamber and incubated for an hour at room temperature in 150 µl/slide of blocking solution (5% normal horse serum in PBS). Slides were then incubated overnight at 4°C with anti-AC antibody diluted to 1:200 or anti-SPHK1 antibody diluted to 1:50 in blocking solution. For negative controls, primary antibody was omitted and replaced by an equal concentration of goat or rabbit IgG in blocking solution. Slides were next washed in PBS three times for 10 minutes each, and then exposed to biotinylated secondary antibody (1:400, donkey anti-goat/anti-rabbit) for 1 hour at room temperature. Following three additional washes in PBS, slides were placed

into a moist chamber and an avidin biotin complex (Vector Laboratories, Burlingame, CA, USA) was applied for 1 hour at room temperature. After the secondary antibody was washed away, positive staining was detected using diaminobenzidine chromogen, which was left on for ~10 minutes or until sufficient staining intensity was observed. For nuclear detection, slides were submerged in hematoxylin for 30 seconds then washed under tap water for 10 minutes. To get rid of background and improve contrast, slides were dipped in acid ethanol (70% EtOH supplemented with 250 μl of concentrated HCl) for 1 second then run under tap water for an additional 10 minutes. Dehydration was performed using an ethanol gradient ending in two 5-minute incubations in xylene. Slides were mounted by applying a drop of mounting solution (Vectashield®, Vector Laboratories, Inc., Burlington, CA, USA) onto the tissue section and placing a glass cover slide on top of the section. Images were captured using bright field microscopy (Qimaging Micropublisher 5.0 RTV, Leica, Solms, Germany) at 20 and 40 time magnifications, and analyzed using QcapturePro 6.0 software.

2.10 SPHK1 enzyme activity analysis

SPHK1 activity was assessed in tissue lysates from IUGR and PTC placentae, villous explants treated with or without SB431542, and TGFβ-treated JEG3 cells using an Echelon SPHK1 Assay Kit (K-3500) (Echelon Bioscience, Salt Lake City, UT) according to the manufacturer's protocol. In brief, 50 μg of protein from placental tissues or 30 μg of protein from JEG3 cell lysates were incubated in reaction buffer, 100 mM sphingosine and 10 mM ATP (adenosine-triphosphate) for 2 hours at room temperature. To stop the kinase reaction, a luminescence attached ATP detector was added. SPHK1 activity was analyzed using a 96-well microtiter plate reader (Tecan Infinite M200). All samples were prepared in duplicate. Samples showing less luminescence were indicative of increased SPHK1 activity (ATP digestion)

whereas samples showing more signal had lower activity. The enzyme activity was therefore calculated as a ratio of the average signal for IUGR samples relative to PTC samples. Villous explants and JEG3 cells did not produce a signal and were therefore omitted from analysis.

2.11 Statistical analysis

Statistical analysis was performed using GraphPad Prism 4 software (San Diego, CA, USA). For comparison of 2 groups an unpaired t-test was used with or without Welch's correction, where applicable. For comparison between multiple groups, one-way analysis of variance (ANOVA) with post-hoc Student-Newman-Keuls test was performed or two-way ANOVA with post-hoc Bonferroni test, where applicable. Statistical significance was defined as $p<0.05$ and results are expressed as the mean ± S.E.M.

Chapter 3

3 Results

Emerging evidence highlights a role for sphingolipids and their metabolites as key bioactive mediators in cell signalling events (4). Altered sphingolipid metabolism is found in a variety of human pathologies including genetic disorders, such as Farber disease (72) and Niemann-Pick disease (73), diabetes (74), cardiovascular disease (3), Alzheimer's (75), and cancer (5,72,76). Intrauterine growth restriction is a pregnancy-related disorder that complicates 4 -7% of all pregnancies, and is defined as failure of the foetus to achieve its inherent growth potential (59). The placenta plays an important role in the pathogenesis of IUGR, which is often accompanied by altered trophoblast cell death and turnover, impaired trophoblast invasion, and inadequate vascular remodelling leading to poor uteroplacental perfusion (47,77). At present, the contribution of sphingolipid metabolism to human placental development and IUGR remains to be established.

3.1 CER metabolism is disrupted in IUGR pregnancies

Recent advances in the field of lipidomics have facilitated the assessment of the complete sphingolipid profile within a tissue or whole organ by HPLC linked to tandem mass spectrometry. Hence, I first examined the sphingolipid profile in placentae from IUGR pregnancies (<10th percentile for gestational age) with no signs of hypertension or other clinical manifestations associated with PE. Placentae from age-matched pre-term deliveries (PTC) with no signs of placental pathology or infection were used as controls. The characteristics of the study population are summarized in **Table 1**. Lipidomics analyses by HPLC-MS/MS revealed significant decreases in ceramide species C:18, C:20, and C:24 in IUGR placentae relative to PTC placentae **(Figure 3.1).**

Table 3.1 Clinical features of the study population.

Criteria	Age-matched Pre-term controls (n=27)	IUGR (n=33)
Mean gestational age at delivery (range in weeks)	33.4 ± 4.8 (25-33) (mean ± SEM)	31.9 ± 1.6 (28-33) (mean ± SEM)
Mean blood pressure (mmHg)	Systolic: 123.9 ± 25.3 Diastolic: 76.4 ± 16.8 (mean ± SEM)	Systolic: 127.9 ± 20.9 Diastolic: 85.1 ± 11.9 (mean ± SEM)
Proteinuria (g/24 h)	Absent	Absent
Mean fetal weight (g)	AGA: 2326.5 ± 1019.1 (mean ± SEM)	IUGR: 1229.9 ± 436.9 (mean ± SEM) <5th percentile for GA
A/REDF (% of women)	0	100
Fetal Sex	Males=69% Females=31%	Males=38% Females=62%
Mode of Delivery	CS 62% VD 38%	CS 100%

Abbreviations: IUGR: Intrauterine growth restriction; AGA: Appropriate for gestational age; A/REDF: Absent or reverse end diastolic flow of the umbilical arteries; CS: Caesarean section delivery; VD: Vaginal delivery.

Tissue ceramide levels are tightly regulated by a balance between their rates of synthesis and breakdown, which is highly dependent on the activity of specific enzymes. Importantly, acid ceramidase (AC) is responsible for CER processing into sphingosine and free fatty acids (10). Since I observed reduced CER levels in IUGR, I next examined *ASAH1* mRNA levels and AC protein levels in IUGR placentae. Quantitative PCR analysis revealed no changes in *ASAH1* mRNA expression between IUGR and PTC placentae (IUGR: 0.73 ± 0.097 fold change *vs*. PTC: 1.0 ± 0.121, $p>0.05$) **(Figure 3.2a)**. AC is synthesized as a 55 kDa precursor protein that undergoes autoproteolytic cleavage in the lysosome, producing a 53 kDa dimeric active form of the enzyme **(Figure 1.4)** (78). Active AC consists of two covalently bonded subunits: 1) 13 kDa α-subunit and 2) the 40 kDa glycosylated β-subunit (79). Western blot analysis of human placental lysates identified AC as a band with an estimated molecular mass between 35 kDa and 55 kDa, which should correspond to the 40 kDa glycosylated β-subunit of the active enzyme (79,80) **(Figure 3.2b)**. The 13 kDa α-subunit was not detected. To validate the specificity of the AC antibody, I preincubated with a commercially available blocking peptide, which competed for the 40 kDa band but left a nonspecific band at 55 kDa **(Figure 3.2b)**. In agreement with enhanced CER turnover in IUGR, I found increased AC protein levels in IUGR placentae relative to PTC placentae (IUGR: 2.24 ± 0.339 fold increase *vs.* PTC: 1.0 ± 0.155, $p=0.006$) **(Figure 3.2c)**.

I next examined the spatial distribution of AC in placentae by immunohistochemical (IHC) analysis. In line with the protein data, IHC revealed strong positive immunoreactivity for AC expression primarily restricted to the trophoblast layer of placental villi from IUGR pregnancies as compared to low staining observed in PTC sections **(Figure 3.3)**. Notably, IUGR sections were characterized by an increased number of forming and shed syncytial knots, which expressed high levels of AC. No signal was observed in the negative control (normal goat IgG),

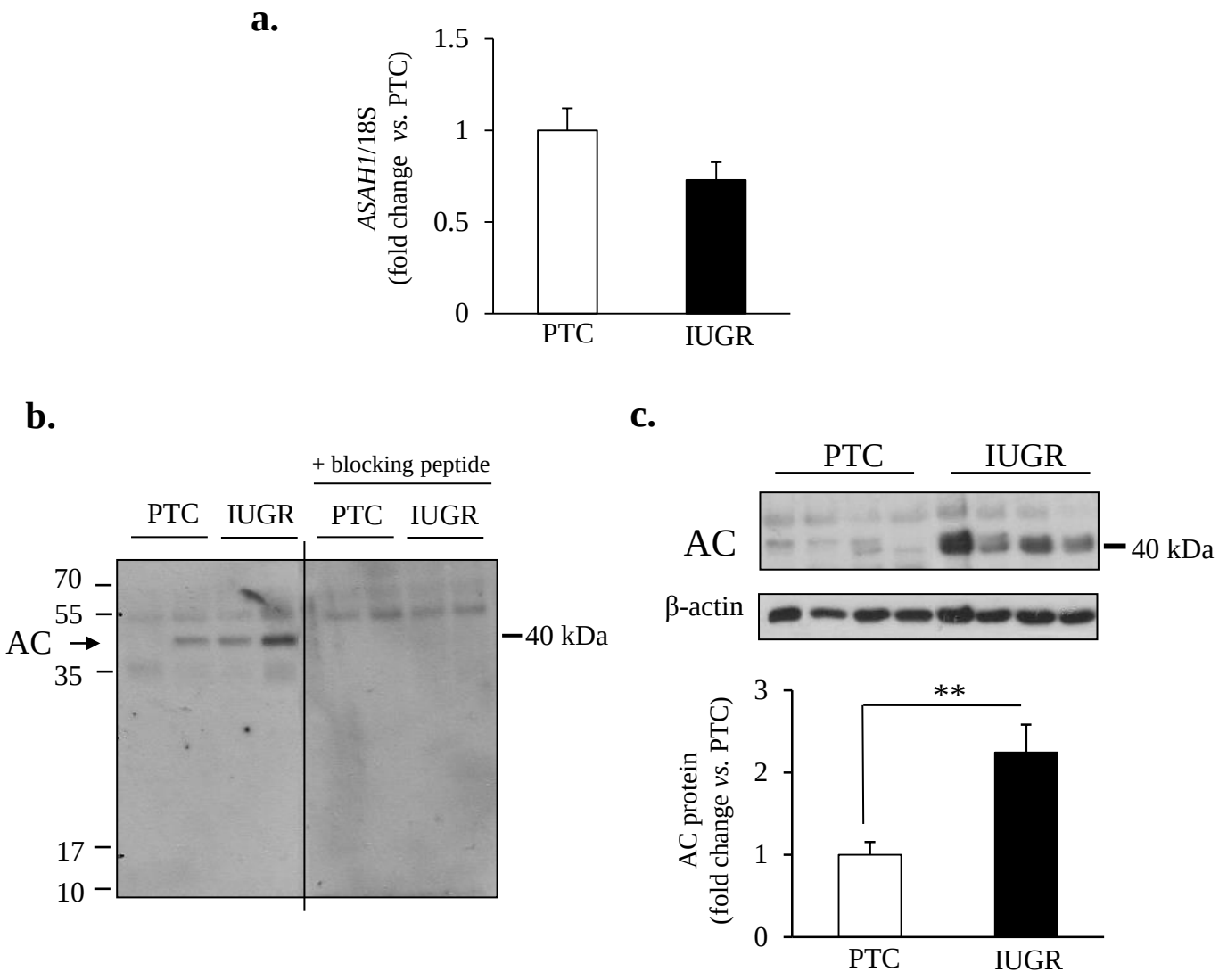

Figure 3.2 AC expression in placentae from PTC and IUGR pregnancies

(a) *ASAH1* mRNA levels in IUGR placentae were not significantly different from PTC placentae as detected by qPCR. Values were normalized to 18S RNA and expressed as a fold change relative to PTC (IUGR, n=19; PTC, n=14). **(b)** Western blot analysis of human placental tissue revealed a major band ranging between 35 kDa and 55 kDa, which according to the literature is likely the 40 kDa active form of AC. The specificity of our antibody was confirmed using a blocking peptide that selectively competed for the reaction with the 40 kDa band, but did not compete for the non-specific band detected at ~55kDa. **(c)** AC protein expression was significantly increased in IUGR placentae relative to PTC placentae as detected by Western blotting. Densitometric analysis of AC expression in IUGR and PTC placentae normalized to β-actin and expressed as a fold change relative to PTC (IUGR, n=14; PTC, n=11). Statistical significance was determined as **$p<0.01$ using an unpaired Student's t-test with or without Welch's correction, where applicable.

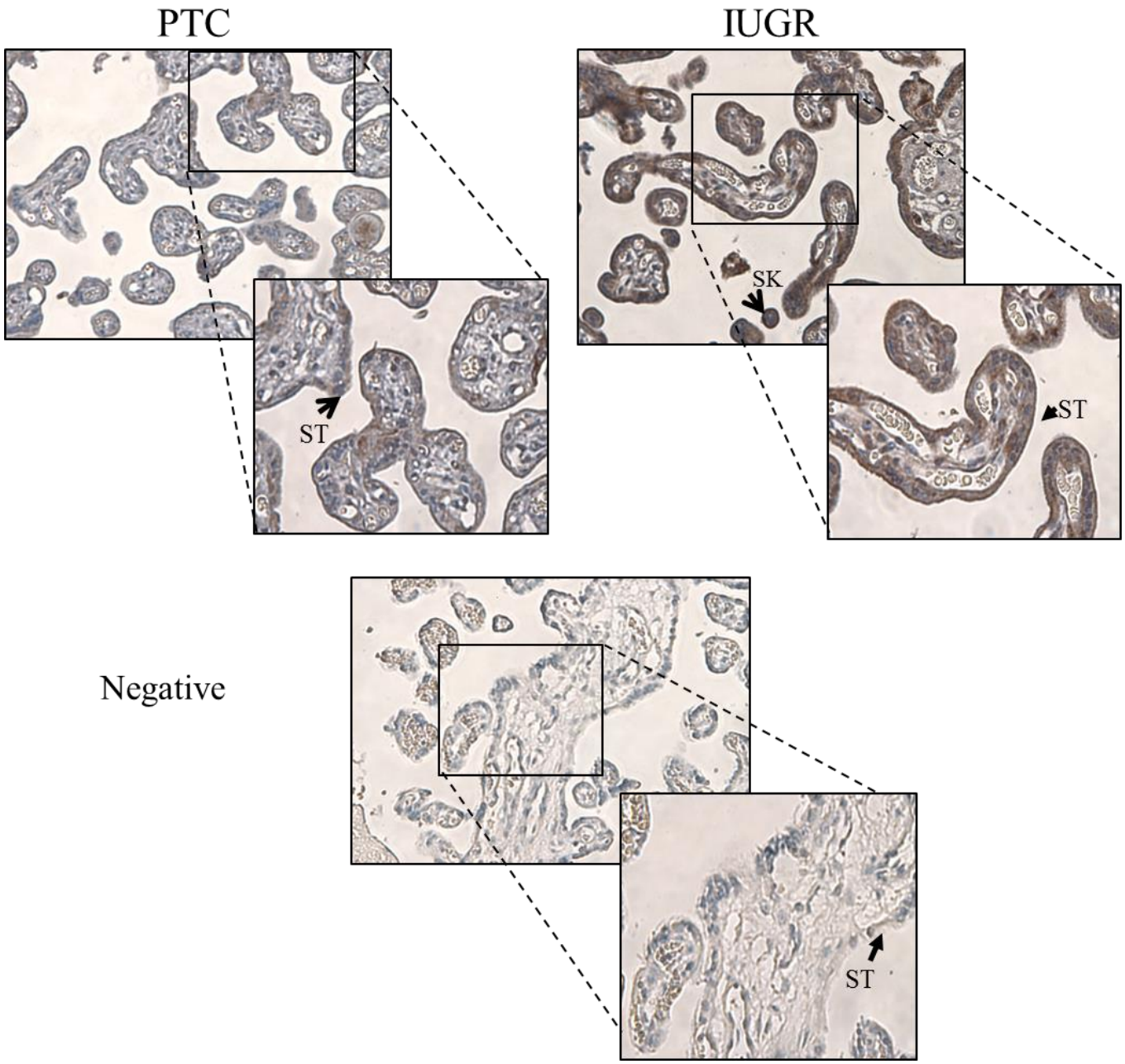

Figure 3.3 AC expression in placental tissue sections from PTC and IUGR pregnancies

Representative images depicting the spatial localization of AC in placental tissue from IUGR and PTC pregnancies using immunohistochemistry and captured by bright field imaging. AC was predominately expressed in the trophoblastic layer of PTC and IUGR sections. Increased AC expression was observed in the budding and shed syncytial knots (SK) found in IUGR placentae (IUGR, n=3, PTC, n=3). Images are shown at 20X and insets at 40X magnifications. Negative (goat IgG); ST: syncytiotrophblast; SK: syncytial knot.

confirming the specificity of the antibody staining. Collectively, the findings indicate enhanced breakdown of CER by AC in the trophoblastic layer of placentae from IUGR pregnancies.

3.2 TGFβ1 and β3 increase AC expression in JEG3 cells.

Early placental development occurs under low oxygen conditions and is associated with high levels of TGFβ1 and β3, which function as key regulators of trophoblast differentiation (17,29,50). In IUGR there is sustained placental hypoxia and high TGFβ3 expression levels, which contribute, in part, to the altered trophoblast phenotype and placental dysfunction typical of this pathology (17,51,60). To establish the mechanism(s) responsible for altered AC expression in IUGR, I examined the role of TGFβ1 and β3 on AC expression using human choriocarcinoma JEG3 cells, an established *in vitro* model of placental origin commonly used to study trophoblast cell fate events (81). This cell line offers a number of experimental advantages as it represents a homogenous population of cells that do not readily fuse, and are amenable to transfection. Hence, I reasoned that JEG3 cells were suitable to systematically decipher the role of TGFβs on sphingolipid metabolism in the placenta. Western blot analysis of JEG3 cell lysates detected the 40 kDa β-subunit of active AC, which was consistent with my previous findings in human placental tissue **(Figure 3.4a)**. The specificity of the antibody in cells was validated using a blocking peptide that outcompeted this band (**Figure 3.4a)**.

Since TGFβs elicit pleiotropic effects on a variety of cell systems in a context-dependent manner (82), I next performed a series of experiments to establish TGFβ1 and β3 effects on AC protein levels in JEG3 cells. Under standard culture conditions, JEG3 cells were exposed to a TGFβ1 or β3 concentration gradient of 1, 5, and 10 ng/ml for 3, 8, and 24 hours. Importantly, cells treated with control vehicle were included as controls. Western blot analysis revealed no changes in AC protein levels following 3 and 8 hours of TGFβ1 or β3 treatment at 1, 5, or 10

ng/ml (**Figure 3.4c)**. However, AC protein levels were upregulated following a 24-hour exposure to 5 and 10 ng/ml of TGFβ1 or β3. Thus, in following experiments I treated cells with 5 ng/ml of TGFβ1 or β3 and examined AC protein levels in JEG3 cells at 24 hours. Western blot analysis showed significantly increased AC protein levels following TGFβ1 or β3 treatment relative to control vehicle JEG3 cells (5 ng/ml TGFβ1 or β3: 1.51 ± 0.085 or 2.26 ± 0.208 fold increase *vs.* control vehicle: 1.0 ± .109, $p<0.05$ and $p<0.001$) **(Figure 3.5a)**. As complete EMEM culture media (10% FBS) contains numerous growth factors that may have confounded my analysis, I also examined AC expression in JEG3 cells cultured in low-serum media (1% FBS). No changes in the TGFβ1 or β3-induced effect on AC expression were observed between JEG3 cells cultured in EMEM supplemented with 10% FBS or 1% FBS **(Figure 3.5a & 3.5b)**. I therefore reasoned that my findings were the direct result of TGFβ1 or β3 treatment, independent of growth factors in the cell culture media.

As TGFβs are known to exert their functions by regulating gene expression (15), I next evaluated *ASAH1* mRNA levels in JEG3 cells. Real-time PCR analysis revealed an increase in *ASAH1* mRNA levels following 3 and 8 hours of TGFβ1 or β3 stimulation as compared to control vehicle treatment (3 hrs, 5 ng/ml TGFβ1 and β3: 2.03 ± .277 or 1.91 ± 0.290 fold increase *vs.* control vehicle: 1.0 ± 0.020, $p<0.01$ and $p<0.01$; 8hrs, 5 ng/ml TGFβ1 or β3: 2.175 ± 0.339 or 1.880 ± 0.204 fold increase *vs.* control vehicle 1.0 ± 0.028, $p<0.01$ and $p<0.001$) **(Figure 3.5c)**. In contrast, *ASAH1* mRNA levels were decreased following 24 hours of TGFβ1 or β3 stimulation relative to control vehicle treatment (24 hrs, 5 ng/ml TGFβ1 and β3: 0.183 ± 0.119/0.337 ± 0.122 *vs*. fold decrease 1.0 ± 0.097, $p<0.01$ and $p<0.01$) (data not shown). I therefore reasoned that 24 hours post-TGFβ treatment is not an appropriate time point to detect

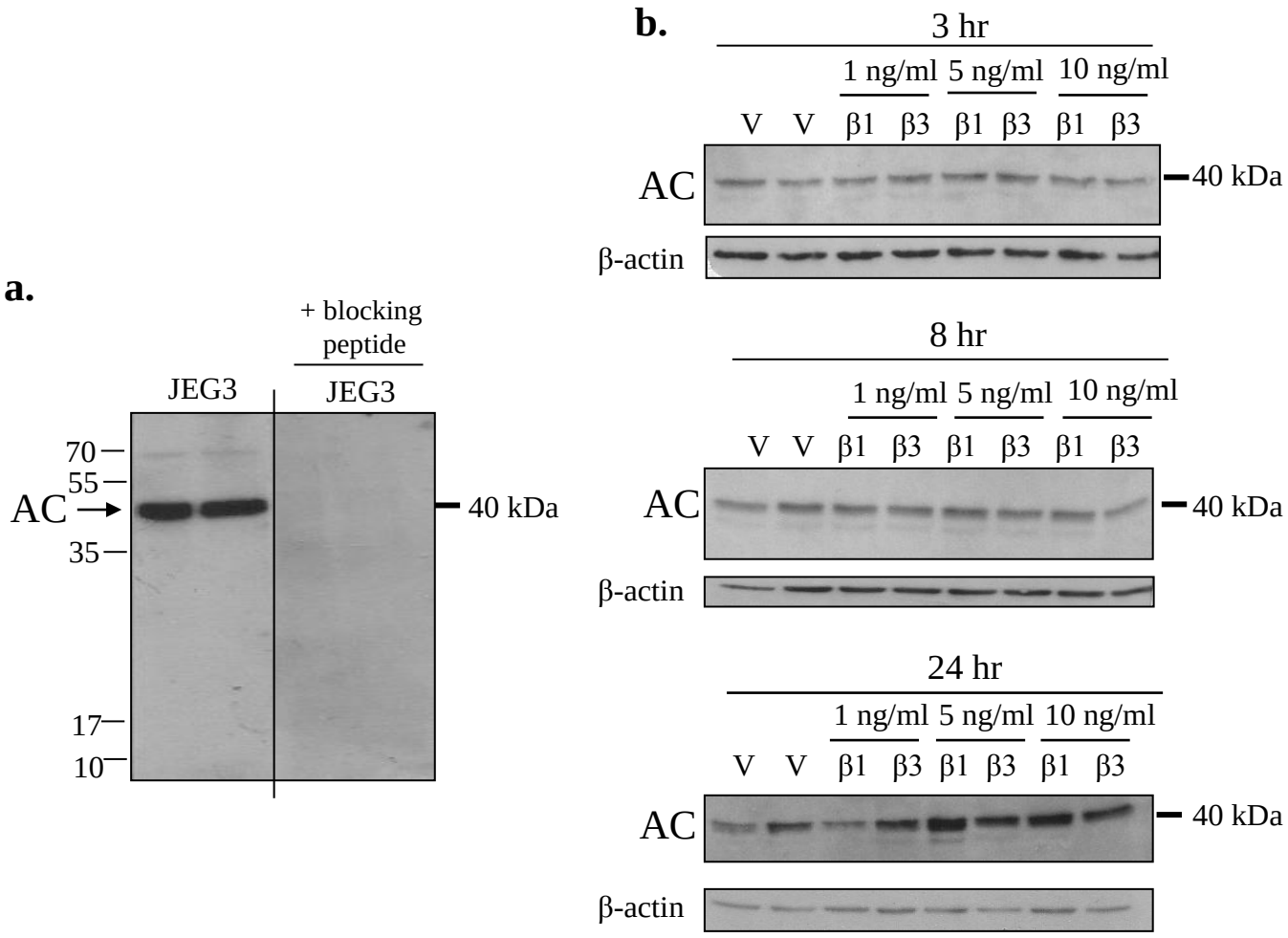

Figure 3.4 AC antibody validation and TGFβ time and dose responses in JEG3 cells

(a) AC was detected as a 40 kDa band in untreated JEG3 cells by Western blotting. The specificity of our antibody was confirmed by using a blocking peptide that selectively outcompeted this band. **(b)** The TGFβ effect on AC expression was examined by treating JEG3 cells with TGFβ1 or β3 for 3, 8, and 24 hours (hr) at 1, 5, and 10 ng/ml. Following 3 and 8 hours no changes in AC expression were observed between control vehicle (V)- and TGFβ-treated cells as detected by Western blotting. However, AC expression was increased following a 24-hr exposure to TGFβ1 or β3 at 5 and 10 ng/ml relative to control vehicle-treated cells (n=3, performed in duplicate).

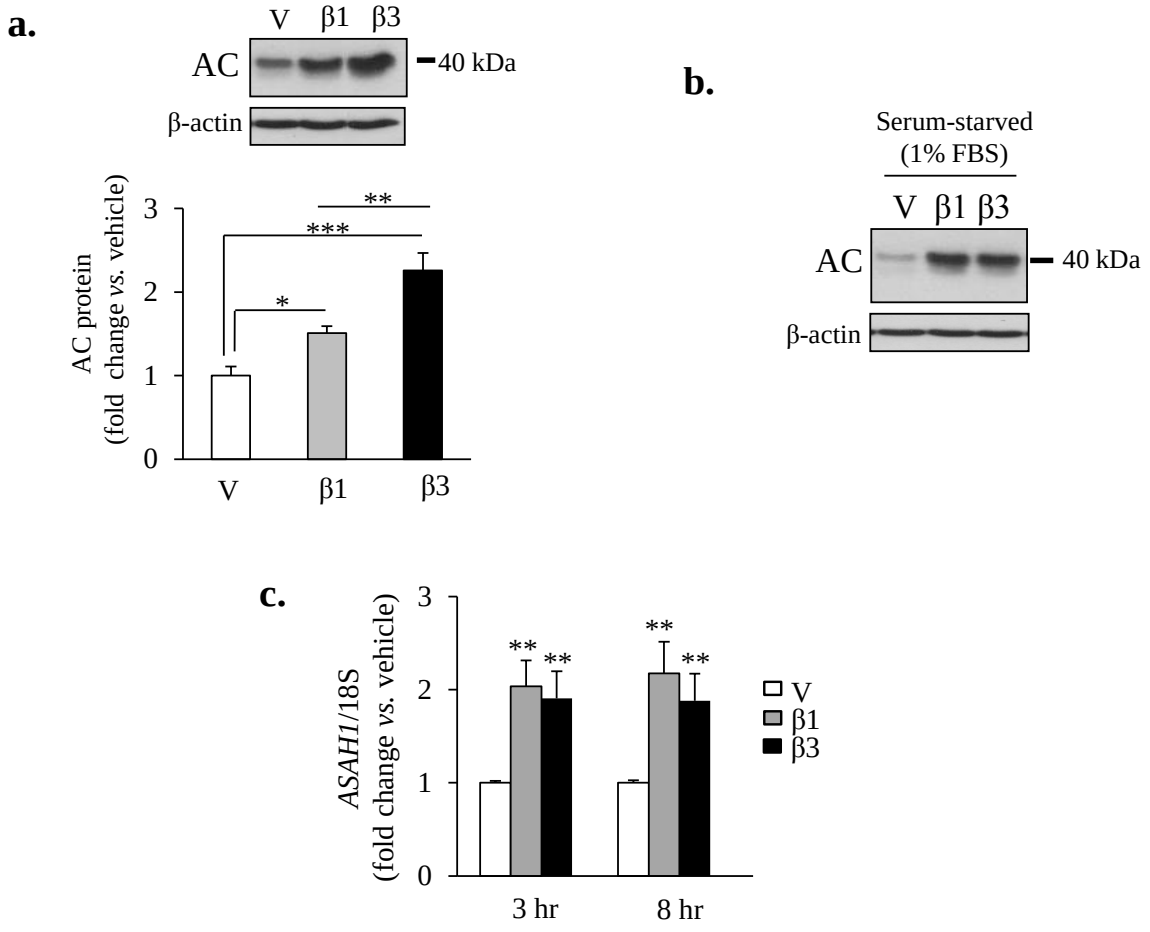

Figure 3.5 AC protein and mRNA expression in TGFβ1 or β3-treated JEG3 cells

(a) Twenty-four hour exposure to TGFβ1 or β3 (5 ng/ml) increased AC protein levels in JEG3 cells relative to control vehicle (V)-treated cells. Densitometric analysis of AC expression normalized to β-actin and expressed as a fold change relative to control vehicle-treated cells (n=12 separate experiments, performed in duplicate). **(b)** JEG3 cells cultured under low-serum media (1% FBS) showed increased AC protein levels following 24-hr TGFβ1 or β3 treatment relative to control vehicle-treated cells. **(c)** Quantitative PCR analysis revealed increased AC mRNA levels following 3 and 8 hours of TGFβ1 or β3 (5 ng/ml) treatment relative to control vehicle (V)-treated cells. Values were normalized to 18S RNA and expressed as a fold change relative to vehicle (V)-treated cells (n=4 separate experiments, performed in duplicate). Statistical significance was determined as *$p<0.05$, **$p<0.01$, and ***$p<0.001$ using one-way ANOVA with post-hoc Student-Newman-Keuls test, or two-way ANOVA with post-hoc Bonferroni test, where applicable.

changes in *ASAH1* mRNA levels. Additionally, these data could be indicative of a negative feedback loop meant to maintain AC protein levels, which is consistent with studies demonstrating that TGFβs exert biphasic effects (early stimulation and late repression) on their target genes (83).

Lastly, to examine AC subcellular localization following TGFβ1 or β3 treatment I performed immunofluorescence staining on JEG3 cells. Positive staining for AC was observed in the cytoplasm and at the cell boundaries of control vehicle-treated cells **(Figure 3.6)**. Uniquely, exposure to TGFβ3, but not TGFβ1, enhanced AC redistribution to the cell boundaries. To confirm AC redistribution to the plasma membrane, I also performed a co-stain for AC and ZO1, a marker for tight junctions (84). In line with previous findings, TGFβ3, but not TGFβ1, stimulated the redistribution of AC from the cytoplasm to the cell boundaries where it colocalized with ZO1 **(Figure 3.6, lower panel)**. No signal was observed in negative control (goat/rabbit IgG) slides. Taken together my data demonstrate that TGFβ1 and β3 have a positive effect on AC expression; however, TGFβ3, but not TGFβ1, induces the unique retribution of AC to the cell boundaries in JEG3 cells.

3.2.1 TGFβ1 and β3 via ALK5/Smad2 signalling regulate AC in JEG3 cells

Canonical TGFβ signalling is initiated by TGFβ binding to a type II serine threonine kinase receptor that subsequently recruits and phosphorylates activin receptor-like kinase 5 (ALK5), thereby leading to Smad2 or Smad3 activation **(Figure 1.5)** (85). Phosphorylated Smad2 or 3 in complex with Smad4 translocate to the nucleus where they associate with transcription factors to regulate the expression of target genes involved in a variety of cellular processes. Since JEG3 cells are Smad3 deficient (81), I reasoned that the TGFβ1 and β3 effect on AC expression was likely mediated via Smad2 signalling. I therefore examined

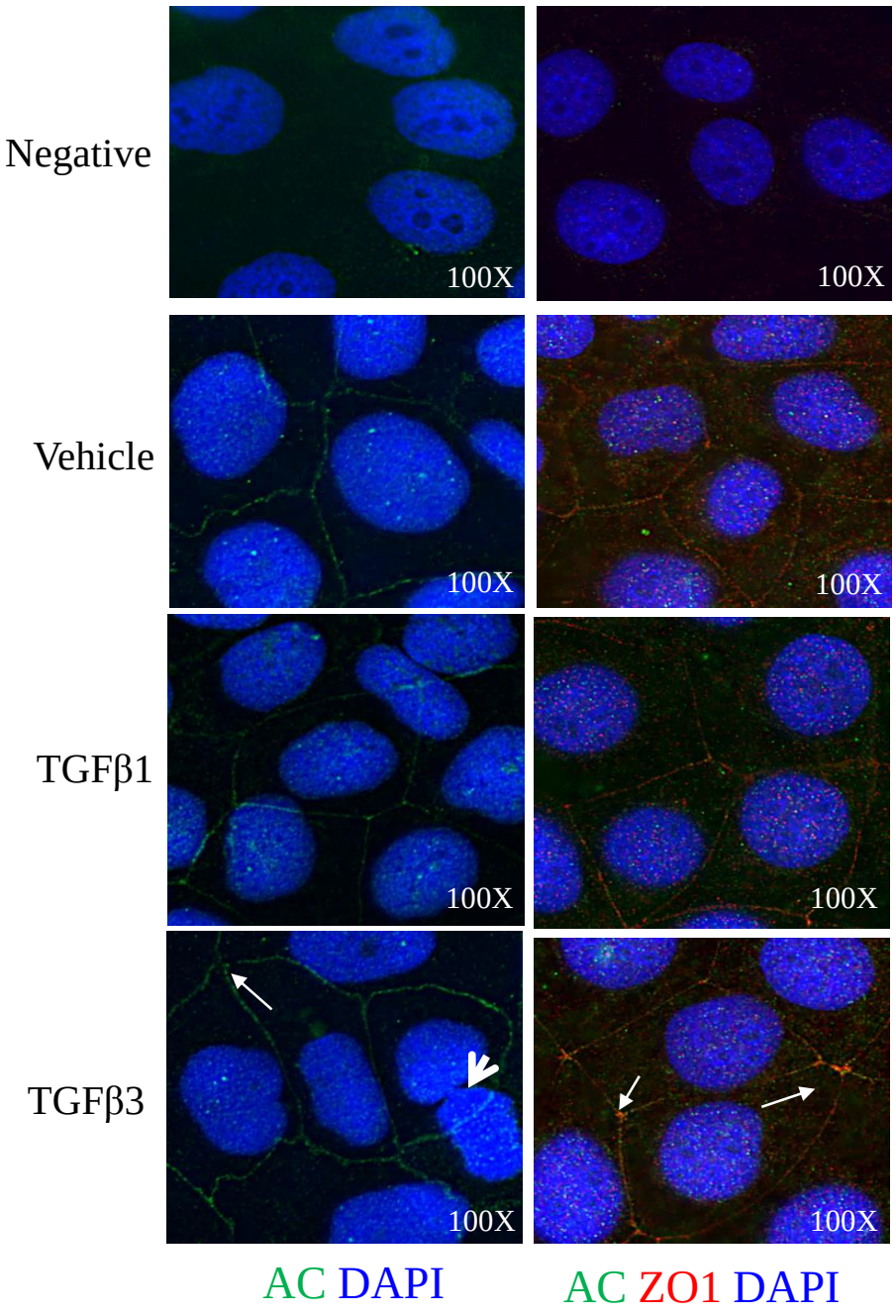

Figure 3.6 Spatial localization of AC expression in TGFβ1 or β3-treated JEG3 cells

Representative images captured by immunofluorescence deconvolution microscopy show AC expression in the cytoplasm as well as at the cell boundaries (white arrows) of control vehicle-treated JEG3 cells. 24-hr exposure to TGFβ3 (5 ng/ml), but not TGFβ1 (5ng/ml), redistributed AC from the cytoplasm to the cell boundaries where it colocalized with ZO1, a marker of tight junctions. AC (green), ZO1 (red) and the nuclei counterstained with DAPI (blue). Negative goat/rabbit IgG. Images are shown at 100X magnification.

SMAD2 mRNA levels, and Smad2 protein levels and activation in JEG3 cells. Real-time PCR analysis showed increased *SMAD2* mRNA levels in JEG3 cells treated for 24 hours with TGFβ1 or β3 (5 ng/ml TGFβ1 or β3: 1.40 ± 0.158 or 1.91 ± 0.098 fold increase *vs.* control vehicle: 1.0 ± 0.031, $p<0.01$ and $p<0.001$) **(Figure 3.7a)**, whereas *SMAD3* levels were not detected by qPCR (data not shown). In addition, Western blot analysis revealed increased Smad2 phosphorylation following 30 minutes of TGFβ1 or β3 treatment (5 ng/ml TGFβ1 or β3: 8.02 ± 1.65 or 7.96 ± 1.45 fold increase *vs.* control vehicle: 1.0 ± 0.382, $p<0.01$ and $p<0.01$) **(Figure 3.7b)**. My data therefore indicate Smad2 activation in JEG3 cells.

To systematically determine if ALK5/Smad2 signalling was responsible for mediating the TGFβ-effect on AC expression in JEG3 cells, I conducted a series of experiments using a pharmacological inhibitor (SB431542) that selectively blocks ALK5 signalling (86). In line with my previous findings, TGFβ1 or β3 treatment significantly increased AC protein levels relative to control treatment as determined by Western blotting (5 ng/ml TGFβ1 or β3: 1.78 ± 0.284 or 2.104 ± 0.233 fold increase *vs.* control vehicle 1.0 ± 0.187, $p<0.05$ and $p<0.01$) **(Figure 3.8a)**. However, the TGFβ1 and β3-stimulatory effect on AC expression was reduced following ALK5 inhibition by SB431542 (5 μM SB431542 & 5 ng/ml TGFβ1 or β3: 0.795 ± 0.280 or 1.358 ± 0.187 decrease *vs.* TGFβ1 or β3: 1.78 ± 0.284 or 2.104 ± 0.233, $p<0.01$ and $p<0.01$). No changes were observed between SB431542-treated cells and control vehicle-treated cells (5 μM SB431542: 1.105± 0.281 fold change *vs*. control vehicle: 1.0 ± 0.187, $p>0.05$). To confirm the specificity of the inhibitor I also measured Smad2 expression and activation following 30 minutes of TGFβ1 and β3 stimulation. SB431542-treatment completely abrogated TGFβ1 and β3 induced Smad2 phosphorylation **(Figure 3.8b)**. As no changes were observed in total Smad2 protein levels, I concluded that SB431542 efficiently blocked ALK5 signalling in JEG3 cells.

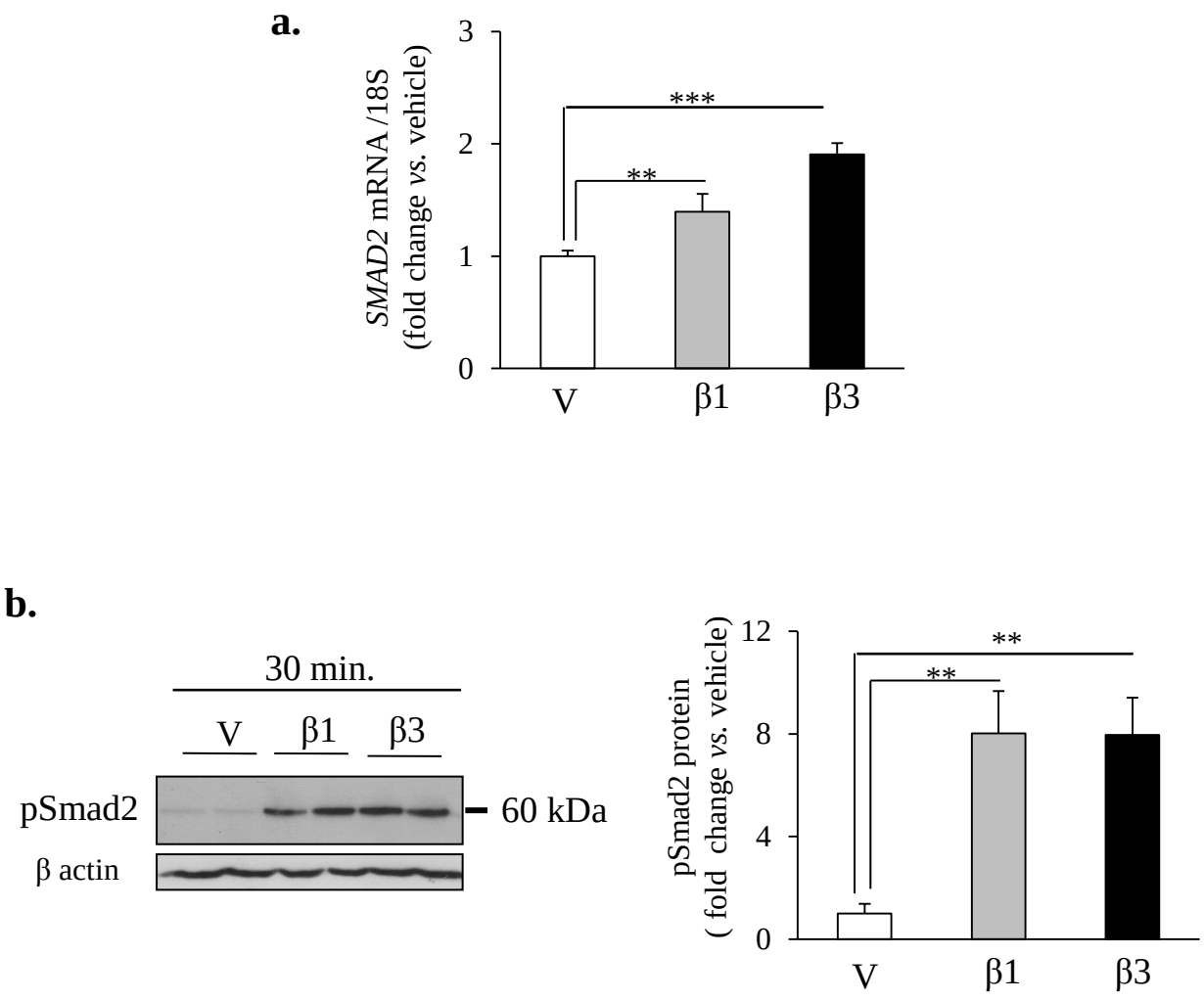

Figure 3.7 TGFβ1 or β3-mediated Smad2 signalling in human choriocarcinoma JEG3 cells

(a) *SMAD2* mRNA levels were significantly increased in JEG3 cells following exposure to TGFβ1 or β3 (5 ng/ml) as detected by qPCR. Values were normalized to 18S and expressed as a fold change relative to control vehicle (V)-treated cells (n=3 separate experiments, performed in duplicate). **(b)** JEG3 cell lysates analyzed by Western blotting showed increased phosphorylated Smad2 (pSmad2) expression following 30 minutes of TGFβ1 or β3 (5 ng/ml) stimulation relative to control vehicle-treated cells. Densitometric analysis of pSmad2 expression normalized to β-actin and expressed as a fold change relative to control vehicle-treated cells (n=4 separate experiments, performed in duplicate). Statistical significance was determined as **p<0.01 and ***p<0.001 using one-way ANOVA with post-hoc Student-Newman-Keuls test.

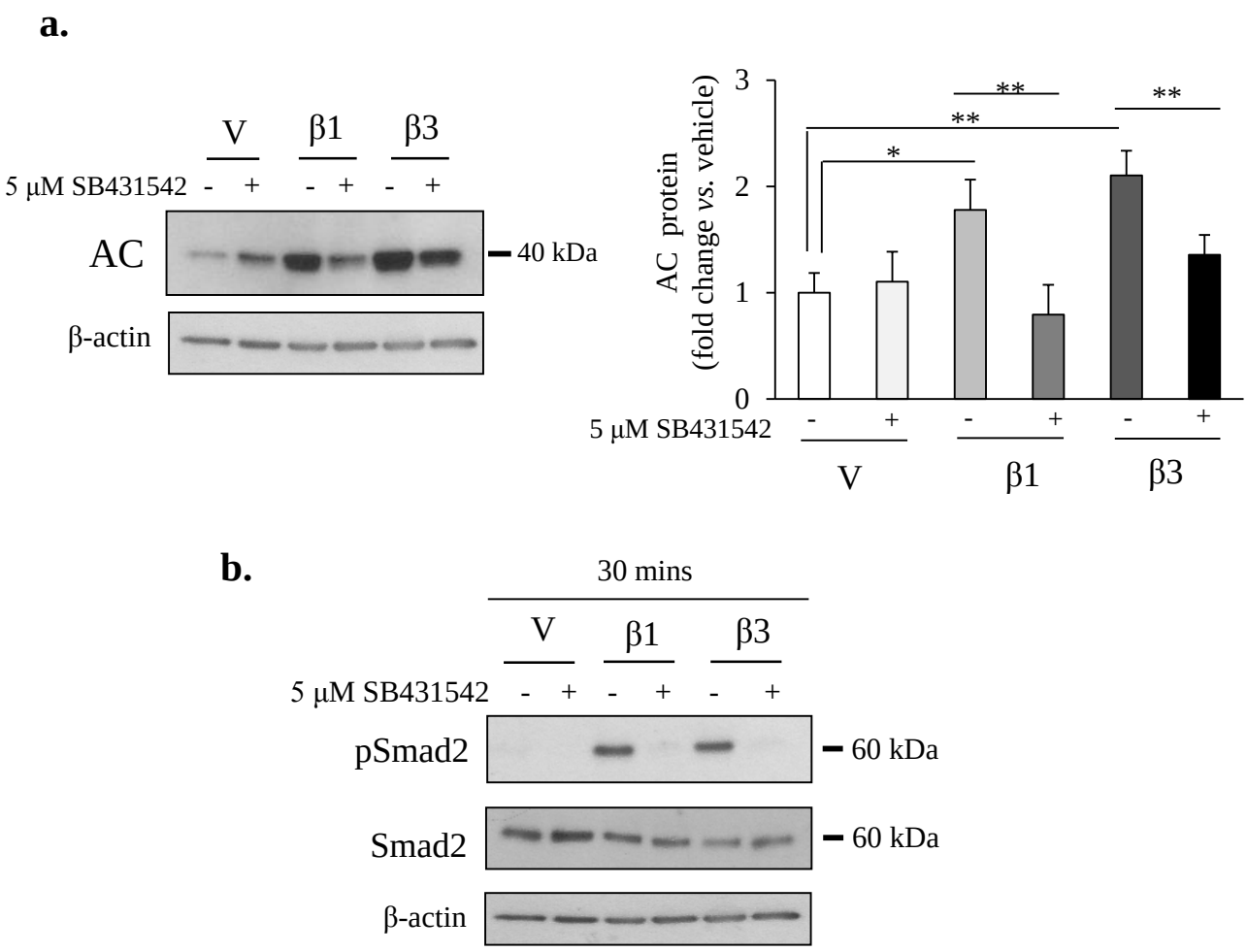

Figure 3.8 AC expression in JEG3 cells treated with the ALK5 inhibitor SB431542

(a) Immunoblot analysis revealed significantly increased AC expression in TGFβ1 or β3-treated JEG3 cells relative to control vehicle (V)-treated cells. ALK5 inhibition by SB431542 in TGFβ1 or β3-treated cells decreased AC expression relative to TGFβ1 or β3-treated cells. No changes were observed between ALK5 inhibited control vehicle-treated cells and control vehicle-treated cells**.** Densitometric analysis of AC protein expression in TGFβ1 or β3-treated JEG3 cells cultured in the absence or presence of SB431542 normalized to β-actin and expressed as a fold change relative to control vehicle-treated cells (n=3 separate experiments, performed in duplicate). **(b)** To confirm ALK5 inhibition by SB431542 total Smad2 and phosphorylated Smad2 (pSmad2) expression were determined by Western blotting in JEG3 cells. SB431542-treatment abrogated pSmad2 expression but did not change total Smad2 expression. Statistical significance was determined as *$p<0.05$, **$p<0.01$, and ***$p<0.001$ using one-way ANOVA with post-hoc Student-Newman-Keuls test.

To further elucidate the downstream signalling mechanism by which TGFβ increases AC expression, I performed a series of Smad2 knockdown experiments by transiently transfecting JEG3 cells with either empty vector (pSuper) or a plasmid encoding Smad2 siRNA. Silencing efficiency was determined by measuring *SMAD2* mRNA levels by qPCR **(Figure 3.9a)**. Consistent with my previous findings, 24-hour exposure to TGFβ1 and β3 significantly increased AC expression in pSuper-transfected cells as compared to control vehicle-treated cells (5 ng/ml TGFβ1 or β3: 2.81 ± 0.909 or 3.24 ± 0.587 fold increase *vs.* control vehicle: 1.0 ± 0.193, $p<0.05$ and $p<0.01$) **(Figure 3.9b)**. In contrast, following Smad2 silencing, AC expression was significantly decreased in siSmad2 cells exposed to TGFβ1 or β3 relative to pSuper cells treated with TGFβ1 or β3 (siSmad2 cells treated with 5 ng/ml TGFβ1 or β3: 0.209 ± 0.0136 or 0.184 ± 0.090 fold decrease *vs.* pSuper cells treated with 5 ng/ml TGFβ1 or β3: 2.81 ± 0.909 or 3.24 ± 0.587, $p<0.001$ and $p<0.001$) **(Figure 3.9b)**. To confirm reduced Smad2 activation in silenced JEG3 cells I measured phosphorylated Smad2 expression following 30 minutes of treatment with TGFβ1 or β3 by Western blotting. Expectedly, pSmad2 expression was decreased in siSmad2-transfected JEG3 cells relative to pSuper-transfected cells **(Figure 3.9b)**. Taken together my data indicate that TGFβ1 and β3 via the ALK5/Smad2 signalling pathway increase AC expression in JEG3 cells.

3.3 ALK5 Inhibition alters CER metabolism in villous explants

Although JEG3 cells are useful in systematically assessing the role of TGFβs on sphingolipid regulatory enzyme expression, first trimester villous explants offer a more physiological relevant model of the human placenta. I therefore examined the TGFβ effect on AC expression in first trimester human villous explants. Since TGFβs are highly expressed in the human placenta during early gestation (51), I reasoned that blocking ALK5 signalling using

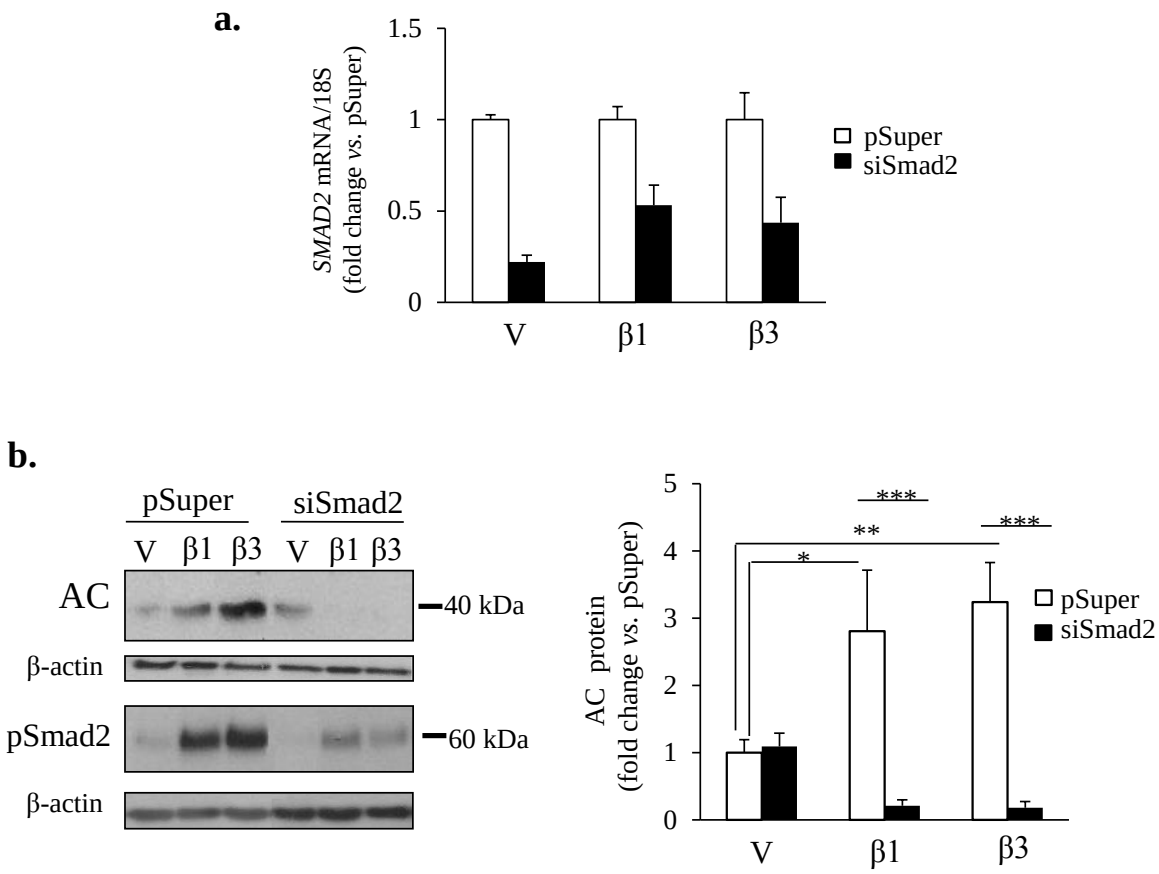

Figure 3.9 AC expression following Smad2 silencing in TGFβ1 or β3-treated JEG3 cells

(a) Total *SMAD2* mRNA levels were decreased in siSmad2-transfected JEG3 cells relative to pSuper-transfected cells (n=1 experiment, performed in triplicate). **(b)** Immunoblot analysis revealed significantly increased AC expression in TGFβ1 or β3-treated pSuper JEG3 cells relative to control vehicle (V)-treated cells. Following Smad2 silencing, AC expression was significantly reduced relative to pSuper JEG3 cells subjected to the same treatments. Phosphorylated Smad2 (pSmad2) expression was also decreased following siSmad2. Densitometric analysis of AC expression in siSmad2 JEG3 cells normalized to β-actin and expressed as a fold change relative to control vehicle (V)-treated pSuper cells (n=3 separate experiments, performed in duplicate). Statistical significance was determined as *$p<0.05$, **$p<0.01$, and ***$p<0.001$ using one-way ANOVA with post-hoc Student-Newman-Keuls test.

SB431542 would be a more suitable experimental approach to address my question. Exposure of villous explants to SB431542 significantly reduced AC protein levels as compared to control vehicle DMSO-treated explants (10μM SB431542: 0.575 ± 0.083 fold decrease *vs.* control vehicle DMSO: 1.0 ± 0.154, $p<0.05$) **(Figure 3.10)**. Total Smad2 and phosphorylated Smad2 expression were also measured to confirm ALK5 inhibition by SB431542. Total Smad2 levels showed no changes while pSmad2 expression was abrogated in explants treated with the inhibitor **(Figure 3.10).**

To establish if impaired ALK5 signalling in SB431542-treated villous explants reduced ceramide turnover by AC I also measured CER levels using LC-MS/MS. Lipidomics analyses revealed significant increases in C:18, C:20, and C:24 ceramide species in SB431542-treated explants relative to control vehicle DMSO-treated explants (C:18, SB431542: 1.958 ± 0.017 *vs.* DMSO: 1.0 ± 0.039, $p<0.001$, C:20, SB431542: 1.647 ± 0.097 vs. DMSO: 1.0 ± 0.011, $p<0.05$, C:24, SB431542: 2.18 ± 0.06 *vs.* DMSO: 1.0 ± 0.062, $p<0.05$) **(Figure 3.11)**. Collectively, these data further support a role for ALK5 signalling in regulating AC expression and CER processing in the human placenta.

3.4 ALK5 and pSmad2 expression are increased in IUGR

Since high levels of AC are accompanied by enhanced ceramide turnover in IUGR, I next examined ALK5 and Smad2 expression levels in IUGR placentae. Previously obtained data revealed increased *ALK5* mRNA levels in IUGR placentae as compared to placentae from PTC and term control (TC) deliveries **(Figure 3.12a)**. In line with mRNA data, ALK5 protein levels were increased in IUGR placentae relative to PTC and TC pregnancies **(Figure 3.12b)**. Notably, no differences in *ALK5* mRNA or protein expression were observed between TC and PTC cases,

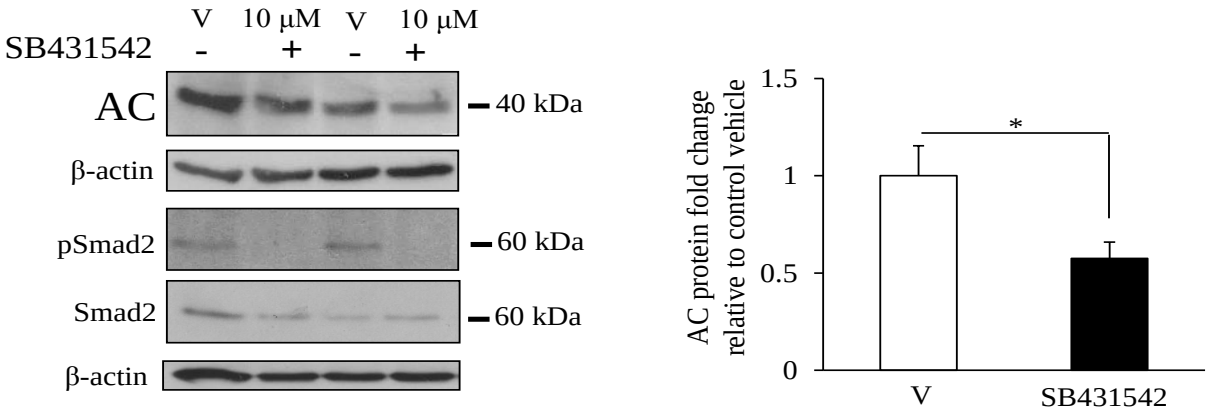

Figure 3.10 AC expression in first trimester human villous explants treated with SB431542

First trimester human villous explants were treated overnight with the pharmacological ALK5 inhibitor (10 μM SB431542) or control vehicle DMSO (V, 0.1% DMSO). AC expression was significantly decreased in first trimester villous explants following 24 hour exposure to SB431542 as shown by Western blotting. Total Smad2 and phosphorylated Smad2 (pSmad2) expression were determined 30 minutes post-treatment to confirm ALK5 inhibition. Densitometric analysis of AC protein expression in SB431542-treated villous explants normalized to β-actin and expressed as a fold change relative to vehicle-treated explants (n=5 experiments). Statistical significance was determined as *$p<0.05$ using an unpaired Student's t-test.

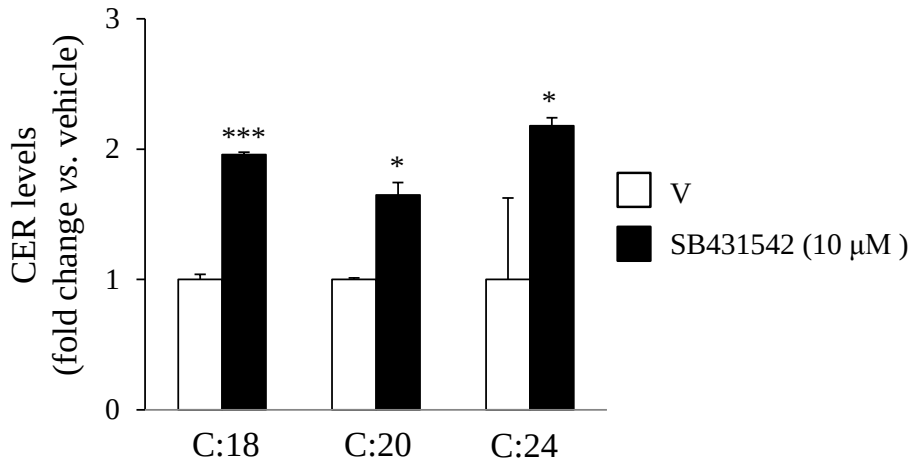

Figure 3.11 Ceramide levels in first trimester human villous explants treated with SB431542

Ceramide levels measured by LC-MS/MS showed significant increases in C:18, C:20, and C:24 CERs in human villous explants treated with ALK5 inhibitor (SB431542). CER species are distinguished by the number of carbons in the fatty acid chain. Values are expressed as a fold change in C:18, C:20, and C:24 levels in SB431542-treated explants relative to control vehicle (V)-treated explants. Statistical significance was determined as $^{**}p<0.05$ or $^{**}p<0.001$ using an unpaired Student's t-test with or without Welch's correction, where applicable (n= 3 experiments, carried out in triplicate).

a.

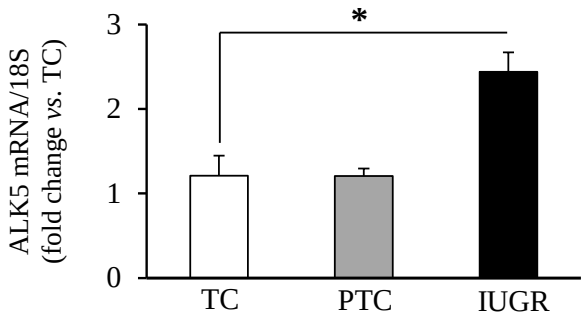

b.

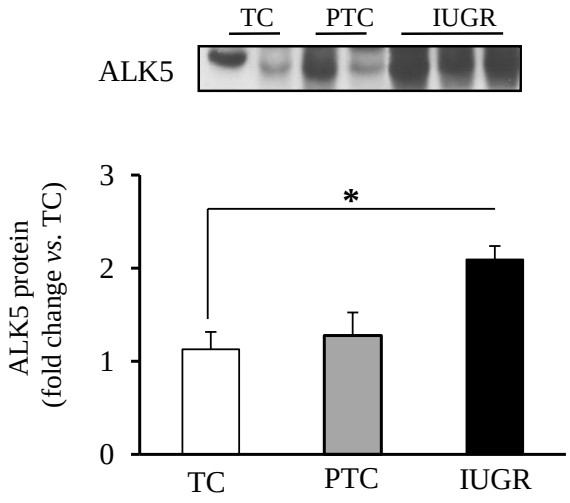

Figure 3.12 ALK5 expression in IUGR placentae

(a) *ALK5* mRNA levels were significantly increased in IUGR placentae relative to pre-term (PTC) and term control (TC) placental tissue as determined by qPCR. Values were normalized to 18S RNA. No changes were observed between TC and PTC. (IUGR n=10; PTC n=8; TC n=8). **(b)** Tissue lysates analyzed by Western blotting revealed significantly increased ALK5 protein expression in IUGR placentae. Densitometric analysis of AC expression in IUGR placentae normalized to β-actin and expressed as a fold change relative to TC placental tissue. No changes were observed between TC and PTC. (IUGR n=10; PTC n=8; TC n=8). Statistical significance was determined as *$p<0.05$ using one-way ANOVA with post-hoc Student-Newman-Keuls test (ns= non-statistical significance). *These data were provided courtesy of Yoav Yinon, Jing Xu, and Isabella Caniggia.*

.

indicating that changes in ALK5 expression are independent of gestational age. In line with these data, immunofluorescence staining showed strong positive immunoreactivity for ALK5 expression primarily localized to the trophoblast layer of placental villi from IUGR pregnancies as compared to the low staining observed in placental sections from PTC deliveries **(Figure 3.13)**. Further, immunofluorescence analysis revealed enhanced pSmad2 expression in placental villi from IUGR pregnancies, suggesting increased activation of ALK5-mediated TGFβ signalling in IUGR relative to PTC deliveries **(Figure 3.13, lower panel).**

3.5 SPH metabolism is disrupted in IUGR pregnancies

Acid ceramidase is the rate-limiting enzyme in the production of sphingosine **(Figure 1.2)** (80). The lipidomics analysis revealed significantly increased sphingosine levels in IUGR when compared to PTC placentae **(Figure 3.14)**, a finding that agrees with the enhanced AC processing of CER that is found in this pathology. Sphingosine can be further modified by SPHK1 to produce S1P, a molecule that opposes the pro-death functions of CER **(Figure 1.3)**. Hence, I next examined SPHK1 expression to determine if SPH was further processed into S1P. Real-time PCR analysis showed a marked decrease in *SPHK1* mRNA levels in IUGR placentae relative to PTC placentae (IUGR 0.243 ± 0.055 fold decrease *vs.* PTC 1.0 ± 0.195, $p<0.01$) **(Figure 3.15a)**. Western blot analysis of human placental lysates identified SPHK1 as a single band at 49 kDa, which was competed out by SPHK1 blocking peptide **(Figure 3.15b)**. In line with mRNA data, SPHK1 protein levels were drastically decreased in IUGR placentae compared to PTC placentae (IUGR: 0.221 ± .107 fold decrease *vs.* PTC: 1.0 ± 0.295, $p<0.01$) **(Figure 3.15c)**. Deficient SPHK1 expression in IUGR may be indicative of its impaired function; hence, I examined SPHK1 activity in human placental lysates and found that it was

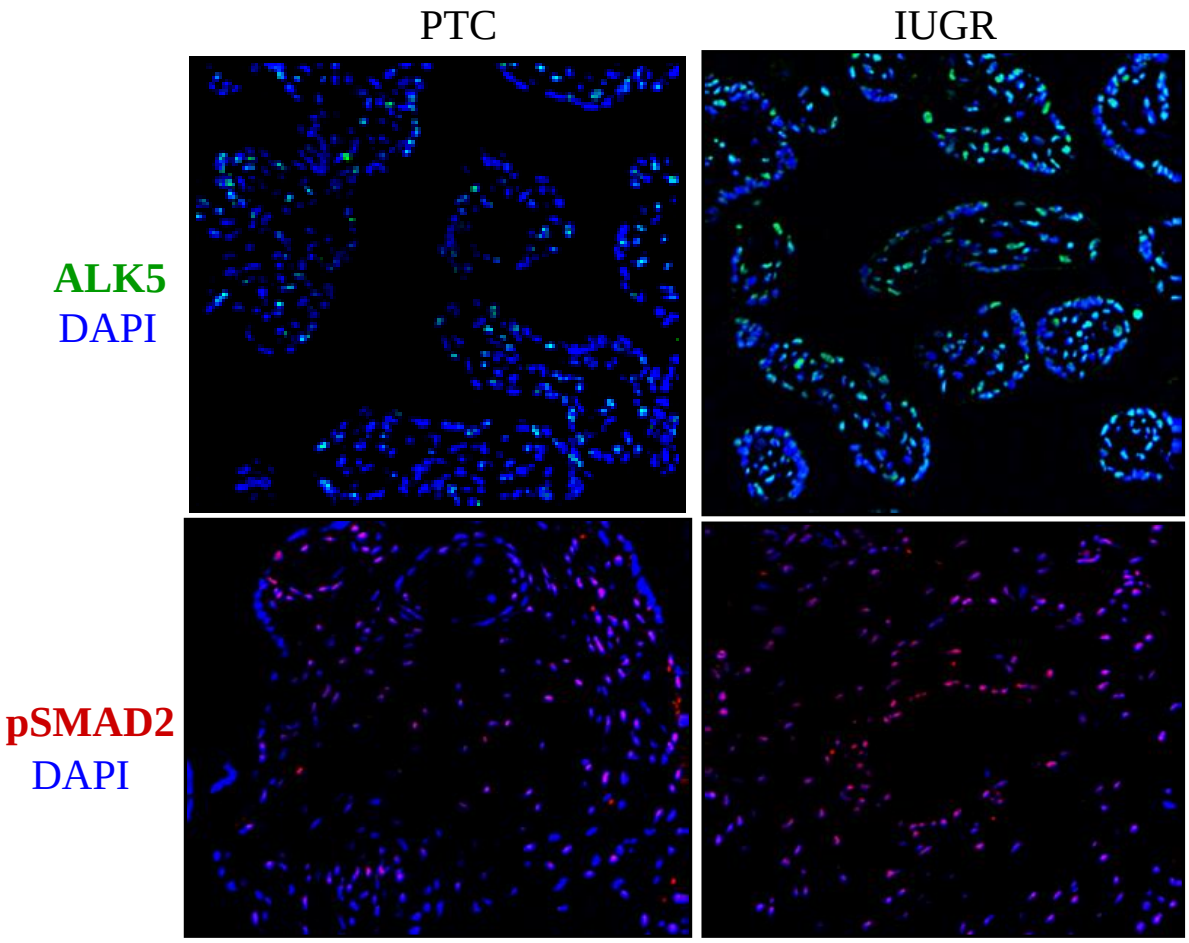

Figure 3.13 Spatial localization of ALK5 and pSmad2 expression in IUGR placentae

Immunofluorescence images showed that ALK5 expression is increased in the trophoblastic layer of placental villi from IUGR pregnancies compared to PTC. This coincided with increased phosphorylated Smad2 (pSmad2) expression in IUGR placentae. ALK5 (green), pSmad2 (red), and the nuclei counterstained with DAPI (blue). Magnification is 40X. *These data were provided courtesy of Yoav Yinon, Jing Xu, and Isabella Caniggia.*

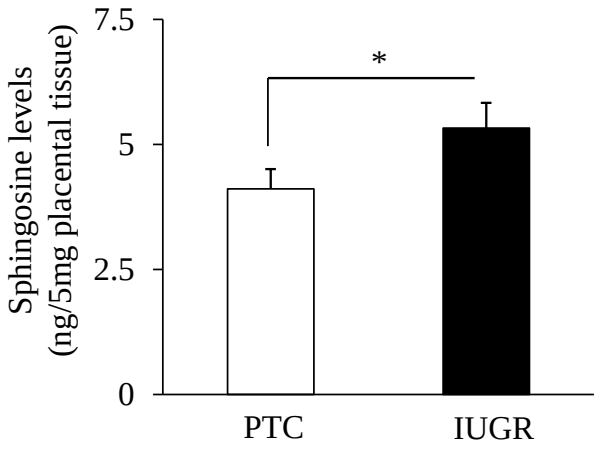

Figure 3.14 Sphingosine levels in placental tissue from IUGR pregnancies and PTC deliveries

Sphingosine levels measured by LC-MS/MS were significantly increased in placentae from IUGR pregnancies compared to age-matched controls from normotensive pregnancies (PTC). Statistical significance was determined as *$p<0.05$ using unpaired Student's t-test (IUGR n=10, PTC n=8).

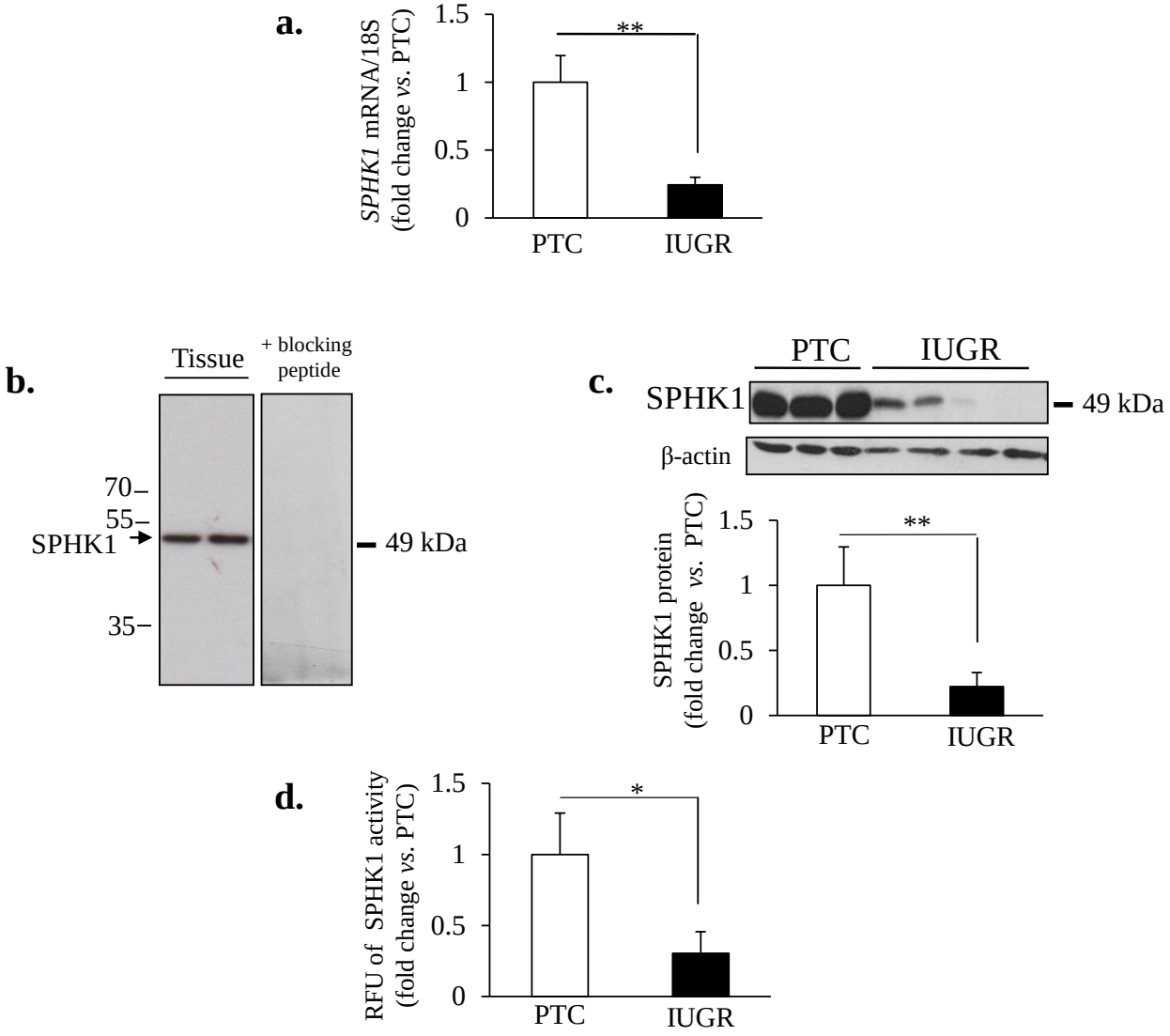

Figure 3.15 SPHK1 expression and activity in placentae from IUGR pregnancies

(a) SPHK1 mRNA levels in IUGR placentae were significantly decreased relative to PTC placentae as detected by qPCR. Values were normalized to 18S RNA and expressed as a fold change relative to PTC (IUGR, n=8; PTC, n=9) (b) Western blot analysis of human placental tissue detected SPHK1 at 49 kDa. The specificity of the antibody was confirmed using a blocking peptide that selectively outcompeted this band. (c) SPHK1 protein levels were significantly increased in IUGR placentae relative to PTC placentae as detected by Western blotting. Densitometric analysis of SPHK1 expression in IUGR and PTC placentae normalized to β-actin and expressed as a fold change relative to PTC (IUGR, n=14; PTC, n=11). (d) SPHK1 activity in IUGR placentae compared to PTC placentae expressed as a fold change relative to PTC (IUGR, n=10; PTC, n=5). Statistical significance was determined as *$p<0.05$ or **$p<0.01$ using unpaired Student's t-test with or without Welch's correction, where applicable. RFU: relative fluorescence units.

significantly decreased in IUGR placentae relative to PTC placentae (IUGR: 0.304 ± 0.153 *vs.* fold decrease PTC: 1.0 ± 0.292, $p<0.05$) **(Figure 3.15d)**. Collectively, these findings show that SPHK1 expression and activity are deficient in IUGR placentae, which may, in part, contribute to the accumulation of sphingosine.

3.6 TGFβ3, not TGFβ1, decreases SPHK1 in JEG3 cells

To establish if altered TGFβ signalling contributed to impaired SPHK1 processing of SPH in IUGR, I conducted a series of *in vitro* experiments using human choriocarcinoma JEG3 cells. Using previously established experimental parameters, JEG3 cells were exposed to TGFβ1 or β3 (5 ng/ml) or vehicle for 3, 8, and 24 hours under standard culture conditions. Real-time PCR analysis revealed significantly decreased *SPHK1* mRNA levels in TGFβ1 or β3-treated JEG3 cells relative to control vehicle-treated cells at all exposure times (3 hrs, 5 ng/ml TGFβ1 or β3: 0.487 ± .177 or 0.324 ± 0.212 fold decrease *vs.* control vehicle 1.0 ± 0.141; 8 hrs, 5 ng/ml TGFβ1 or β3: 0.142 ± 0.055 or 0.171 ± 0.042 fold decrease *vs.* control vehicle 1.0 ± 0.076; 24 hrs TGFβ1 or β3: 0.219 ± .099 or 0.232 ± 0.089 fold decrease *vs.* control vehicle 1.0 ± 0.084, $p<0.05$ and $p<0.001$) **(Figure 3.16a)**. Western blot analysis of JEG3 cell lysates identified SPHK1 as a single band at 49 kDa, which was confirmed using blocking peptide that outcompeted this band **(Figure 3.16b)**. In line with mRNA data, TGFβ3 significantly decreased SPHK1 expression relative to control vehicle-treated cells (5 ng/ml TGFβ3: 0.424 ± 0.072 fold decrease *vs.* control vehicle 1.0 ± 0.108, $p<0.001$) **(Figure 3.16c)**. Importantly, no changes in SPHK1 protein levels were observed following TGFβ1 treatment (5 ng/ml TGFβ1: 0.753 ± 0.084 fold change *vs.* control vehicle 1.0 ± 0.108, $p>0.05$) **(Figure 3.16c)**. In line with protein data, immunofluorescence staining of SPHK1 in JEG3 cells showed low immunoreactivity for SPHK1

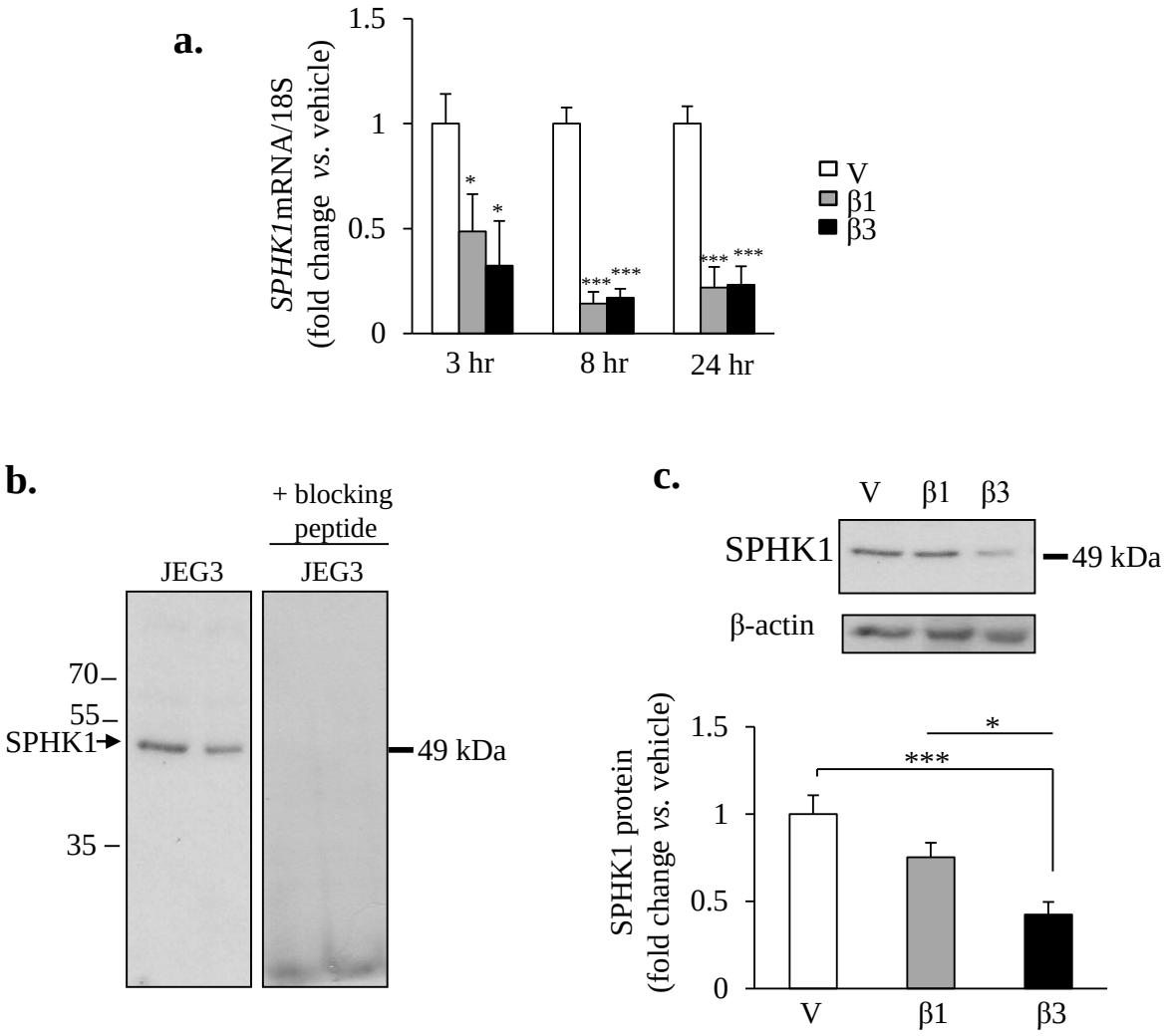

Figure 3.16 *SPHK1* mRNA and SPHK1 protein expression in TGFβ-treated JEG3 cells

(a) *SPHK1* mRNA levels were decreased following TGFβ1 or β3 (5 ng/ml) treatment for 3, 8, and 24 hours (hr) as detected by qPCR. Values were normalized to 18S RNA and expressed as a fold change relative to control vehicle (V)-treated cells (n=3 separate experiments, performed in duplicate). (b) SPHK1 was detected as a 49 kDa band in JEG3 cells by Western blotting. The specificity of our antibody was confirmed by using a blocking peptide that selectively outcompeted this band. (c) Immunoblot analysis showed decreased SPHK1 protein levels in TGFβ3-treated JEG3 cells compared to control vehicle (V)-treated cells. No changes were observed between TGFβ1-treated cells and control vehicle-treated cells. Densitometric analysis of SPHK1 expression in TGFβ1 or β3-treated cells normalized to β-actin and expressed as a fold change relative to control vehicle (n=8 separate experiments, performed in duplicate). Statistical significance was determined as *$p<0.05$, or ***$p<0.001$ using one-way ANOVA with post-hoc Student-Newman-Keuls test, or two-way ANOVA with post-hoc Bonferroni test, where applicable.

in the cytoplasm of TGFβ3-treated cells as compared to control vehicle-treated cells **(Figure 3.17)**. Notably, in contrast to AC, no changes in the subcellular localization of SPHK1 were observed following TGFβ3 treatment. Together these data show a prominent TGFβ3 effect on SPHK1 expression in JEG3 cells.

3.6.1 ALK5 inhibition does not alter SPHK1expression in JEG3 cells or villous explants

To determine if canonical TGFβ signalling contributed to reduced SPHK1 expression, I next blocked ALK5 signalling and examined SPHK1 expression in JEG3 cells. Under standard culture conditions, JEG3 cells were exposed to 5 ng/ml of vehicle, TGFβ1, or TGFβ3 in the presence or absence of SB431542 (5 μM) for 24 hours. Consistent with my previous findings, TGFβ3 treatment alone significantly decreased SPHK1 expression relative to control vehicle treatment (5 ng/ml TGFβ3: 0.418 ± 0.098 fold decrease *vs.* control vehicle: 1.0 ± 0.337, $p<0.05$) **(Figure 3.18)**. However, ALK5 inhibition by SB431542 did not significantly alter SPHK1 expression within treatment groups **(Figure 3.18)**. To confirm activity of the ALK5 inhibitor I measured pSmad2 expression following 30 minutes of TGFβ1 or β3 stimulation by Western blotting. TGFβ1 or β3 treatment induced Smad2 phosphorylation whereas ALK5 inhibition by SB431542 markedly reduced pSmad2 expression **(Figure 3.18)**.

I subsequently knocked down Smad2 expression by transiently transfecting JEG3 cells with either empty vector (pSuper) or a plasmid encoding Smad2 siRNA. Consistent with my previous findings, TGFβ3, but not TGFβ1, reduced SPHK1 expression in pSuper-transfected cells relative to control vehicle-treated cells **(Figure 3.19)**. However, no changes in SPHK1 expression were observed between pSuper- and siSmad2-transfected cells exposed to TGFβ1 or β3 treatment **(Figure 3.19)**. To confirm that Smad2 was silenced, I measured pSmad2

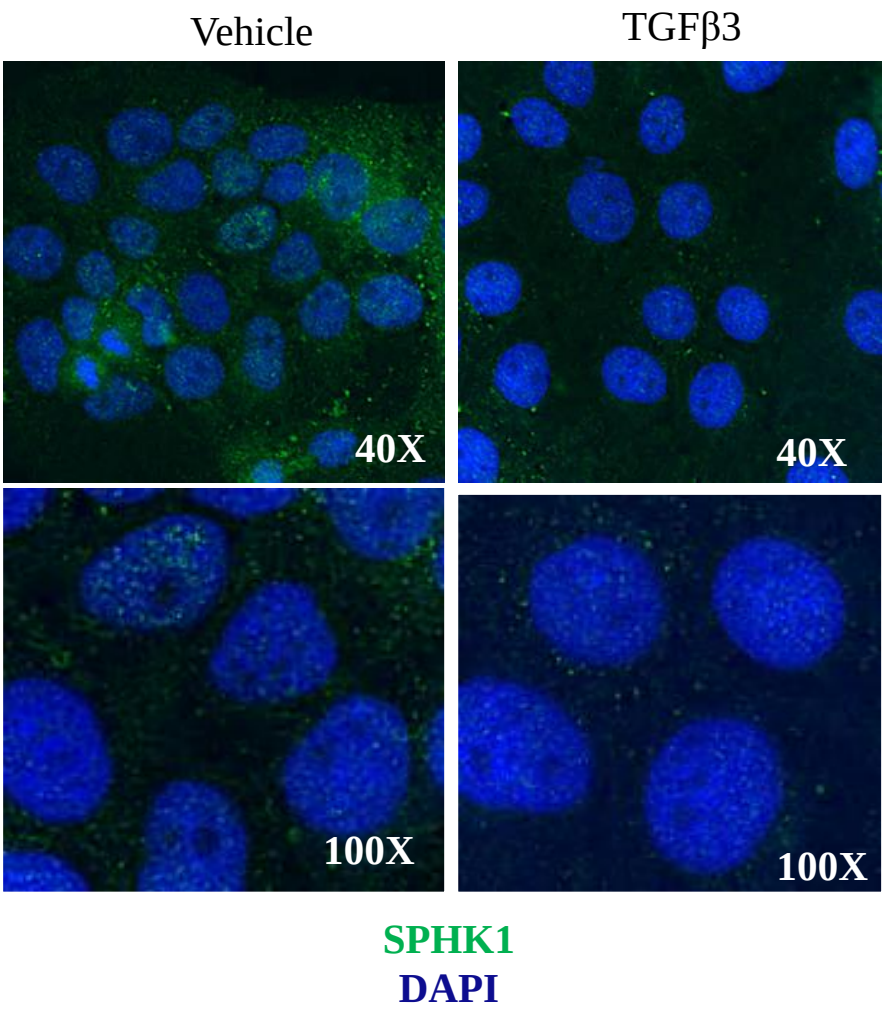

Figure 3.17 SPHK1 subcellular localization in TGFβ3-treated JEG3 cells

Immunofluorescence images showed reduced signal for SPHK1 in the cytoplasm following a 24-hour exposure to TGFβ3 relative to control vehicle cells (n=3 separate experiments, performed in duplicate). AC (green) and the nuclei counterstained with DAPI (blue).

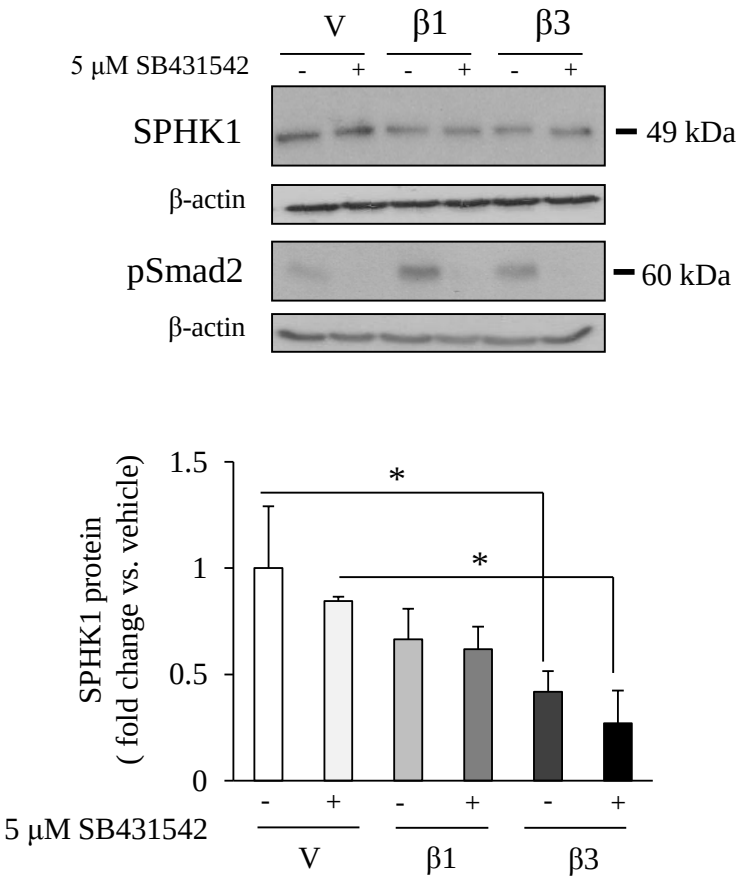

Figure 3.18 SPHK1 expression in JEG3 cells following ALK5 inhibition by SB431542

Immunoblot analysis revealed decreased SPHK1 expression following TGFβ3 treatment of JEG3 cells relative to control vehicle (V)-treated cells. No changes in SPHK1 expression were observed following SB431542 (5 μM) treatment. Densitometric analysis of SPHK1 protein expression in TGFβ1 or β3-treated JEG3 cells cultured in the absence or presence of SB431542 normalized to β-actin and expressed as a fold change relative to control vehicle-treated cells (n=3 separate experiments, performed in duplicate). Statistical significance was determined *$p<0.05$ using one-way ANOVA with post-hoc Student-Newman-Keuls test.

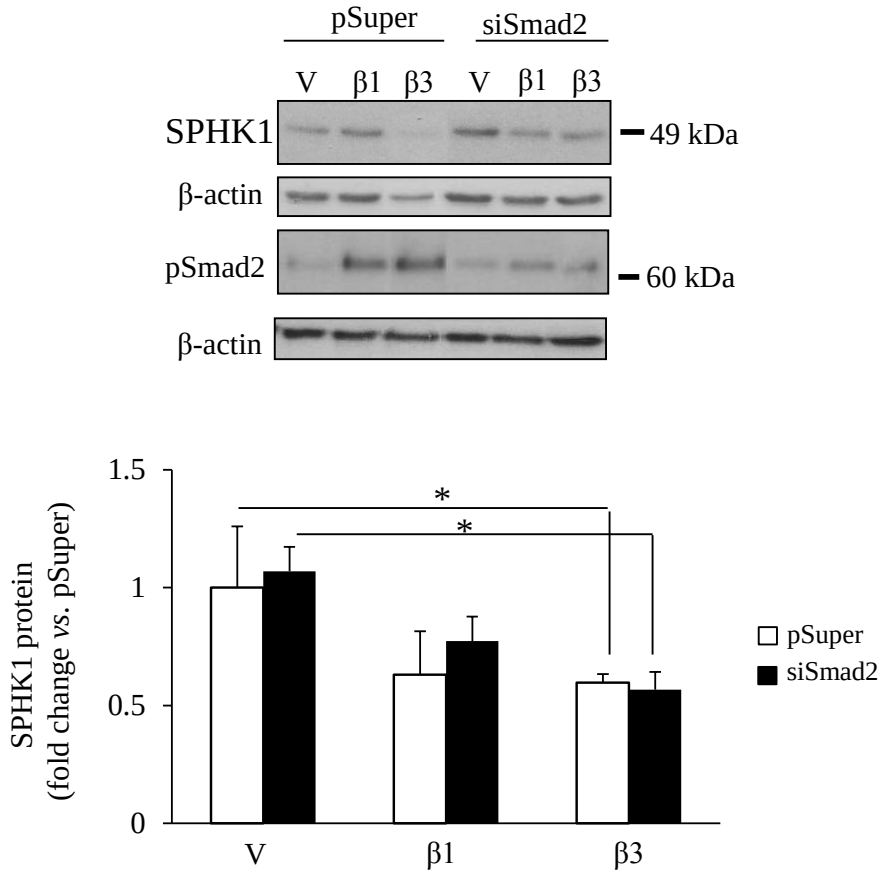

Figure 3.19 SPHK1 expression following Smad2 silencing in TGFβ1 or β3-treated JEG3 cells

Western blot analysis revealed reduced SPHK1 expression in TGFβ3-treated pSuper JEG3 cells relative to control vehicle (v)-treated pSuper JEG3 cells. No significant (ns) changes in SPHK1 expression were observed following Smad2 silencing when compared to pSuper JEG3 cells subjected to the same treatments. Phosphorylated Smad2 (pSmad2) expression was decreased in siSmad2 JEG3 cells relative to pSuper JEG3 cells following 30 minutes of TGFβ1 or β3 treatment. Densitometric analysis (lower panel) of SPHK1 expression in siSmad2 JEG3 cells normalized to β-actin and expressed as a fold change relative to control vehicle (V)-treated pSuper JEG3 cells (n=3 separate experiments, performed in duplicate). Statistical significance was determined as *$p<0.05$ using one-way ANOVA with post-hoc Student-Newman-Keuls test.

expression following 30 minutes of TGFβ1 or β3 stimulation. Immunoblot analysis revealed decreased pSmad2 expression in SiSmad2-transfected JEG3 cells relative to pSuper-transfected cells following TGFβ1 and β3 treatment **(Figure 3.19)**. I therefore reasoned that the TGFβ3 effect on SPHK1 in JEG3 cells is likely ALK5-and Smad2-independent.

To support these findings I also examined SPHK1 expression in human villous explants treated with SB431542 by Western blotting. No changes in SPHK1 expression were observed between ALK5 inhibited explants and control vehicle DMSO-treated explants (10 μM SB431542: 1.17 ± 0.181 fold change *vs.* control vehicle DMSO: 1.0 ± 0.136, $p>0.05$) **(Figure 3.20a)**. Reduced pSmad2 expression following SB431542 treatment confirmed the specificity of this inhibitor in explants **(Figure 3.20a)**. Additionally, my lipidomics data indicated no changes in sphingosine levels in ALK5 inhibited explants relative to control vehicle DMSO-treated explants (10 μM SB431542: 0.825 ± 0.141 fold change *vs.* control vehicle DMSO: 1.0 ± 0.031, $p>0.05$) **(Figure 3.20b)**. Hence, my findings suggest that ALK5 has no direct effect on SPHK1 expression.

3.6.2 TGFβ via ALK1 signalling alters SPHK1 expression in JEG3 cells

TGFβs have also been shown to elicit their function by activating ALK1 (36). In contrast to ALK5, ALK1 activation leads to the phosphorylation and subsequent activation of Smad1, 5, and 8 **(Figure 1.5)**. Interestingly, studies have suggested that the balance between ALK5- and ALK1-mediated signalling is needed to regulate angiogenesis, and that ALK5 may be required for ALK1 function (87). To determine if ALK1-mediated signalling was involved in the downregulation of SPHK1 expression, JEG3 cells were exposed to vehicle, TGFβ1 or TGFβ3 in the presence or absence of the ALK1 inhibitor Dorsomorphin (10 μM) for 24 hours. Consistent with my previous findings, exposure of JEG3 cells to TGFβ3, not TGFβ1, significantly

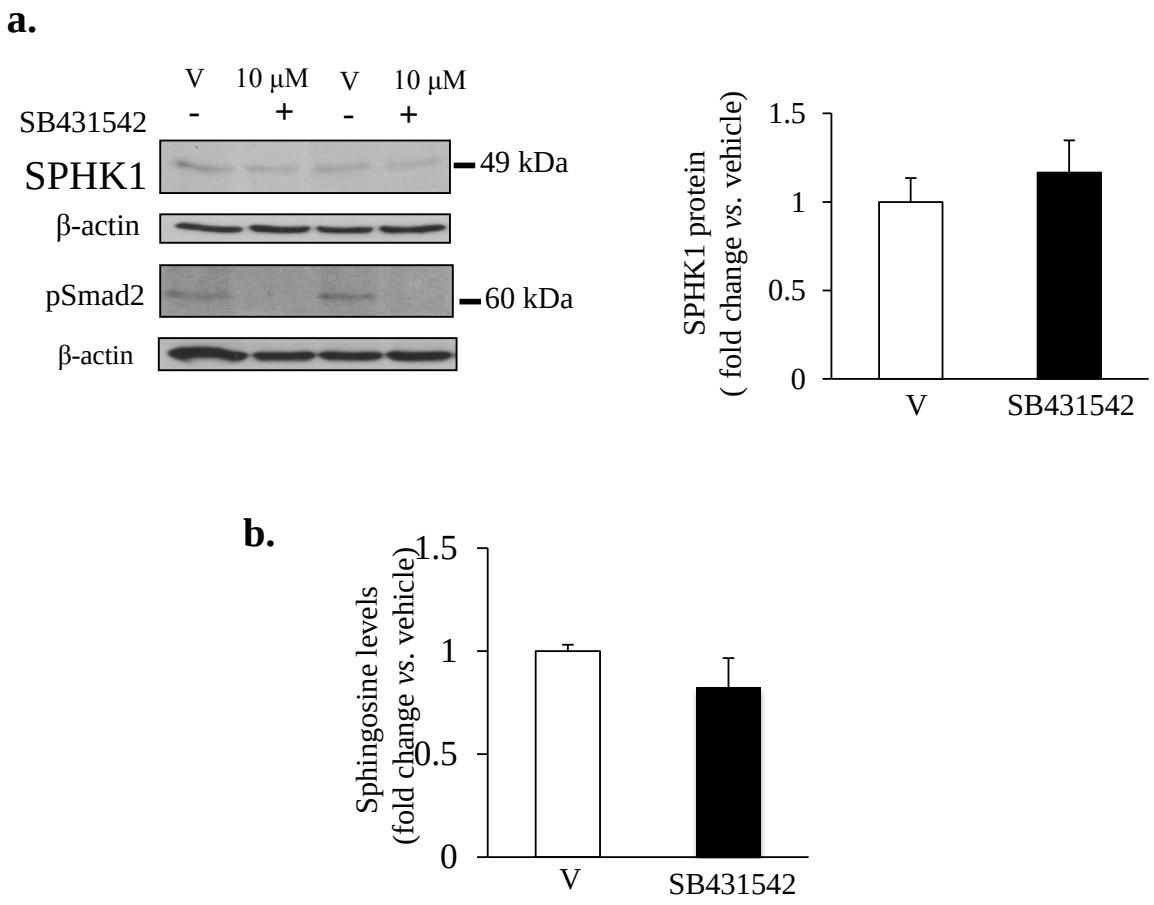

Figure 3.20 SPHK1 expression and SPH levels in human villous explants treated with SB431542

(a) SPHK1 expression in first trimester human villous explants treated with pharmacological ALK5 inhibitor (10 μM SB431542) or control vehicle (V) DMSO (0.1% DMSO) was analyzed by Western blotting. SPHK1 expression was not changed following a 24-hour exposure to SB431542. Phosphorylated Smad2 (pSmad2) expression was determined 30 minutes post treatment to confirm ALK5 inhibition. Densitometric analysis of SPHK1 protein expression in SB431542-treated villous explants normalized to β-actin and expressed as a fold change relative to control vehicle-treated explants (n=5, carried out in quadruplicate). **(b)** No changes in Sphingosine levels measured by LC-MS/MS were found between vehicle (V)-treated and SB431542-treated villous explants. Values are expressed as a fold change relative to vehicle-treated explants (n=3 experiments, carried out in triplicate). Statistical significance was determined using an unpaired Student's t-test with or without Welch's correction, where applicable.

decreased SPHK1 expression relative to control vehicle-treated cells (5 ng/ml TGFβ3: 0.226 ± 0.084 fold decrease *vs.* control vehicle: 1.0 ± 0.191, $p<0.001$) **(Figure 3.21a)**. Exposure to Dorsomorphin markedly reduced SPHK1 expression within all treatment groups **(Figure 3.21a)**. To confirm the activity of Dorsomorphin as an ALK1 inhibitor, I measured pSmad1 expression following 30 minutes of TGFβ1 and β3 stimulation. Exposure of JEG3 cells to TGFβ1 or β3 induced Smad1 phosphorylation whereas Dorsomorphin reduced pSmad1 expression **(Figure 3.21b)**. Total Smad1 expression was unaffected by Dorsomorphin treatment **(Figure 3.21b)**. These data indicate that that impaired ALK1 signalling represses SPHK1 expression in JEG3 cells.

3.6.3 Inhibition of MAPK signalling does not alter SPHK1 expression in JEG3 cells

TGFβs are also capable of exerting their functions by activating "non-Smad pathways" (38). Namely, TGFβs activate downstream mitogen-activated protein kinases (MAPKs), which encompass the extracellular-receptor regulated kinases (ERKs), c-JUN n-terminal kinases (JNKs), and p38 proteins. Interestingly, TGFβ1 via ERK pathway was shown to upregulate and activate SPHK1 in human fibroblast cells (88). To rule out the possibility that the TGFβ3-effect on SPHK1 was mediated via MAPKs I conducted a series of experiments using specific pharmacological inhibitors of ERK (U0126), p38 (SB239063), or JNK (SP600125), and examined SPHK1 expression by Western blotting. Consistent with previous findings, SPHK1 expression was reduced following TGFβ3 treatment relative to control vehicle treatment **(Figure 3.22)**. However, no changes in SPHK1 expression were observed within treatment groups following MAPK inhibition **(Figure 3.22)**. Hence, my data indicate no direct involvement of the MAPKs in the TGFβ regulation over SPHK1 expression in JEG3 cells.

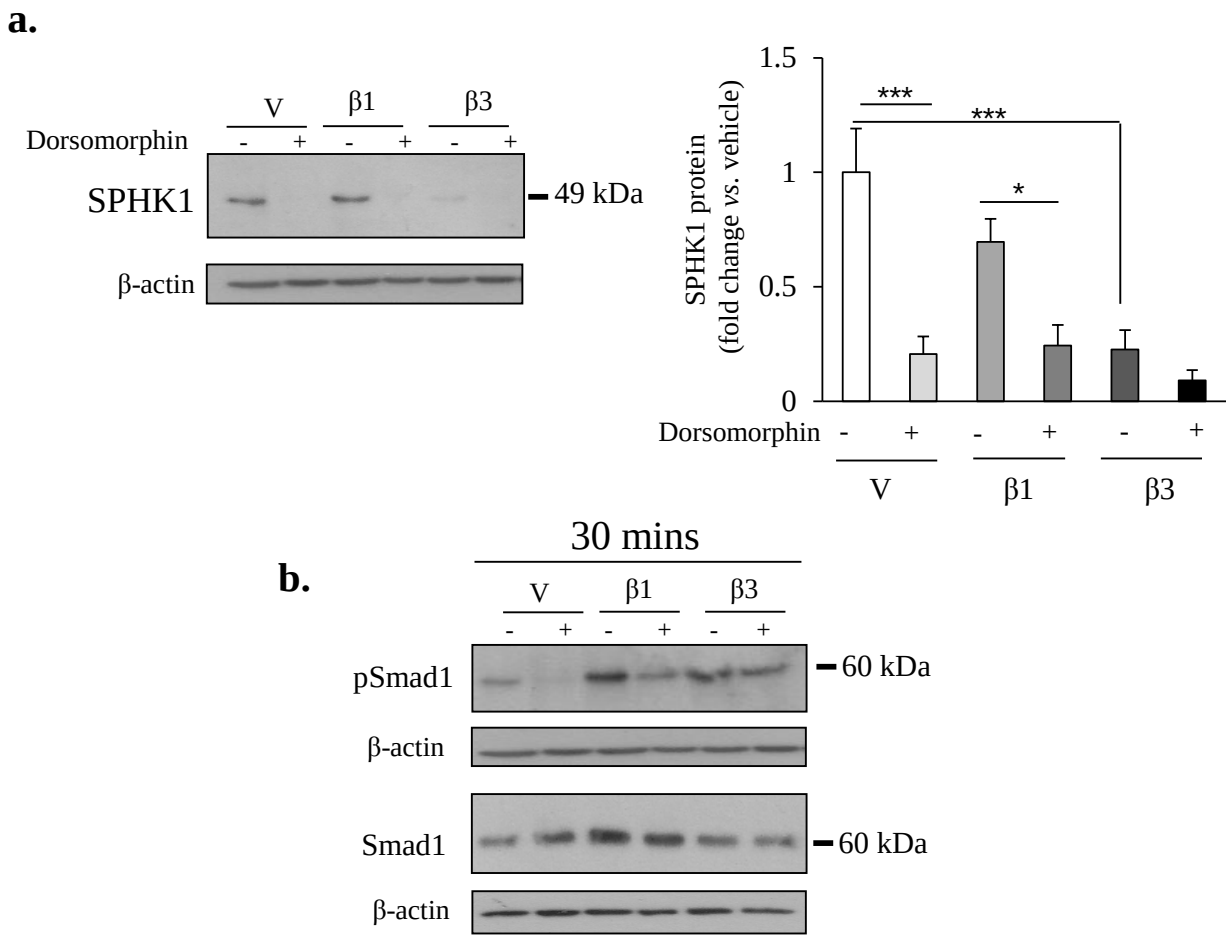

Figure 3.21 SPHK1 expression in JEG3 cells treated with the ALK1 inhibitor Dorsomorphin

(a) Immunoblot analysis revealed significantly reduced SPHK1 expression following TGFβ3, but not TGFβ1, treatment in JEG3 cells relative to control vehicle (V)-treated cells. ALK1 inhibition by Dorsomorphin (10 μM) significantly reduced SPHK1 expression within the control vehicle and TGFβ1 treatment groups. No changes were observed within the TGFβ3 treatment group. Densitometric analysis of SPHK1 protein expression in TGFβ1 or β3-treated JEG3 cells in the absence or presence of Dorsomorphin normalized to β-actin and expressed as a fold change relative to control vehicle-treated cells (n=3 separate experiments, performed in duplicate). **(b)** To confirm ALK1 inhibition by Dorsomorphin total Smad1 and phosphorylated Smad1 (pSmad1) expression were determined by Western blotting in JEG3 cells following 30 minutes of TGFβ1 or β3 treatment. Dorsomorphin reduced pSmad1 expression but did not change total Smad1 expression. Statistical significance was determined as *$p<0.05$, and **$p<0.01$ using one-way ANOVA with post-hoc Student-Newman-Keuls test.

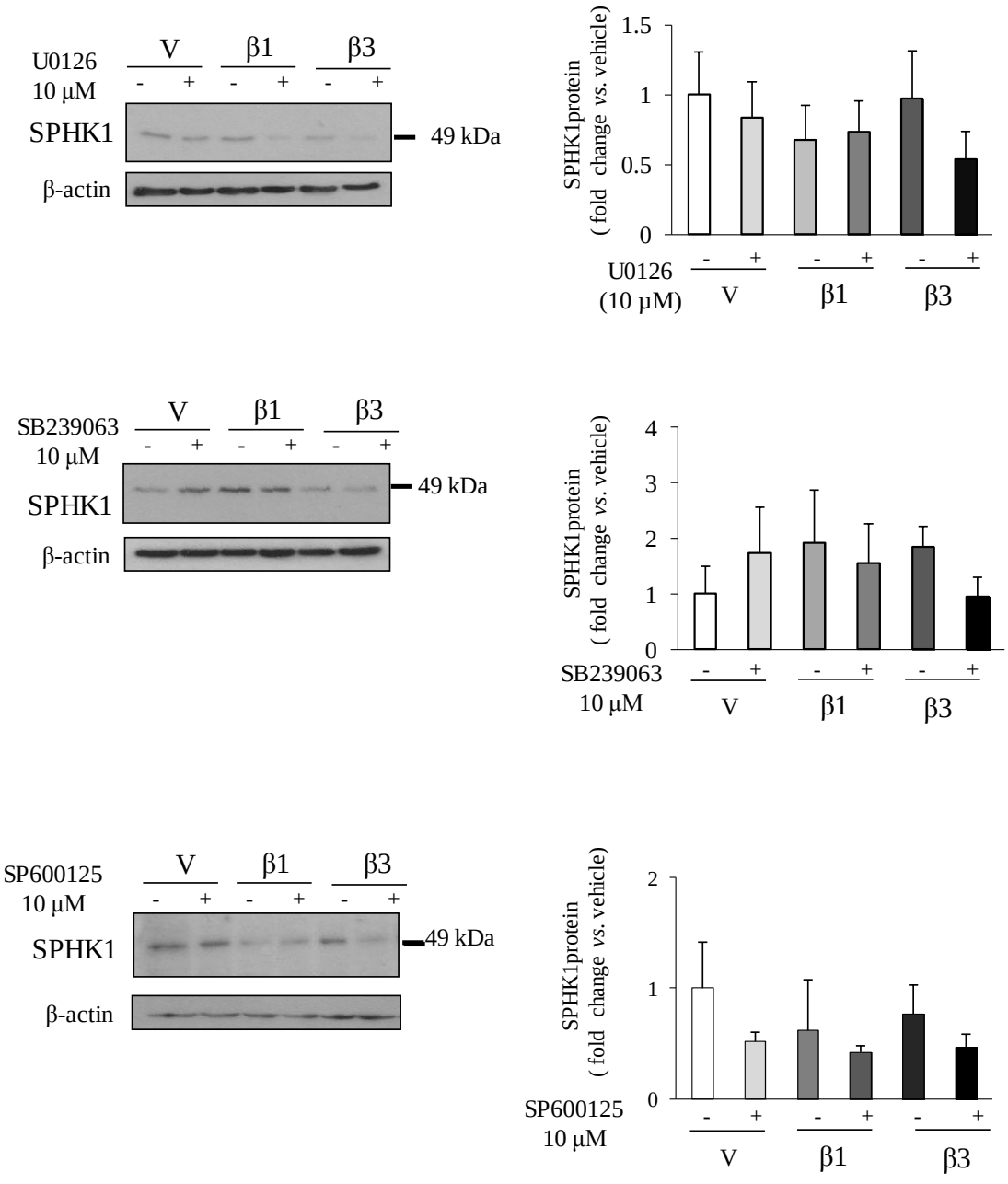

Figure 3.22 SPHK1 expression in JEG3 cells following inhibition of MAPK pathways

Immunoblot analysis revealed no changes in SPHK1 expression in JEG3 cells treated with pharmacological inhibitors of ERK (U0126), p38 (SB239063), or JNK (SP600125) relative to control vehicle or TGFβ1 or β3 treatment groups. (n=3 separate experiments, performed in duplicate).

Chapter 4

4 Discussion

I report, for the first time, that sphingolipid metabolism is altered in IUGR placentae (89). In particular I found that an accumulation of SPH in IUGR is secondary to the enhanced processing of CER by AC and impaired expression and function of SPHK1. Moreover, I show that TGFβ1 and β3 are responsible for altering AC and SPHK1 expression. Importantly, TGFβ1 and β3 utilize different downstream signalling pathways whereby ALK5 signalling regulates AC expression and ALK1 signalling regulates SPHK1 expression. Of clinical significance, ALK5 expression and activation is enhanced in IUGR placentae.

Sphingolipid accumulation characterizes several human pathologies. Classical sphingolipid storage disorders are caused by rare, genetic alterations in key sphingolipid regulatory enzymes (90). For instance, Niemann-Pick disease is due to mutations in the gene encoding ASM (*SMPD1),* leading to lysosomal accumulation of SM (91). Symptoms of this disease include enlargement of the spleen and/or liver, osteoporosis, pulmonary insufficiency, and cardiovascular disease (91). Conversely, Farber disease is a fatal disorder due to inherited deficiencies in AC (*ASAH1*), and subsequent accumulation of CERs in the lysosome (72). This disease is associated with impaired cognitive function, swollen joints, and hoarseness. Disrupted sphingolipid metabolism has also been implicated in complex diseases such as cancers, diabetes, and Alzheimer's disease (92). Specifically, increased S1P levels due to SPHK1 overexpression have been documented in stomach, lung, brain, colon, kidney, prostate, and breast cancers as well as non-Hodgkin's lymphoma (93). In contrast, accumulation of pro-death CERs has been implicated in the pathogenesis of obesity and type 2 diabetes (94). Lastly, Alzheimer's disease is

characterized by SPH accumulation in the brain due to enhanced AC processing of CER and reduced S1P synthesis by SPHK1 (95). To my knowledge I am the first to report disrupted sphingolipid metabolism in IUGR.

Fetal sex has been shown to influence gene expression in the human placenta thereby affecting fetal development (Cvitic, S et al., Plos One, 2013). For instance, male fetuses have an increased risk of perinatal mortality and are generally larger than female fetuses. Furthermore, during complicated pregnancies, males generally have poorer outcomes than females and are more inclined to develop metabolic disorders later in life. This is likely attributed to the expression of sex-specific hormones that are capable of impinging on a variety of signalling pathways. Interestingly, a pilot study conducted in our laboratory revealed no changes in sphingolipid levels in the placental tissue of male fetuses relative to that of female fetuses. Hence, we reason that SPH accumulation in IUGR is independent of fetal sex.

Sphingolipids function as key bioactive mediators in cell signalling events (4). Of critical importance is the balance between pro-death CERs and SPH, and pro-survival S1P, which is tightly regulated via the action of specific sphingolipid regulatory enzymes. Namely, acid ceramidase catalyzes the hydrolysis of CERs into SPH and free fatty acids. Its overexpression has been implicated in contributing to the onset of several malignancies including prostate cancer and melanoma (76,96). *In vitro* studies conducted in murine L929 fibosarcoma cells indicate that AC overexpression leads to decreased endogenous ceramide levels as well as the suppression of apoptosis induced by the tumour necrosis factor alpha (TNFα) signalling pathway (97). Moreover, enhanced AC processing of CER results in increased levels of SPH, the precursor for S1P production by SPHK1. In cancers, S1P is considered as a “tumour promoting” lipid that stimulates cell growth, cell motility, and angiogenesis causing cells to acquire a malignant

phenotype (4,9). Enhanced AC processing of CER in IUGR may be indicative of an adaptive mechanism whereby the placenta attempts to promote trophoblast cell survival by increasing S1P production. However, the placenta fails due to deficiencies in SPHK1 expression, thereby resulting in the accumulation of pro-death SPH. A similar sphingolipid prolife was observed in Alzheimer's disease, which is associated with increased neuronal cell death (95). Hence, it is possible that SPH accumulation, in part, contributes to the accelerated trophoblast cell turnover that is typical of IUGR.

During pregnancy SPHK1 expression is thought to mediate the growth and differentiation of uterine tissues (8,54,55). In pregnant rat models, an approximate 30-fold increase in SPHK1 expression was observed in the glandular epithelium, vasculature, and myometrium in response to rising progesterone levels (54). Disruptions to the SPHK1 gene caused defective decidualization with poor blood vessel formation, resulting in miscarriage (54). Female, homozygous knockouts for SPHK1 (*Sphk1*$^{-/-}$) also presented with a massive accumulation of sphingosine in the uterine tissues (7). This was accompanied by increased decidual cell death, reduced proliferation of stromal cells, and breakage of decidual blood vessels. Similarly, pregnant ewes expressed high levels of SPHK1 in the uterine vasculature, as well as in the trophectoderm cells and epithelial syncytium, supporting a role for SPHK1 in uterine/placental angiogenesis (55). In line with these studies, my findings underscore the importance of SPHK1 expression in reproductive tissues.

Although I have focused on sphingolipid metabolism in trophoblast cells, impaired SPHK1 expression/activity in IUGR may also have implications on blood vessel formation in the human placenta. It is well established that S1P is a potent angiogenic factor that stimulates endothelial cell invasion and sprouting *in vitro* (98). During human pregnancy S1P has also been

shown to regulate the vascular tone of arteries from the chorionic plate and stem villous (99). Reduced S1P production by SPHK1 may therefore contribute to the shallow trophoblast invasion and hypovascular phenotype typical of IUGR placentae. Future studies using placental endothelial cells are required to further explore this hypothesis.

In the context of the human placenta, bioactive sphingolipids have been shown to affect trophoblast differentiation and syncytialization. In culture, human term cytotrophoblasts display high levels of endogenous CER at the onset of differentiation, but very low levels of CER upon syncytialization, coinciding with an increase in the CER metabolizing enzyme AC (6,53). Additionally, treatment of primary isolated cytotrophoblast cells with exogenous sphingosine or an inhibitor of SPHK1 also inhibited trophoblast differentiation as measured by decreased levels of human chorionic gonadotropin (hCG) secretion (6). Hence, my finding of disrupted AC/SPHK1 expression in the trophoblastic layer of placental villi from IUGR pregnancies may also add to the altered rates of trophoblast differentiation and syncytialization observed in IUGR.

Of clinical relevance, the sphingolipid profile that I found in IUGR is in stark contrast to that of preeclampsia (PE), which is characterized by an accumulation of CERs due to the impaired expression and processing of AC in the placentae (*Melland-Smith, M., manuscript under consideration*). Similar to IUGR, PE can arise due to placental insufficiency, which is characterized by accelerated cell death and turnover, leading to the excessive shedding of syncytial debris into the maternal circulation (30,48). Previously obtained data from my laboratory showed that C16 ceramide treatment of human choriocarcinoma JEG3 cells resulted in increased cell death and autophagy. As SPH is also a potent cell death inducer (100), PE and IUGR may utilize different sphingolipid pathways to contribute to the increased cell death and turnover typical of both pathologies. This is consistent with a report demonstrating that the E3

ubiquitin ligase MULE (Mcl-1 Ubiquitin Ligases E3) differentially targets myeloid cell leukemia factor 1 (Mcl-1) and tumor suppressor p53 for degradation in PE and IUGR to promote apoptosis via two different mechanisms (61,65). Thus, my data lends further support to the notion that PE and IUGR have distinct molecular signatures.

While the majority of studies have focused on characterizing the sphingolipid profile in disease states, studies have failed to systematically define the mechanism(s) responsible for altered sphingolipid metabolism. In the present study I used human villous explants and human choriocarcinoma JEG3 cells to demonstrate a role for TGFβ1 and β3 in the regulation of AC in the human placenta. To my knowledge I am the first to report a direct TGFβ-mediated upregulation of AC expression in any cell system. My *in vitro* studies revealed an early inductive effect on the AC gene (*ASAH1*) in JEG3 cells following 3 and 8 hours of TGFβ1 or β3 treatment, but a decrease at 24 hours when AC protein expression increased. This discrepancy may be explained by the TGFβ biphasic effect, meaning that after 8 hours of exposure, TGFβ was no longer stimulatory but inhibitory (101). This is consistent with the body of literature that suggests TGFβ effects are dose- and time- dependent (101,102). Additionally, previous work conducted using the rat insulinoma cell line, INS-1 β-cells, showed that cytokine treatment leads to biphasic changes in AC activity leading to early and late phases of SPH production (103). The authors conclude that the biphasic regulation of sphingolipid metabolites by cytokines may be ubiquitous given that IL-1β and TNF-α stimulation of rat mesangial cells also resulted in the transient activation of neutral sphingomyelinase, and a delayed second increase hours after treatment (104). Although there are currently no commercially available kits to measure AC activity, future studies warrant the investigation of AC activity in response to TGFβ1 and β3 treatment.

I also observed the unique TGFβ3-mediated redistribution of AC to the plasma membrane and tight junctions of JEG3 cells. In the human placenta, tight junctions between polarized progenitor cytotrophoblast cells maintain these cells in an undifferentiated state; whereas the loss of tight junctions is accompanied by CT cell differentiation and fusion, which are needed to form the syncytium. A key regulator of trophoblast cell fusion is partitioning defective protein 6 (Par6), which is involved in the establishment and maintenance of tight junctions (84). Recently, Par6 was shown to bind to CER enriched compartments in the plasma membrane of primitive ectoderm cells, inducing the formation of an apicolateral polarity complex (105). Investigators also found that depletion of CERs by inhibition of ceramide *de novo* synthesis prevented formation of the primitive ectoderm layer (41). Together these studies suggest that CERs in conjunction with Par6 are functionally involved in regulating embryonic cell polarity. Intriguingly, TGFβs have also been shown to regulate Par6 activation, leading to loss of tight junctions during cancer progression (40). It is therefore possible that TGFβ3 plays a role in enhancing AC processing of CER at the tight junctions to regulate trophoblast cell polarity. Future studies are required to explore this hypothesis.

Although I am the first to report a TGFβ-mediated regulation of AC expression, it was previously reported that TGFβ1 upregulates the activity and expression of SPHK1 in human cardiac, lung, and skin fibroblasts (106-108). This is in stark contrast to my findings in JEG3 cells, an epithelial-like cell line, which showed no changes in SPHK1 expression following TGFβ1 treatment. This discrepancy may be explained by the cell type-specific effects of TGFβs (15). For instance, TGFβs have been shown to inhibit lymphocyte and epithelial cell proliferation (109), but stimulate mesenchymal and fibroblast cell growth and proliferation (110,111). Interestingly, enhanced S1P production due to a TGFβ1-mediated upregulation of SPHK1 expression/activity in fibroblasts has been shown to stimulate cell proliferation (106). While, my

finding of a TGFβ3-mediated downregulation of SPHK1 in JEG3 cells is consistent with TGFβ inhibitory effects on epithelial cell proliferation.

There is currently no literature considering a role for TGFβ3 in sphingolipid metabolism; and yet TGFβ3, not TGFβ1, significantly reduced SPHK1 expression in JEG3 cells. Although TGFβ1 and TGFβ3 isoforms share high structural homology and an overlap in function (28), TGFβ3 has been shown to be an important regulator of placentation (17,29,52). In contrast to TGFβ1 and TGFβ2, TGFβ3 has a unique pattern of developmental regulation as it is highly expressed between 7 and 8 weeks of gestation but declines dramatically around 10 weeks as oxygen tension rises (17). This is likely due to the inhibitory effects of TGFβ3 on trophoblast cell differentiation and invasion during early placental development (17). As S1P is known to promote cell differentiation and growth, the TGFβ3-mediated downregulation of SPHK1 expression may be to prevent S1P production in trophoblast cells (4). Given that I observed no changes in response to TGFβ1, this finding also reinforces the notion that TGFβ3 has important and distinctive functions from other TGFβ isoforms in the human placenta.

Another issue to consider is the potential for cross-talk between bioactive lipid mediators and TGFβ signalling cascades (106). For instance, TGFβs and S1P have both been shown to induce Smad2 and Smad3 phosphorylation in primary isolated human keratinocytes (112). It was further demonstrated that Smad2/3 phosphorylation by S1P required crosstalk between S1P and TGFβ receptors. In contrast, S1P-mediated Smad1/2 phosphorylation in renal mesangial cells was found to be S1P receptor-independent (113). The authors conclude that this discrepancy is likely caused by differential TGFβ signalling in these cell types (106). Lastly, S1P was shown to phosphorylate and activate ERK1/2 proteins in renal mesangial cells, thereby mimicking the

effects of TGFβs (113). It would therefore be interesting to examine the interplay between S1P and TGFβ signalling in JEG3 cells.

TGFβs regulate gene expression by binding to a heterodimeric complex of type I and type II serine threonine kinase receptors thereby activating intracellular Smad proteins **(Figure 1.5)**. In most cell systems, TGFβs signal via ALK5/Smad2/3 pathway; however, recent studies on endothelial cells have demonstrated that TGFβ1 and β3, but not TGFβ2, can bind to and transduce signals via ALK1/Smad1/5 pathway in addition to ALK5 (114). Remarkably, these pathways have opposing downstream effects on endothelial cell behaviour whereby ALK1 stimulates endothelial cell migration and proliferation, while ALK5 inhibits these processes. Moreover, the ALK1 and ALK5 pathways activate different downstream targets (36), which is consistent with my findings of an ALK5-mediated effect on AC, but an ALK1-dependent regulation of SPHK1 in the human placenta.

Studies aimed at establishing the mechanism regulating ALK1 and ALK5 activation in endothelial cells have found that ALK1 activity is dependent on ALK5 expression, as it recruits ALK1 into the TGFβ signalling complex (37). Moreover, ALK5 activity is needed for optimal ALK1 activation; however, ALK1 signalling directly inhibits ALK5 activation of Smad2/3 in order to exert its biological function (37). The decision for TGFβ to activate the ALK5 or ALK1 pathway likely depends on the expression levels, ratio, and functionality of these receptors on endothelial cells (87). Endoglin, a TGFβ accessory receptor, might also function to maintain the balance between the positive and negative regulation of angiogenesis by ALK1 and ALK5, respectively (114). Interestingly, inherited deficiencies in ALK1 and endoglin have been linked to the human vascular disorder hereditary hemorrhagic telangietctasia (HHT), which is clinically characterized by localized vascular arteriovenous malformations (115,116). Hence, the balance

between ALK1 and ALK5 signalling may play an important role in the development of human pathology.

Despite being predominately expressed on the surface of endothelial cells, ALK1 and endoglin are both expressed on trophoblast cells during the early stages of placental development (117,118). Specifically, endoglin is transiently upregulated on trophoblast cells differentiating along the invasive pathway, and was shown to contribute to the TGFβ1 and β3-inhibitory effects on trophoblast outgrowth and migration (118). Remarkably, IUGR is associated with significantly increased levels of TGFβ3 and endoglin expression in the placenta (60). Moreover, our laboratory found increased ALK5 expression and Smad2 phosphorylation in IUGR placentae. Hence, it is possible that in IUGR, TGFβ1 and β3, with or without the aid of Endoglin, preferentially bind and activate ALK5 and Smad2 signalling, thereby increasing AC processing of CER into SPH **(Figure 4.1)**. This may be accompanied by deficient ALK1 signalling via Smad1 resulting in impaired SPHK1 expression/activity and SPH accumulation **(Figure 4.1)**. Future studies warrant the investigation of ALK1 expression and activity in IUGR.

4.1 Conclusion

Although great efforts have been made to characterize the regulatory mechanisms of sphingolipid metabolism in a variety of cell systems, its regulation in the human placenta remains elusive. Herein, I used a systematic approach to demonstrate a novel role for TGFβ1 and TGFβ3 in regulating sphingolipid metabolism in the human placenta. I found that TGFβ1 and β3 utilize different downstream signalling pathways to upregulate AC expression and downregulate SPHK1 expression, mimicking the expression profile observed in IUGR placentae. I therefore reason that altered TGFβ signalling may, in part, contribute to pro-death SPH accumulation in IUGR placentae, which may, in turn, contribute to altered trophoblast cell turnover typical of this pathology.

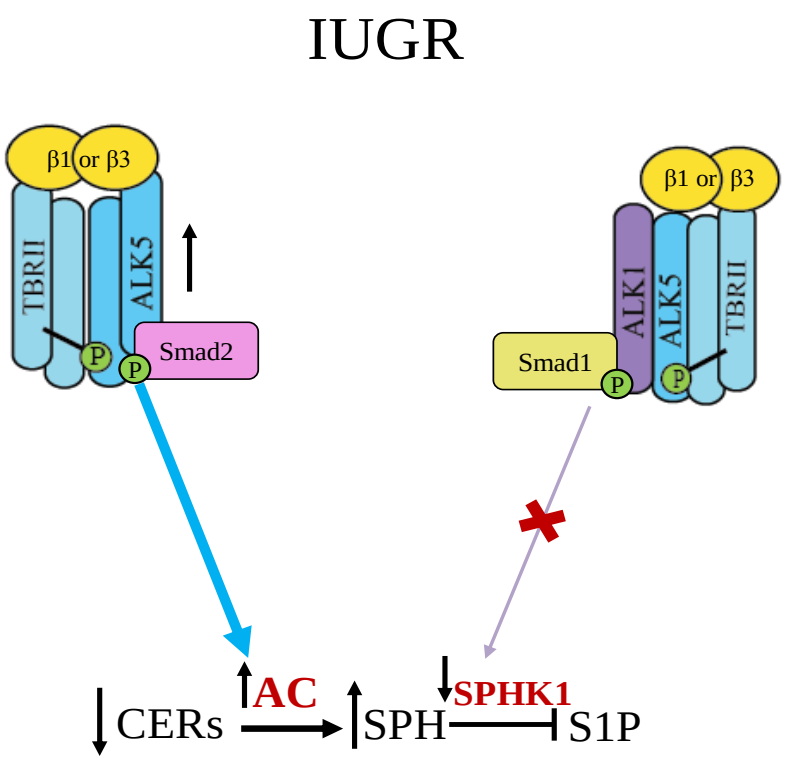

Figure 4.1 Putative model of TGFβ1 or β3 effect on sphingolipid metabolism in IUGR

Canonical TGFβ signalling involves TGFβ binding to a TβRII and activin receptor-like kinase 1 (ALK1) or ALK5, which in turn phosphorylate and activate distinct intracellular Smad proteins that regulate gene expression. In IUGR, increased ALK5 expression may lead to the preferential activation of Smad2 thereby increasing AC expression and enhancing ceramide (CER) processing into sphingosine (SPH). This may be accompanied by deficient ALK1 signalling via Smad1, 5, 8 thereby suppressing SPHK1 expression. As a result, SPH fails to be converted into S1P by SPHK1 contributing to increased SPH levels in IUGR.

Chapter 5

5 Future Directions

5.1 Is sphingosine detectable in the maternal circulation?

The complex structure of sphingolipids allows them to be largely amphiphilic in nature (119). This allows for lipids to exist in a dynamic equilibrium between plasma membrane molecules and free monomers present in the extracellular environment and circulation. In fact, in most living organisms significant amounts of sphingolipids have been detected in the serum and cerebrospinal fluid as components of serum lipoproteins or associated with albumin (120,121). The presence of sphingolipids in biological fluids has served as a platform to study their role as contributors in the manifestation of diseases such as diabetes, cardiac disease, and inflammation. Specifically, increased SPH levels were observed in the sera of patients suffering from coronary artery disease (122). The authors concluded that SPH accrual may contribute to the inflammation and/or ischemic injury associated with this disease. Further, type 2 diabetes patients were found to have increased plasma SPH and sphinganine (55% and 45%, respectively) levels relative to healthy subjects, which were attributed to increased *de novo* synthesis of CER and enhanced CER processing (123). Our laboratory has also recently detected elevated CER levels in the sera of preeclamptic patients (*Melland-Smith, M., manuscript under consideration*). Resultantly, blood sphingolipid levels have been considered as a potential biomarker in the diagnosis of diseases associated with dysregulated sphingolipid metabolism (124). As SPH was demonstrated to accumulate in IUGR placentae, I should now consider whether SPH could be used as a sensitive biomarker for IUGR. To test these hypotheses I would first need to obtain blood samples from consenting patients, and subsequently perform lipidomics analysis by HPLC-MS/MS to analyze the sphingolipid composition. If SPH is detectable and elevated in the sera of IUGR patients, one could consider the long-range usage of SPH as a biomarker for IUGR.

However, that would require that SPH offers high levels of specificity and sensitivity, and that the gestational age at which it is detected permits earlier diagnosis.

5.2 Are changes in CER/SPH content spatially localized in IUGR placentae?

Lipid microdomains (*i.e.*, lipid rafts), rich in cholesterol, long-chain saturated fatty acids, and importantly sphingolipids, are involved in specialised pathways of protein/lipid transport and signalling (125). In particular, lipid rafts strategically cluster transmembrane proteins, glycosylphosphatidylinisotol-anchored proteins, and raft receptor proteins that play central roles in the maintenance of the balance between cell proliferation and cell death. Studies show that TGFβ responsiveness can be either potentiated or suppressed by altering the cell-surface environment and plasma membrane components (126). Moreover, TGFβ downstream targets such as matrix metalloproteinases, which trigger extracellular-matrix remodelling and tumour invasion, are also associated with lipid rafts (127). Hence, my finding of TGFβ3-mediated redistribution of AC to the plasma membrane and tight junctions of JEG3 cells **(Figure 3.6)** may have implications on lipid microdomain composition thereby affecting TGFβ signal transduction events. It would therefore be of interest to define the spatial localization of CER turnover in TGFβ3-treated JEG3 cells as well as IUGR placentae. To do so I could isolate lipid detergent resistant membranes (DRMs) from TGFβ1 or β3-treated JEG3 cells and placental tissue using sucrose density gradient centrifugation followed by lipid extraction. Using defined markers of lipid rafts (*e.g.*, Flotillin-1/2 and Caveolin-1) and non-lipid raft markers (*e.g.*, human transferase), I could next distinguish insoluble fractions (lipid microdomains) from soluble fractions. Using the insoluble fractions I could examine AC protein levels by Western blotting, and sphingolipid content by lipidomics analysis using HPLC-MS/MS. These findings may

further clarify the mechanism by which TGFβ3 regulates AC expression and indicate whether AC functions on non-lysosomal ceramide.

5.3 Does TGFβ have a direct genetic regulation over AC and SPHK1?

In the present study I observed an early induction of *ASAH1* mRNA levels, and a reduction in *SPHK1* mRNA levels following TGFβ1 and β3 treatment of JEG3 cells. While I have demonstrated a role for ALK5 and ALK1 signalling in the regulation of AC and SPHK1 protein levels, it would be of interest to define this mechanism of regulation at the mRNA level. Upon phosphorylation, receptor-regulated Smad proteins typically form complexes with co-Smad proteins that are capable of translocating to the nucleus (14). Within the nucleus this complex binds to DNA via the Smad MH1 domain thereby interacting with a number of transcriptional cofactors to enhance or suppress gene expression (128). Accordingly, target genes have Smad-responsive promoter regions that contain one or more Smad binding elements (SBE), which are specific oligonucleotide sequences. Originally defined as 5′-GTCAGAC-3′ (129), SBE was later shown to be 5′-GTCT-3′, or its complement 5′-AGAC-3′, and in many instances this sequence may contain an extra base (128,130). Hence, the MH1–SBE complex consists of Smads that recognize the 5′-GTCT-3′ sequence through the β-hairpin in the MH1 domain (128,130). Direct binding of Smad4/1/5 to GC-rich sequences has also been observed in oligonucleotide binding assays and so GC-rich regions are sometimes referred to as "Smad1-binding elements" (131). However, the original Smad1-binding element defined in vertebrates is a canonical SBE (132). I therefore thought to perform an *in silico* analysis of the *ASAH1* and *SPHK1* promoter regions to determine putative SBEs. Remarkably, rudimentary analysis of the *ASAH1* promoter revealed approximately 8 SBEs clustered closely to the 5′ region of the promoter **(Figure 5.1)**. Further, the putative *ASAH1* promoter region was previously

5′-------TGCCCTGCTCTCCTTAACTAAATACTTTGTCTATTAATACTTCTTTCTTCTTTTCCCCTT
GTTCTTTCTGTGCCAGACCCACACACGTCTGCTGTAATTGAACATGCCAGGCACATTCTC
CATTTAAAGCCTTTTAACAGCTGCTGTCTCTGCCTAGAATACTCTTACTTGGGCACACAC
AAAACTAGCTTCCTGGTCTCCCTCAACTGTCTGCTCAAACTTCACCTCCTTAATCATGTC
TATCTGTCCCTCTTATTTAAAATTGTAACTCTACCACTTCTGATCTCCACACTTGATGCC
CCTGGCCTCCCTTTTCCTCCACTGCATTTGTCACTAACATCCCGTATAATTTTCTTAGGT
ATTATGTTTATTGCCCATTTCTCACCGAGAACATACGCCTCAGGGTGGAAGAAGTTTGTC
TTTTTGTTGTTGTTCACTGCTTATCCCCAGTGTCAGGAGACATGCTTGGCACATTGTAGG
TCCGCAGTAAATATTTTTTGAATTAATAAAGAATATTTCTACCATCTGCTAGCTTACTGT
TCATGCAGGAGCTCAAATGTGCTTTAAGCATGTGATATGTTTCAAAAGTCAAACTTCATC
CTTAGGGAGAACACTGTCATCTTCTCCTCCTTTAAAAAAAAAAAAATAGGAAAAAAAGCAA
AACAAAACATCACCTTCTCATTTCCCCACCTCCAACAAAAAGAGTGTTGAGTTTTCTAAA
GAAATAATACAAATGGATAAAACTGCAATTTGTTGTCCTTTCTCTCACATGCAAAAAGAA
AAGAAAAAATACTGCCGAGATTTCGGCAGCGTGCTGAGCTTCATCAAAGCATTAAAACAA
TGCTGCTTGAGACGTCAGAGGCTCATCCAGGAAGTGCAACCCAGAGGGCAGGATTTCCTG
CTGGACTTTGAAATCCAACCCGGTCACCTACCCGCGCGACTGTGTCCACGGATGGCACGA
AAGCCAAGCGAGTCCCCCTGCCGAGCTACTCGCGTCCGCCTCCTCCCAAGCTGAGCTCTG
CTCCGCCCACCTGAGTCCTTCGCCAGTTAGGAGGAAACACAGCCGCTTAATGAACTGCTG
CATCGGGCTGGGAGAGAAAG------3′

Figure 5.1 Putative Smad binding elements (SBE) present in the *ASAH1* gene promoter

In silico analysis of the AC gene (*ASAH1*) promoter region revealed 7 putative SBEs. Specifically, four 5'-GTCT-3' sites and three 5'-AGAC-3' sites. The above promoter sequence was obtained from SwitchGear Genomics company's online website: (http://switchgeargenomics.com/genecards.php?id=701467).

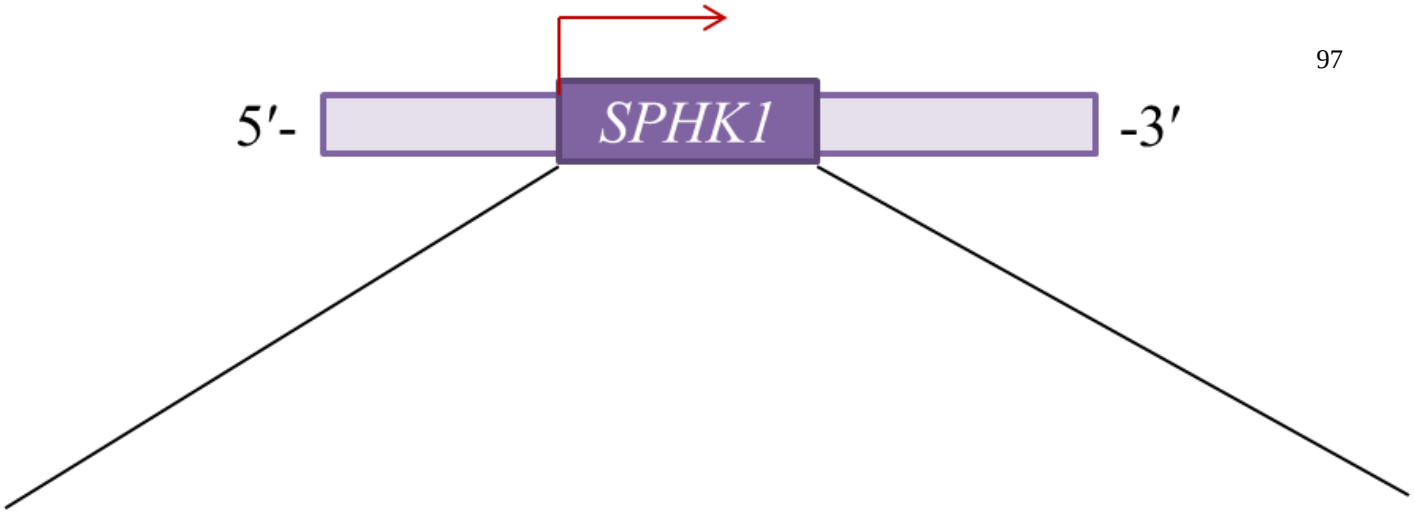

5′---TTGACCTTCAGAAGACAAGCCTCCAGGGGAGGGGAATTTCTATTTTTTGGCATGTGGATA
ATGAACACAGGGGAGGGCAATCCCTGCTCCGGGCTCCATGTCTTTTTCCAGCTTGTCAAA
ATAGGACGTCCACACCCTCCTTTGCCCCCAAGTCCCCCCACTAATTGGCATCAATCGAGG
AAGTCTGAGCGACTGCATGTTTAGGTAAAAGAGGAAAGGGGTGGGGTGGGGCGCAGTGGC
TCACGCCTGTAATCCCAGCACTTTGGGAGGCCGAGGCGGGCAGATCACAAGGTCAGGAGT
TCGAGACTGGCCTGAACAACATGGAGAAACACCGTCTCTACTAAAAATATAAAAATTAGC
CGGGCATGGTGGTGCATGCCTGTAATCCCAGCTACTCAGGAGGCTGAGGCAGGAGAATCG
CTTGAACCCAGGAGACGGAGGTTGCAGTGAGCCAAGATTGCGCCACTGCACTCCAGCCTG
GGTGACAGAGCAAGACTCCATCTCAAAAAAAAAAAAAAAAAAAAAATAGAGGAAAGGAGT
GAACCCCTGAGTGGCCAGCTGGGTGCCTCAACGGGGTGTCTCCAAAGGCAGCTTGTGCTT
GTTTGTGACCAGGGTGACAAAGGACTTCACTGTCCTGTAGCACAGATGAGGTTCCACCCT
CAGGTGGGTGGAAACAGCCCAGGCCATTAGTGCAAATCCCCTGCCTGGCCCAGGGCCACG
TTCAGCCCACTGTCTGTTTGCTTTGGGACCCACCCAAGGTCACATTTTAGCTTTTGAGAA
ATGTGAAAGTGGAAAACATTGCAAAACAAAAAGCCCCTGGAAAACTGTGCACACACCCAT
CCCCTCAGCCTGATGCTCCAGCTTGGCTGCTAGGAGATCAATGCAGCTCTGCCTTCCTGC
TCCCTGTGCAGAGGTGCCGGCTCCTGCTTCCTGGTTCCCAGCTTTCCTTTTGGGAACTGC
CTGAGGTGGTTTGACACACAGCTGTTGGGCTTCTCTTCCCTTGAGGTCTCTGA---3′

Figure 5.2 Putative Smad binding elements (SBE) present in the *SPHK1* gene promoter

In silico analysis of the SPHK1 gene (*SPHK1*) promoter region revealed 10 putative SBEs. Specifically, six 5'-GTCT-3' sites and four 5'-AGAC-3' sites. The above promoter sequence was obtained from SwitchGear Genomics company's online website: (http://switchgeargenomics.com/genecards.php?id=718825).

shown to contain approximately 60% GC content, whereby Smad4/5 have been shown to bind GC rich regions (133). Likewise we detected 10 SBEs throughout the promoter region of *SPHK1* **(Figure 5.2)**. It would therefore be interesting to follow up this analysis with promoter bashing, whereby I would mutate the Smad regulatory elements and assess *ASAH1/SPHK1* transcription by way of luciferase activity and chromatin immunoprecipitation assays.

5.4 Does TGFβ alter the post-translational modifications of AC in IUGR?

The AC enzyme contains six N-linked oligosaccharide chains, which are critical to its lysosomal trafficking and enzyme activation (79). Our laboratory has recently detected alterations in the glycosylation status of AC following exposure to oxidative stress conditions in human villous explants and JEG3 cells. Furthermore, the laboratory detected reduced AC glycosylation and expression in preeclampsia, a disease associated with oxidative stress. We therefore concluded that reactive oxide species in PE disrupted glycosylation events and may contribute to the impaired trafficking and bioactivity of AC in PE. In the present study, I observed a significant upregulation of total AC protein levels in IUGR placentae relative to healthy pre-term controls **(Figure 3.2)**. I also demonstrated a role for TGFβ1 and β3 in the regulation of AC expression. It would therefore be of interest to examine AC glycosylation status in IUGR, and the role of TGFβ1 and β3 in AC glycosylation. To do so, I could perform an immunoprecipitation of AC from placental tissue or TGFβ1 and β3-treated JEG3 followed by immunoblotting for Concanavalin A, a mannose binding lectin that binds specifically to N-linked oligosaccharide chains. If AC glycosylation were affected, I would expect to see changes in Concanavalin A expression between treatments. Samples treated with Tunicamycin, an inhibitor of N-linked glycoprotein synthesis, could be included as a positive control**.**

5.5 Are other points in the sphingolipid metabolic pathway affected in IUGR?

In addition to the *de novo* ceramide synthesis pathway, CERs can be regenerated through the breakdown of sphingomyelin (SM) via acid sphingomyelinase (ASM) in the lysosome (134). ASM is synthesized at the ER as a 75 kDa proform, glycosylated in the Golgi complex, and shuttled to the lysosome where it is cleaved into its mature 70kDa form (10). Inherited deficiencies in the gene encoding ASM (*SMPD1*) are associated with the manifestation of Niemann-Pick disease, a lysosomal storage disorder clinically characterized by SM accumulation in acidic compartments (92). Given the central role of CER in sphingolipid metabolism and the role of ASM in human pathology, it would of interest to examine ASM expression in IUGR placentae, and to define a role for TGFβ1 and β3 in its regulation. Interestingly, I found a significant reduction in *SMPD1* mRNA levels and active (70kDa) ASM protein levels in IUGR relative to PTC placentae **(Figure 5.3a & b)**. To establish TGFβ1 and β3-effect on ASM expression, JEG3 cells were treated with TGFβ1 or β3 (5 ng/ml) or control vehicle for 3, 8, and 24 hours. I found significantly reduced *SMPD1* mRNA levels following exposure to TGFβ1 or β3 at all time points **(Figure 5.4a)**. Notably, I observed significantly reduced active (70kDa) ASM expression in TGFβ1 and β3-treated JEG3 cells **(Figure 5.4b)**. Of clinical significance my *in vitro* data mimicked our observations in IUGR. Using human villous explants, I further demonstrated that overnight incubation with the ALK5 inhibitor, SB431542, significantly enhanced ASM activity **(Figure 5.5)**. These data are indicative of a role for ALK5 signalling in ASM regulation. Together, deficient SM breakdown by ASM, and enhanced CER processing by AC could account for the reduced CER levels in IUGR **(Figure 3.1)**. Future studies are needed to define the precise mechanism by which TGFβ1 and β3 regulate ASM expression, similar to experiments examining AC and SPHK1.

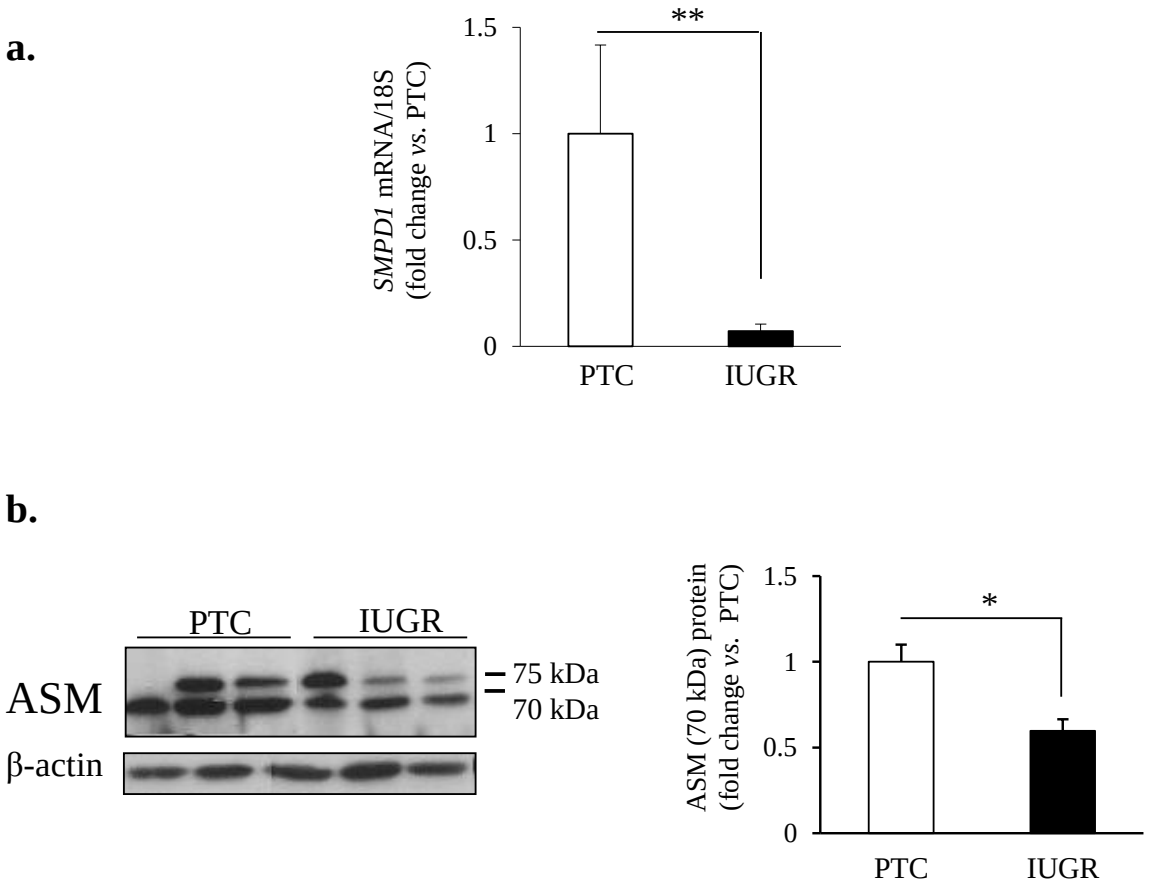

Figure 5.3 ASM expression in placentae from IUGR pregnancies

(a) *SMPD1* mRNA levels in IUGR placentae were significantly decreased relative to PTC placentae, as detected by qPCR. Values were normalized to 18S and expressed as a fold change relative to PTC (IUGR, n=5; PTC, n=8). **(b)** Active (70 kDa) ASM protein expression was significantly decreased in IUGR placentae relative to PTC placentae as detected by Western blotting. Densitometric analysis of ASM active band in IUGR and PTC placentae normalized to β-actin and expressed as a fold change relative to PTC (IUGR n=14; PTC n=11). Statistical significance was determined as *$p<0.05$ and **$p<0.01$ using an unpaired Student's t-test with or without Welch's correction, where applicable.

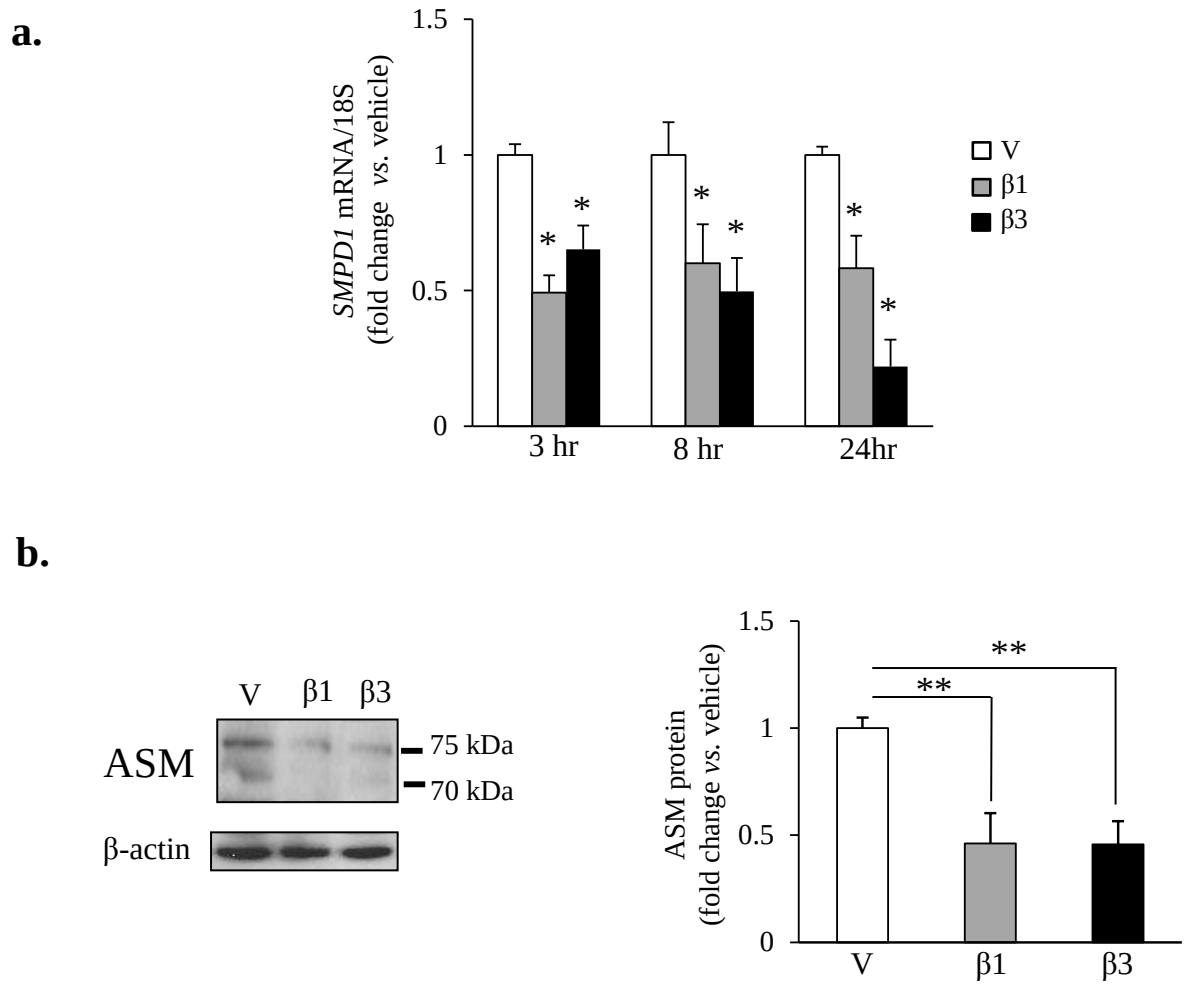

Figure 5.4 ASM mRNA and protein expression in TGFβ1 or β3-treated JEG3 cells

(a) *SMPD1* mRNA levels were significantly decreased in JEG3 cells treated with TGFβ1 or β3 (β1/β3: 5 ng/ml) for 3, 8, and 24 hours (hr) as detected by qPCR. Values were normalized to 18S RNA and expressed as a fold change relative to control vehicle (V)-treated cells (n=3 separate experiments, duplicate). **(b)** Immunoblot analysis showed decreased active ASM protein levels in TGFβ1 or β3-treated JEG3 cells compared to control vehicle-treated cells. Densitometric analysis of ASM expression in TGFβ1 or β3-treated cells normalized to β-actin and expressed as a fold change relative to control vehicle (n=3 separate experiments, performed in duplicate). Statistical significance was determined as *$p<0.05$ and **$p<0.01$ using one-way ANOVA with post-hoc Student-Newman-Keuls test, or two-way ANOVA with post-hoc Bonferroni test, where applicable

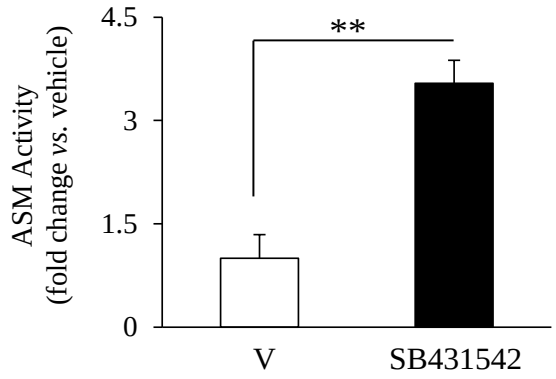

Figure 5.5 ASM activity in human villous explants treated with SB431542

ASM activity was significantly increased in first trimester villous explants following a 24-hour exposure period to ALK5 inhibitor SB431542. Values are expressed as a fold change relative to control vehicle (V)-treated explants (n=5 explants, performed in quadruplicate). Statistical significance was determined as p<**0.01 using unpaired Student's t-test.

5.6 What cell fate outcomes are associated with SPH accumulation in trophoblast cells?

As previously discussed SPH accrual is associated with accelerated cell death, organelle stress, and membrane fragmentation (100). Specifically, SPH has been shown to mediate lysosomal membrane permeablization leading to the release of cathepsins and the initiation of cell death (135). Cells undergo apoptosis via two major pathways, namely the extrinsic pathway (receptor-mediated cell death) or the intrinsic pathway (mitochondrial cell death) (136). However, recent evidence suggests that autophagy may function as an alternative cell death pathway (136). Autophagy is a catabolic process by which cytoplasmic constituents are sequestered by double-membrane vacuoles termed autophagosomes, and delivered to lysosomes for degradation and recycling (137,138). Under stress conditions, such as hypoxia or nutrient deprivation, autophagy promotes cell survival by removing damaged proteins and/or organelles; however, in excess, autophagy can result in caspase-dependent and –independent cell death (136). Interestingly, specific sphingolipid species have been shown to promote opposing autophagic processes, some in favour of cell death whereas others promote cell survival (138). For example, CERs, known to promote apoptosis, have been shown to induce autophagic cell death (138). In contrast, S1P-induced autophagy has been shown to function as a survival mechanism following nutrient deprivation in human breast cancer MCF-7 cells (139). Moreover, our laboratory has recently reported increased autophagy in PE (140), which may, in part, be due to an accumulation of CERs in preeclamptic placentae (*Melland-Smith, M., manuscript under consideration*). As IUGR is associated with altered trophoblast cell turnover, and exuberant shedding of cell death fragments (61) it would be interesting to establish a role for TGFβs via SPH in regulating autophagy in the human placenta.

To do so I first exposed JEG3 cells to TGFβ1 and β3, then examined LC3B (microtubule-associated protein 1 light chain 3) and p62 protein expression (Sequestosome 1), markers of autophagosome formation (23). My preliminary data revealed increased LC3BII and p62 expression at 3 and 8 hours following TGFβ1 and β3 treatment of JEG3 cells **(Figure 5.6a & 6b)**. However, LC3BII and p62 expression decreased 24 hours following TGFβ1 and β3 treatment **(Figure 5.6a & 6b)**. These data indicates that TGFβ1 and β3 induces autophagy in JEG3 cells. However, when autophagosomes fuse with lysosomes and autophagy is complete, LC3B and p62 are degraded and recycled. To show flux through autophagy it is recommended to use an inhibitor of autophagy such as bafilomycin A1 (BafA1), which prevents fusion of the autophagosome with the lysosome. Cells treated with BafA1 should show an accumulation of LC3B, but even more so when the treatment (*ex.* TGFβ1 and β3) induces autophagy. Thus we intend on examining LC3BI/II and p62 expression in the absence and presence of TGFβ1 and β3 and BafA1. In order to link it back to sphingolipids we could impinge on sphingolipid metabolism using pharmacological inhibitors of AC (*ex.* Ceranib-2 (141)) or SPHK1 (*ex.* SK1-I (BML-258) (142)) and examine changes in LC3B and p62. Moreover, we could treat JEG3 cells with exogenous sphingosine with and without TGFβ1 and β3 to determine if TGFβ enhances the sphingosine-mediated effect on cell fate.

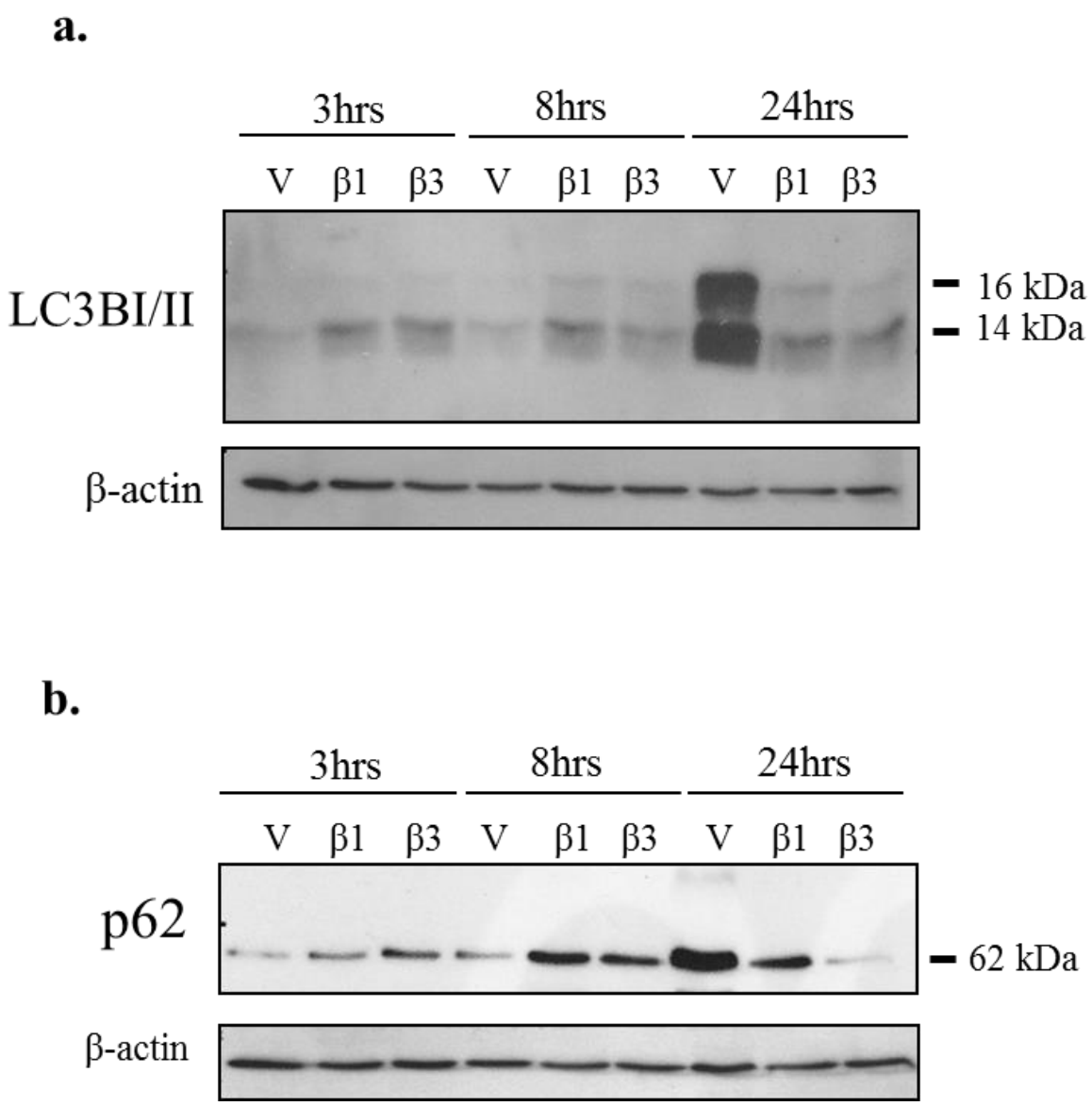

Figure 5.6 AC protein expression in TGFβ1 or β3-treated human choriocarcinoma JEG3 cells

(a) Marker of autophagosome formation, LC3BII (14 kDa), was increased in JEG3 cells following 3 and 8 hours (hrs) of TGFβ1 or β3 treatment as indicated by Western blotting**.** Twenty-four hour exposure to TGFβ1 or β3 reduced LC3BII levels relative to control vehicle (V)-treated cells (n=1, performed in duplicate) **(b)** The p62 protein is a ubiquitin scaffold binding protein that may link proteins targeted for degradation to the autophagic machinery. Protein levels of p62 were increased at 3 and 8 hours of TGFβ1 or β3 treatment, but decreased at 24 hours as compared to control vehicle-treated JEG3 cells (n=1, performed in duplicate).

References

1. Thudichum, J. L. W. (1884) *A Treatise on the Chemical Constitution of the Brain*, Bailliere, Tindall, and Cox, London, UK

2. Gault, C. R., Obeid, L. M., and Hannun, Y. A. (2010) *Adv Exp Med Biol* **688**, 1-23

3. Kolter, T. (2011) *Chem Phys Lipids* **164**, 590-606

4. Hannun, Y. A., and Obeid, L. M. (2008) *Nat Rev Mol Cell Biol* **9**, 139-150

5. Oskouian, B., and Saba, J. D. (2010) *Adv Exp Med Biol* **688**, 185-205

6. Singh, A. T., Dharmarajan, A., Aye, I. L., and Keelan, J. A. (2012) *Mol Cell Endocrinol* **362**, 48-59

7. Mizugishi, K., Li, C., Olivera, A., Bielawski, J., Bielawska, A., Deng, C. X., and Proia, R. L. (2007) *J Clin Invest* **117**, 2993-3006

8. Kaneko-Tarui, T., Zhang, L., Austin, K. J., Henkes, L. E., Johnson, J., Hansen, T. R., and Pru, J. K. (2007) *Biol Reprod* **77**, 658-665

9. Hannun, Y. A., and Bell, R. M. (1989) *Science* **243**, 500-507

10. Hannun, Y. A., Luberto, C., and Argraves, K. M. (2001) *Biochemistry* **40**, 4893-4903

11. Rosen, H., Gonzalez-Cabrera, P. J., Sanna, M. G., and Brown, S. (2009) *Annu Rev Biochem* **78**, 743-768

12. Roberts, A. B., and Sporn, M. B. (1992) *Mol Reprod Dev* **32**, 91-98

13. Roberts, A. B., Flanders, K. C., Heine, U. I., Jakowlew, S., Kondaiah, P., Kim, S. J., and Sporn, M. B. (1990) *Philos Trans R Soc Lond B Biol Sci* **327**, 145-154

14. Wrana, J. L., Attisano, L., Wieser, R., Ventura, F., and Massague, J. (1994) *Nature* **370**, 341-347

15. Piek, E., Heldin, C. H., and Ten Dijke, P. (1999) *Faseb J* **13**, 2105-2124

16. Massague, J., Blain, S. W., and Lo, R. S. (2000) *Cell* **103**, 295-309

17. Caniggia, I., Grisaru-Gravnosky, S., Kuliszewsky, M., Post, M., and Lye, S. J. (1999) *J Clin Invest* **103**, 1641-1650

18. Roberts, A. B., Kim, S. J., Kondaiah, P., Jakowlew, S. B., Denhez, F., Glick, A. B., Geiser, A. G., Watanabe, S., Noma, T., Lechleider, R., and et al. (1990) *Annals of the New York Academy of Sciences* **593**, 43-50

19. Marquardt, H., Lioubin, M. N., and Ikeda, T. (1987) *J Biol Chem* **262**, 12127-12131

20. ten Dijke, P., Geurts van Kessel, A. H., Foulkes, J. G., and Le Beau, M. M. (1988) *Oncogene* **3**, 721-724

21. Barbara, N. P., Wrana, J. L., and Letarte, M. (1999) *J Biol Chem* **274**, 584-594

22. Cheifetz, S., Bellon, T., Cales, C., Vera, S., Bernabeu, C., Massague, J., and Letarte, M. (1992) *J Biol Chem* **267**, 19027-19030

23. Cheifetz, S., Andres, J. L., and Massague, J. (1988) *J Biol Chem* **263**, 16984-16991

24. Dickson, M. C., Martin, J. S., Cousins, F. M., Kulkarni, A. B., Karlsson, S., and Akhurst, R. J. (1995) *Development* **121**, 1845-1854

25. Shull, M. M., Ormsby, I., Kier, A. B., Pawlowski, S., Diebold, R. J., Yin, M., Allen, R., Sidman, C., Proetzel, G., Calvin, D., and et al. (1992) *Nature* **359**, 693-699

26. Sanford, L. P., Ormsby, I., Gittenberger-de Groot, A. C., Sariola, H., Friedman, R., Boivin, G. P., Cardell, E. L., and Doetschman, T. (1997) *Development* **124**, 2659-2670

27. Kaartinen, V., Voncken, J. W., Shuler, C., Warburton, D., Bu, D., Heisterkamp, N., and Groffen, J. (1995) *Nat Genet* **11**, 415-421

28. ten Dijke, P., Hansen, P., Iwata, K. K., Pieler, C., and Foulkes, J. G. (1988) *Proc Natl Acad Sci U S A* **85**, 4715-4719

29. Graham, C. H., Lysiak, J. J., McCrae, K. R., and Lala, P. K. (1992) *Biol Reprod* **46**, 561-572

30. Adelman, D. M., Gertsenstein, M., Nagy, A., Simon, M. C., and Maltepe, E. (2000) *Genes Dev* **14**, 3191-3203

31. Munger, J. S., Harpel, J. G., Giancotti, F. G., and Rifkin, D. B. (1998) *Mol Biol Cell* **9**, 2627-2638

32. Barcellos-Hoff, M. H. (1996) *J Mammary Gland Biol Neoplasia* **1**, 353-363

33. Jullien, P., Berg, T. M., and Lawrence, D. A. (1989) *International journal of cancer. Journal international du cancer* **43**, 886-891

34. Oh, S. P., Seki, T., Goss, K. A., Imamura, T., Yi, Y., Donahoe, P. K., Li, L., Miyazono, K., ten Dijke, P., Kim, S., and Li, E. (2000) *Proc Natl Acad Sci U S A* **97**, 2626-2631

35. Chen, Y. G., and Massague, J. (1999) *J Biol Chem* **274**, 3672-3677

36. Goumans, M. J., Valdimarsdottir, G., Itoh, S., Rosendahl, A., Sideras, P., and ten Dijke, P. (2002) *Embo J* **21**, 1743-1753

37. Goumans, M. J., Valdimarsdottir, G., Itoh, S., Lebrin, F., Larsson, J., Mummery, C., Karlsson, S., and ten Dijke, P. (2003) *Mol Cell* **12**, 817-828

38. Zhang, Y. E. (2009) *Cell Res* **19**, 128-139

39. Kowar, J., Eriksson, A., and Jemt, T. *Clin Implant Dent Relat Res* **15**, 37-46

40. Viloria-Petit, A. M., and Wrana, J. L. (2010) *Cell Cycle* **9**, 623-624

41. Krishnamurthy, K., Wang, G., Silva, J., Condie, B. G., and Bieberich, E. (2007) *J Biol Chem* **282**, 3379-3390

42. Lawler, S., Feng, X. H., Chen, R. H., Maruoka, E. M., Turck, C. W., Griswold-Prenner, I., and Derynck, R. (1997) *J Biol Chem* **272**, 14850-14859

43. Gude, N. M., Roberts, C. T., Kalionis, B., and King, R. G. (2004) *Thromb Res* **114**, 397-407

44. Boyd, J. D. H., W.J. . (1970) *The Human Placenta*, Cambridge

45. Morrish, D. W., Dakour, J., and Li, H. (1998) *J Reprod Immunol* **39**, 179-195

46. Graham, C. H. (1997) *Placenta* **18**, 137-143

47. Ishihara, N., Matsuo, H., Murakoshi, H., Laoag-Fernandez, J. B., Samoto, T., and Maruo, T. (2002) *American journal of obstetrics and gynecology* **186**, 158-166

48. Buurma, A. J., Penning, M. E., Prins, F., Schutte, J. M., Bruijn, J. A., Wilhelmus, S., Rajakumar, A., Bloemenkamp, K. W., Karumanchi, S. A., and Baelde, H. J. (2013) *Hypertension* **62**, 608-613

49. Lysiak, J. J., Hunt, J., Pringle, G. A., and Lala, P. K. (1995) *Placenta* **16**, 221-231

50. Morrish, D. W., Bhardwaj, D., and Paras, M. T. (1991) *Endocrinology* **129**, 22-26

51. Ietta, F., Wu, Y., Winter, J., Xu, J., Wang, J., Post, M., and Caniggia, I. (2006) *Biol Reprod* **75**, 112-121

52. Caniggia, I., Mostachfi, H., Winter, J., Gassmann, M., Lye, S. J., Kuliszewski, M., and Post, M. (2000) *J Clin Invest* **105**, 577-587

53. Singh, A. T., Dharmarajan, A., Aye, I. L., and Keelan, J. A. (2012) *Reprod Biomed Online* **24**, 224-234

54. Jeng, Y. J., Suarez, V. R., Izban, M. G., Wang, H. Q., and Soloff, M. S. (2007) *Am J Physiol Endocrinol Metab* **292**, E1110-1121

55. Dunlap, K. A., Kwak, H. I., Burghardt, R. C., Bazer, F. W., Magness, R. R., Johnson, G. A., and Bayless, K. J. (2010) *Biol Reprod* **82**, 876-887

56. (2013) *Obstetrics and gynecology* **122**, 1122-1131

57. Romanowicz, L., and Bankowski, E. (2010) *Pathobiology : journal of immunopathology, molecular and cellular biology* **77**, 78-87

58. Baig, S., Lim, J. Y., Fernandis, A. Z., Wenk, M. R., Kale, A., Su, L. L., Biswas, A., Vasoo, S., Shui, G., and Choolani, M. (2013) *Placenta* **34**, 436-442

59. (2013) *Obstetrics and gynecology* **121**, 1122-1133

60. Yinon, Y., Nevo, O., Xu, J., Many, A., Rolfo, A., Todros, T., Post, M., and Caniggia, I. (2008) *Am J Pathol* **172**, 77-85

61. Rolfo, A., Garcia, J., Todros, T., Post, M., and Caniggia, I. (2012) *Cell Death Dis* **3**, e305

62. (2002) *Obstetrics and gynecology* **99**, 159-167

63. Mandruzzato, G., Antsaklis, A., Botet, F., Chervenak, F. A., Figueras, F., Grunebaum, A., Puerto, B., Skupski, D., and Stanojevic, M. (2008) *J Perinat Med* **36**, 277-281

64. Pollack, R. N., and Divon, M. Y. (1992) *Clin Obstet Gynecol* **35**, 99-107

65. Newhouse, S. M., Davidge, S. T., Winkler-Lowen, B., Demianczuk, N., and Guilbert, L. J. (2007) *Placenta* **28**, 999-1003

66. Major, M. B., and Jones, D. A. (2004) *J Biol Chem* **279**, 5278-5287

67. Bligh, E. G., and Dyer, W. J. (1959) *Can J Biochem Physiol* **37**, 911-917

68. Tibboel, J., Joza, S., Reiss, I., de Jongste, J. C., and Post, M. (2013) *Eur Respir J* **42**, 776-784

69. Yoo, H. H., Son, J., and Kim, D. H. (2006) *J Chromatogr B Analyt Technol Biomed Life Sci* **843**, 327-333

70. Soleymanlou, N., Wu, Y., Wang, J. X., Todros, T., Ietta, F., Jurisicova, A., Post, M., and Caniggia, I. (2005) *Cell Death Differ* **12**, 441-452

71. MacPhee, D. J., Mostachfi, H., Han, R., Lye, S. J., Post, M., and Caniggia, I. (2001) *Lab Invest* **81**, 1469-1483

72. Sugita, M., Dulaney, J. T., and Moser, H. W. (1972) *Science* **178**, 1100-1102

73. Takahashi, T., Suchi, M., Desnick, R. J., Takada, G., and Schuchman, E. H. (1992) *J Biol Chem* **267**, 12552-12558

74. Summers, S. A., and Nelson, D. H. (2005) *Diabetes* **54**, 591-602

75. Haughey, N. J., Bandaru, V. V., Bae, M., and Mattson, M. P. (2010) *Biochim Biophys Acta* **1801**, 878-886

76. Seelan, R. S., Qian, C., Yokomizo, A., Bostwick, D. G., Smith, D. I., and Liu, W. (2000) *Genes Chromosomes Cancer* **29**, 137-146

77. Crocker, I. P., Cooper, S., Ong, S. C., and Baker, P. N. (2003) *Am J Pathol* **162**, 637-643

78. Shtraizent, N., Eliyahu, E., Park, J. H., He, X., Shalgi, R., and Schuchman, E. H. (2008) *J Biol Chem* **283**, 11253-11259

79. Ferlinz, K., Kopal, G., Bernardo, K., Linke, T., Bar, J., Breiden, B., Neumann, U., Lang, F., Schuchman, E. H., and Sandhoff, K. (2001) *J Biol Chem* **276**, 35352-35360

80. Park, J. H., and Schuchman, E. H. (2006) *Biochim Biophys Acta* **1758**, 2133-2138

81. Xu, G., Chakraborty, C., and Lala, P. K. (2001) *Biochem Biophys Res Commun* **287**, 47-55

82. Chaudhury, A., and Howe, P. H. (2009) *IUBMB Life* **61**, 929-939

83. de Gorter, D. J., van Dinther, M., Korchynskyi, O., and ten Dijke, P. (2011) *J Bone Miner Res* **26**, 1178-1187

84. Sivasubramaniyam, T., Garcia, J., Tagliaferro, A., Melland-Smith, M., Chauvin, S., Post, M., Todros, T., and Caniggia, I. (2013) *Endocrinology* **154**, 1296-1309

85. Ten Dijke, P., Goumans, M. J., Itoh, F., and Itoh, S. (2002) *J Cell Physiol* **191**, 1-16

86. Laping, N. J., Grygielko, E., Mathur, A., Butter, S., Bomberger, J., Tweed, C., Martin, W., Fornwald, J., Lehr, R., Harling, J., Gaster, L., Callahan, J. F., and Olson, B. A. (2002) *Molecular pharmacology* **62**, 58-64

87. Goumans, M. J., Lebrin, F., and Valdimarsdottir, G. (2003) *Trends Cardiovasc Med* **13**, 301-307

88. Pitson, S. M., Moretti, P. A., Zebol, J. R., Lynn, H. E., Xia, P., Vadas, M. A., and Wattenberg, B. W. (2003) *Embo J* **22**, 5491-5500

89. Henckel, E., Luthander, J., Berggren, E., Kapadia, H., Naver, L., Norman, M., Bennet, R., and Eriksson, M. (2004) *Pediatr Infect Dis J* **23**, 27-31

90. Schulze, H., and Sandhoff, K. (2011) *Cold Spring Harb Perspect Biol* **3**

91. Dacremont, G., Kint, J. A., and Cocquit, G. (1973) *The New England journal of medicine* **289**, 592-593

92. Hla, T., and Dannenberg, A. J. (2012) *Cell Metab* **16**, 420-434

93. Pyne, N. J., and Pyne, S. (2010) *Nat Rev Cancer* **10**, 489-503

94. Haus, J. M., Kashyap, S. R., Kasumov, T., Zhang, R., Kelly, K. R., Defronzo, R. A., and Kirwan, J. P. (2009) *Diabetes* **58**, 337-343

95. He, X., Huang, Y., Li, B., Gong, C. X., and Schuchman, E. H. (2010) *Neurobiology of aging* **31**, 398-408

96. Musumarra, G., Barresi, V., Condorelli, D. F., and Scire, S. (2003) *Biol Chem* **384**, 321-327

97. Strelow, A., Bernardo, K., Adam-Klages, S., Linke, T., Sandhoff, K., Kronke, M., and Adam, D. (2000) *The Journal of experimental medicine* **192**, 601-612

98. Su, S. C., and Bayless, K. J. (2012) *Methods Mol Biol* **874**, 201-213

99. Hemmings, D. G., Hudson, N. K., Halliday, D., O'Hara, M., Baker, P. N., Davidge, S. T., and Taggart, M. J. (2006) *Biol Reprod* **74**, 88-94

100. Cuvillier, O. (2002) *Biochim Biophys Acta* **1585**, 153-162

101. Shinar, D. M., and Rodan, G. A. (1990) *Endocrinology* **126**, 3153-3158

102. Allen-Hoffmann, B. L., Crankshaw, C. L., and Mosher, D. F. (1988) *Mol Cell Biol* **8**, 4234-4242

103. Zhu, Q., Shan, X., Miao, H., Lu, Y., Xu, J., You, N., Liu, C., Liao, D. F., and Jin, J. (2009) *FEBS letters* **583**, 2136-2141

104. Kaszkin, M., Huwiler, A., Scholz, K., van den Bosch, H., and Pfeilschifter, J. (1998) *FEBS letters* **440**, 163-166

105. Bieberich, E. (2011) *J Lipids* **2011**, 610306

106. Lebman, D. A., and Spiegel, S. (2008) *J Lipid Res* **49**, 1388-1394

107. Gellings Lowe, N., Swaney, J. S., Moreno, K. M., and Sabbadini, R. A. (2009) *Cardiovasc Res* **82**, 303-312

108. Yamanaka, M., Shegogue, D., Pei, H., Bu, S., Bielawska, A., Bielawski, J., Pettus, B., Hannun, Y. A., Obeid, L., and Trojanowska, M. (2004) *J Biol Chem* **279**, 53994-54001

109. Moses, H. L. (1992) *Mol Reprod Dev* **32**, 179-184

110. Clark, R. A., McCoy, G. A., Folkvord, J. M., and McPherson, J. M. (1997) *J Cell Physiol* **170**, 69-80

111. Kim, D. S., Korting, H. C., and Schafer-Korting, M. (1998) *Pharmazie* **53**, 51-57

112. Sauer, B., Vogler, R., von Wenckstern, H., Fujii, M., Anzano, M. B., Glick, A. B., Schafer-Korting, M., Roberts, A. B., and Kleuser, B. (2004) *J Biol Chem* **279**, 38471-38479

113. Xin, C., Ren, S., Kleuser, B., Shabahang, S., Eberhardt, W., Radeke, H., Schafer-Korting, M., Pfeilschifter, J., and Huwiler, A. (2004) *J Biol Chem* **279**, 35255-35262

114. Lux, A., Attisano, L., and Marchuk, D. A. (1999) *J Biol Chem* **274**, 9984-9992

115. McAllister, K. A., Grogg, K. M., Johnson, D. W., Gallione, C. J., Baldwin, M. A., Jackson, C. E., Helmbold, E. A., Markel, D. S., McKinnon, W. C., Murrell, J., and et al. (1994) *Nat Genet* **8**, 345-351

116. Johnson, D. W., Berg, J. N., Baldwin, M. A., Gallione, C. J., Marondel, I., Yoon, S. J., Stenzel, T. T., Speer, M., Pericak-Vance, M. A., Diamond, A., Guttmacher, A. E., Jackson, C. E., Attisano, L., Kucherlapati, R., Porteous, M. E., and Marchuk, D. A. (1996) *Nat Genet* **13**, 189-195

117. Roelen, B. A., van Rooijen, M. A., and Mummery, C. L. (1997) *Dev Dyn* **209**, 418-430

118. Caniggia, I., Taylor, C. V., Ritchie, J. W., Lye, S. J., and Letarte, M. (1997) *Endocrinology* **138**, 4977-4988

119. Formisano, S., Johnson, M. L., Lee, G., Aloj, S. M., and Edelhoch, H. (1979) *Biochemistry* **18**, 1119-1124

120. Valentino, L. A., and Ladisch, S. (1994) *Blood* **83**, 2872-2877

121. Cotterchio, M., and Seyfried, T. N. (1994) *J Lipid Res* **35**, 10-14

122. Deutschman, D. H., Carstens, J. S., Klepper, R. L., Smith, W. S., Page, M. T., Young, T. R., Gleason, L. A., Nakajima, N., and Sabbadini, R. A. (2003) *Am Heart J* **146**, 62-68

123. Gorska, M., Dobrzyn, A., and Baranowski, M. (2005) *Med Sci Monit* **11**, CR35-38

124. Ribar, S., Mesaric, M., and Sedic, M. (2003) *Croat Med J* **44**, 165-170

125. Lingwood, D., and Simons, K. (2010) *Science* **327**, 46-50

126. Huang, S. S., and Huang, J. S. (2005) *J Cell Biochem* **96**, 447-462

127. Philips, N., Keller, T., and Gonzalez, S. (2004) *Wound Repair Regen* **12**, 53-59

128. Shi, Y., Wang, Y. F., Jayaraman, L., Yang, H., Massague, J., and Pavletich, N. P. (1998) *Cell* **94**, 585-594

129. Zawel, L., Dai, J. L., Buckhaults, P., Zhou, S., Kinzler, K. W., Vogelstein, B., and Kern, S. E. (1998) *Mol Cell* **1**, 611-617

130. Massague, J., Seoane, J., and Wotton, D. (2005) *Genes Dev* **19**, 2783-2810

131. Ishida, W., Hamamoto, T., Kusanagi, K., Yagi, K., Kawabata, M., Takehara, K., Sampath, T. K., Kato, M., and Miyazono, K. (2000) *J Biol Chem* **275**, 6075-6079

132. Hata, A., Seoane, J., Lagna, G., Montalvo, E., Hemmati-Brivanlou, A., and Massague, J. (2000) *Cell* **100**, 229-240

133. Li, C. M., Park, J. H., He, X., Levy, B., Chen, F., Arai, K., Adler, D. A., Disteche, C. M., Koch, J., Sandhoff, K., and Schuchman, E. H. (1999) *Genomics* **62**, 223-231

134. Smyth, M. J., Perry, D. K., Zhang, J., Poirier, G. G., Hannun, Y. A., and Obeid, L. M. (1996) *Biochem J* **316 (Pt 1)**, 25-28

135. Ullio, C., Casas, J., Brunk, U. T., Sala, G., Fabrias, G., Ghidoni, R., Bonelli, G., Baccino, F. M., and Autelli, R. (2012) *J Lipid Res* **53**, 1134-1143

136. Yu, L., Strandberg, L., and Lenardo, M. J. (2008) *Autophagy* **4**, 567-573

137. Harris, J. (2011) *Cytokine* **56**, 140-144

138. Young, M. M., Kester, M., and Wang, H. G. (2012) *J Lipid Res*

139. Lavieu, G., Scarlatti, F., Sala, G., Carpentier, S., Levade, T., Ghidoni, R., Botti, J., and Codogno, P. (2006) *J Biol Chem* **281**, 8518-8527

140. Kalkat, M., Garcia, J., Ebrahimi, J., Melland-Smith, M., Todros, T., Post, M., and Caniggia, I. (2013) *Autophagy* **9**, 2140-2153

141. Draper, J. M., Xia, Z., Smith, R. A., Zhuang, Y., Wang, W., and Smith, C. D. (2011) *Mol Cancer Ther* **10**, 2052-2061

142. Paugh, S. W., Paugh, B. S., Rahmani, M., Kapitonov, D., Almenara, J. A., Kordula, T., Milstien, S., Adams, J. K., Zipkin, R. E., Grant, S., and Spiegel, S. (2008) *Blood* **112**, 1382-1391